

**DESIGNING FOR SUSTAINABILITY: APPLICATIONS OF  
TUNABLE SOLVENTS, SWITCHABLE SOLVENTS, AND  
CATALYSIS TO INDUSTRIAL PROCESSES**

A Thesis  
Presented to  
The Academic Faculty

by

Ali Zuhair Fadhel

In Partial Fulfillment  
of the Requirements for the Degree  
Doctor of Philosophy in the  
School of Chemical & Biomolecular Engineering

Georgia Institute of Technology

April, 2011

**DESIGNING FOR SUSTAINABILITY: APPLICATIONS OF  
TUNABLE SOLVENTS, SWITCHABLE SOLVENTS, AND  
CATALYSIS TO INDUSTRIAL PROCESSES**

Approved by:

Dr. Charles A. Eckert, Advisor  
School of Chemical & Biomolecular  
Engineering  
*Georgia Institute of Technology*

Dr. Charles L. Liotta, Advisor  
School of Chemistry & Biochemistry  
*Georgia Institute of Technology*

Dr. Michael A. Filler  
School of Chemical & Biomolecular  
Engineering  
*Georgia Institute of Technology*

Dr. Dennis W. Hess  
School of Chemical & Biomolecular  
Engineering  
*Georgia Institute of Technology*

Dr. Carsten Sievers  
School of Chemical & Biomolecular  
Engineering  
*Georgia Institute of Technology*

Date Approved: December 17, 2010

To my parents Nedaa and Zuhair for teaching me to be honest and work hard and for their continuous support, for my wife Lisa Marie for her love and support, and for everyone who tries hard.

## ACKNOWLEDGEMENTS

I am deeply grateful to my Advisors Dr. Charles A. Eckert and Charles L. Liotta for investing their priceless time in my education and scientific growth. They helped me develop as an independent researcher, a critical thinker, an effective communicator, and as a professional. I truly feel that their guidance and trust have prepared me to undertake novel and challenging research and to contribute to the field of Chemical Engineering. I appreciate the challenges they provided me with and their trust in my scientific and communication abilities. Their innovation and excitement about research will always be a motivation for me to carry out sustainability-related projects.

I want to thank my Ph.D. committee members Dr. Michael Filler, Dr. Dennis Hess, and Dr. Carsten Sievers for their valuable time, challenging questions, and feedback on my research projects. I also want to thank Dr. Aryn Teja for his time and help.

I want to thank the Eckert-Liotta group members for their outstanding teamwork spirit and constant willingness to help me achieve and go further in my research. I am especially grateful to Dr. Pamela Pollet for the many exciting chemistry-related discussions and for her creative suggestion to overcome challenges in my projects. I am also thankful for Dr. Rani Jha and Dr. Veronica Llopis Mestre for their valuable time and excitement about results.

Finally, I am forever in debt to my family; their love and kind support is a constant source of motivation. Thank you to all my friends and especially Malek Hajaya for the many insightful and inspiring late-night discussions.

# TABLE OF CONTENTS

	Page
<b>ACKNOWLEDGEMENTS</b>	<b>iv</b>
<b>LIST OF TABLES</b>	<b>vii</b>
<b>LIST OF FIGURES</b>	<b>viii</b>
<b>CHAPTER 1: INTRODUCTION</b>	<b>1</b>
<b>CHAPTER 2: COUPLING HOMOGENEOUS REACTIONS AND HETEROGENEOUS SEPARATIONS WITH ORGANIC-AQUEOUS TUNABLE SOLVENTS</b>	<b>7</b>
2.1: Background	7
2.1.1: Tunable Solvents	10
2.1.2: Phase Behavior of Tunable Solvents	12
2.1.3: Reported Reactions and Separations in Tunable Solvents	13
2.1.3.1: Rhodium Catalyzed Hydroformylation of 1-octene in OATS	13
2.1.3.2: Enzyme Catalyzed Reactions in OATS	17
2.2: Materials and Experimental Methods	21
2.2.1: Materials	21
2.2.2: Experimental Methods	21
2.3: Results and Discussion	28
2.3.1: Phase Behavior of propane-OATS	29
2.3.2: Application of propane-OATS to Enzymatic Reactions	31
2.3.3: Application of propane-OATS to Hydroformylation Reactions	32
2.3.4: Application of CO <sub>2</sub> -OATS to Hydroformylation of p-methylstyrene	33
2.4: Conclusions	47
<b>CHAPTER 3: REVERSIBLE CAPPING AGENTS FOR THE SYNTHESIS AND DEPOSITION OF GOLD NANOPARTICLES</b>	<b>48</b>
3.1: Background	48
3.2: Materials and Experimental Methods	54
3.2.1: Materials.	54
3.2.2: Experimental Methods	55
3.3: Results and Discussions	58
3.3.1: Two-component Reversible Ionic Liquid Systems	58
3.3.2: One-component Reversible Ionic Liquid Systems	64

3.4: Conclusions	68
<b>CHAPTER 4: CATALYST SYNTHESIS AND TESTING FOR A DUAL PURPOSE HYDRAZINE THRUSTER</b>	<b>69</b>
4.1: Background	69
4.2: Materials and Experimental Methods	74
4.2.1: Materials	74
4.2.2: Experimental Methods	74
4.3: Results and Discussion	78
4.3.1: Metal Nanoparticles Synthesis	78
4.3.2 Supported Metal Nanoparticle Synthesis	80
4.3.3: Reactor Environment Safety	84
4.3.4: Hydrazine Reactor Design	85
4.3.5: Decomposition of Hydrazine	90
4.4: Conclusions	93
<b>CHAPTER 5: CONCLUSIONS AND RECOMMENDATIONS</b>	<b>94</b>
<b>REFERENCES</b>	<b>99</b>

## LIST OF TABLES

	Page
Table 2.1: Liquid-liquid equilibria of H <sub>2</sub> O(1)/CO <sub>2</sub> (2)/ACN(3) OATS at 40°C.	13
Table 2.2: Mass Composition of H <sub>2</sub> O(1)/propane(2)/ acetone(3) OATS at 40°C.	30
Table 2.3: Mass Composition of H <sub>2</sub> O(1)/propane(2)/ THF(3) OATS at 30°C.	31
Table 2.4: Mass Composition of H <sub>2</sub> O(1)/propane(2)/ THF(3) OATS at 40°C.	31
Table 2.5: Phenylethyl acetate hydrolysis in organic-aqueous OATS mixtures.	32
Table 2.6: <i>p</i> -methylstyrene conversion and branched product selectivity after 1 hour reaction time in different homogeneous solvents systems.	35
Table 2.7: Effect of TPPMS:Rh on the conversion and selectivity of <i>p</i> -methylstyrene hydroformylation in ACN:H <sub>2</sub> O (70 vol% ACN).	40
Table 4.1: Size of metal nanoparticles as determined by TEM analysis.	79
Table 4.2: Comparison of conversion, metal loading, surface area and pore volume.	81
Table 4.3: Results from supported nanoparticle catalyst decomposition tests.	92

## LIST OF FIGURES

	Page
Figure 1.1: Growth in the number of research articles containing the word “sustainable” based on a SciFinder® search (accessed August, 2010).	2
Figure 1.2: Relationship of sustainability, green engineering, and green chemistry.	2
Figure 1.3: General schematic of a process using tunable and smart solvents.	5
Figure 2.1: Solvent power and transport ability of various solvents.	8
Figure 2.2: Kamlet-Taft dipolarity and polarizability ( $\pi^*$ ) of acetonitrile/CO <sub>2</sub> mixture as a function of CO <sub>2</sub> mole fraction.	11
Figure 2.3: Schematic of catalyzed reaction with CO <sub>2</sub> -OATS mediated separation.	12
Figure 2.4: Hydroformylation of 1-octene to 1-nonanal and Side Products.	15
Figure 2.5: Hydrophilic ligands for hydroformylation reactions.	15
Figure 2.6: Partitioning of hydrophilic TPPMS and TPPTS in the aqueous phase as a function of CO <sub>2</sub> pressure in THF/H <sub>2</sub> O (70:30 v:v) at 25°C.	16
Figure 2.7: Hydrolysis of 2-phenylethyl acetate to 2-phenylethanol using CAL B.	19
Figure 2.8: Monophasic Ester Hydrolysis Reaction Rates for 8mM (+) and Near-Saturation (O) of 2PEA Solutions as a Function of 1,4-dioxane Fraction in dioxane/H <sub>2</sub> O at room temperature.	19
Figure 2.9: CAL B Recycles for Ester Hydrolysis in dioxane/H <sub>2</sub> O (40:60 v:v) (conversion $\blacklozenge$ and measured solution pH $\blacklozenge$ ).	20
Figure 2.10: Sample loop internal mechanism.	24

Figure 2.11: Experimental set-up for phase separation experiments under CO <sub>2</sub> -pressure.	27
Figure 2.12: Hydroformylation of <i>p</i> -methylstyrene with Rh/TPPMS to produce branched (desired) and linear aldehydes.	29
Figure 2.13: <i>p</i> -methylstyrene conversion after one hour of reactions time.	36
Figure 2.14: 2-( <i>p</i> -tolyl)-propanal selectivity after one hour of reaction time.	37
Figure 2.15: <i>p</i> -methylstyrene conversion and branched product yield as a function of time at 60°C and 3.1 MPa of syngas.	38
Figure 2.16: Differences in OATS on the separation of 2-( <i>p</i> -tolyl)-propanal in the organic Phase as a function of CO <sub>2</sub> pressure.	41
Figure 2.17: Effect of temperature on the separation of 2-( <i>p</i> -tolyl)-propanal in the organic-rich phase in ACN/H <sub>2</sub> O OATS.	42
Figure 2.18: Separation of branched product (2-( <i>p</i> -tolyl)-propanal) and <i>p</i> -methylstyrene in ACN/H <sub>2</sub> O OATS as a function of CO <sub>2</sub> pressure.	44
Figure 2.19: Retention of the ligand TPPMS in the aqueous phase in ACN/H <sub>2</sub> O OATS as a function of CO <sub>2</sub> pressure.	46
Figure 2.20: Hydroformylation catalyst recycles in ACN/H <sub>2</sub> O OATS with 3.1 MPa of CO <sub>2</sub> .	46
Figure 3.1: Room temperature ionic liquids that form microemulsions with <i>N</i> -EtFOSA surfactant in compressed CO <sub>2</sub> .	51
Figure 3.2: TEM Image of gold nanoparticles synthesized with <i>N</i> -EtFOSA (0.06 g/ml) and TMGT ( $w = 0.41$ ) in compressed CO <sub>2</sub> (35°C, 20MPa) with $W_{\text{HAuCl}_4}/W_{\text{IL}} = 0.01$ .	52
Figure 3.3: TEM Image of gold nanoparticles synthesized with <i>N</i> -EtFOSA (0.06 g/ml) and TMGT ( $w = 0.41$ ) in compressed CO <sub>2</sub> (35°C, 20MPa) with $W_{\text{HAuCl}_4}/W_{\text{IL}} = 0.04$ .	52

Figure 3.4: 2-component reversible ionic liquids formed by a switch from a molecular liquid mixture of N,N,N',N'-tetramethyl-N''-butylguanidine (TMBG) and alcohol (ROH) to the ionic liquid [TMBGH] <sup>+</sup> [O <sub>2</sub> COR] <sup>-</sup> upon addition of CO <sub>2</sub> . R= C <sub>1</sub> to C <sub>12</sub> .	54
Figure 3.5: 1-component reversible ionic liquids formed by a switch from a molecular liquid trialkoxysilylpropylamine to its corresponding ionic liquid upon addition of CO <sub>2</sub> .	54
Figure 3.6: Synthesis of surfactant molecule <i>N</i> -propyl octylsulfonamide.	55
Figure 3.7: Chemical structure of ionic dye methyl orange (4-dimethylaminoazobenzene-4'-sulfonic acid sodium salt)	59
Figure 3.8: UV-Vis experiments demonstrating the formation, reversal, and reformation of micellar structure consisting of [TMBGH] <sup>+</sup> [O <sub>2</sub> COCH <sub>3</sub> ] <sup>-</sup> / <i>N</i> -propyl-octylsulfon-amide/dodecane and polar dye methyl orange.	60
Figure 3.9: Dissolution of chloroauric acid in [TMBGH] <sup>+</sup> [O <sub>2</sub> COCH <sub>3</sub> ] <sup>-</sup> / <i>N</i> -propyl-octylsulfonamide/dodecane (left) and gold nanoparticles formed after reduction with hydrazine (right).	60
Figure 3.10: TEM image of Au <sup>0</sup> prepared in [TMBGH] <sup>+</sup> [O <sub>2</sub> COCH <sub>3</sub> ] <sup>-</sup> / <i>N</i> -propyl-octylsulfon amide/dodecane.	61
Figure 3.11: TEM image of Au <sup>0</sup> prepared in [TMBGH] <sup>+</sup> [O <sub>2</sub> COCH <sub>3</sub> ] <sup>-</sup> / <i>N</i> -propyl-octylsulfon amide/hexane.	63
Figure 3.12: Size distribution of Au <sup>0</sup> particle prepared in fresh and recycled [TMBGH] <sup>+</sup> [O <sub>2</sub> COCH <sub>3</sub> ] <sup>-</sup> / <i>N</i> -propyl-octylsulfon amide/hexane solvent system.	63
Figure 3.13: Formation, reversal, and reformation of micellar structure consisting of TPSAC RevIL indicated by color change due to dissolution of methyl orange.	65
Figure 3.14: UV-Vis spectra demonstrating the formation, reversal, and reformation of micellar structure consisting of TPSAC as evident by methyl orange absorption peak around 410 nm.	66
Figure 3.15: TEM Image of gold nanoparticles synthesized with THSAC in hexane (0.035 g/ml) with $W_{\text{HAuCl}_4}/W_{\text{IL}}=0.054$ .	67
Figure 3.16: TEM Image of gold nanoparticles synthesized with TPSAC in hexane (0.012 g/ml) with $W_{\text{HAuCl}_4}/W_{\text{IL}}=0.007$ .	68

Figure 4.1: Decomposition pathways of hydrazine.	71
Figure 4.2: Proposed hydrazine decomposition mechanism.	73
Figure 4.3: Schematic of GC-TCD analysis set-up.	77
Figure 4.4: TEM images of nickel nanoparticles (top) and the corresponding particle size distribution histogram (bottom).	79
Figure 4.5: TEM images of iridium nanoparticles (top) and the corresponding particle size distribution histogram (bottom).	80
Figure 4.6: SEM images of nickel particles supported on silica surface.	82
Figure 4.7: SEM images of copper particles supported on silica surface.	83
Figure 4.8: SEM image of iridium particles supported on a silica surface.	83
Figure 4.9: ChemCasette hydrazine monitoring system and hydrazine monitoring badges.	85
Figure 4.10: Reactor designed and built to test the hydrazine decomposition abilities of metal catalysts supported on silica.	87
Figure 4.11: Schematic of second generation reactor.	89
Figure 5.1: 2,2'-Bis-(diiphenylphosphinomethyl)-1,1'-binaphthyl chiral ligand.	96

## SUMMARY

The focus of this research was to improve the sustainability of various processes by employing tunable solvents, switchable solvents, and catalysis. In Chapter 2, we report applications of tunable solvents to metal and enzyme catalyzed reactions of hydrophobic substrates. Tunable solvents are defined as solvent that change properties rapidly but continuously upon the application of an external physical stimulus and we utilize these solvents to couple homogeneous reactions with heterogeneous separations. We developed organic-aqueous tunable solvents that utilize propane for efficient phase separation at moderate pressures around 1 MPa; for example the water contents in the propane-expanded THF is 3 wt% at 0.8MPa at 30°C. Also, we extended the use of CO<sub>2</sub>-organic-aqueous tunable solvents to a pharmaceutically-relevant reaction—the hydroformylation of *p*-methylstyrene. The homogeneous reactions provide fast rates with excellent yields. At 60°C, the reaction reaches completion after 180 minutes with 95% branched aldehyde yield. The CO<sub>2</sub>-induced heterogeneous separation of the product from the catalyst provides an efficient and simple way to remove 99% of the product, to retain 99.9% of catalyst, and to recycle the Rh-TPPMS catalyst for five consecutive reactions.

In chapter 3, we investigated the use of reversible ionic liquids (RevILs) for synthesis of nanoparticles. RevILs are formed by the reversible reaction of compounds with basic nitrogen functionalities (molecular liquid) with CO<sub>2</sub> at ambient pressure to form a liquid salt (ionic liquid). We demonstrated that RevILs form microemulsions that can be switched-on by bubbling CO<sub>2</sub> and switched-off by heating. These microemulsions solubilize ionic compounds such as chloroauric acid. We utilized these microemulsions

as a template for controlled synthesis of gold nanoparticles. With 2-component RevILs, [TMBGH]<sup>+</sup>[O<sub>2</sub>COCH<sub>3</sub>]<sup>-</sup>/*N*-propyl-octylsulfonamide/hexane were used to form particles in the size range of 6-20 nm with an average particles size of 11.4±3.3. With 1-component RevILs, (3-aminopropyl)-tripropylsilane was used to prepare semi-spherical gold particles with an average size of about 20nm. The 1-component RevILs systems provide a simpler method to form microemulsions when compared to the 2-component RevILs systems since they eliminate the need for alcohols and surfactants.

In chapter 4, we developed a catalyst that efficiently decomposes hydrazine to selectively produce ammonia. This enables the use of the chemical propulsion hydrazine for electric propulsion as well. We prepared nickel, copper, cobalt, ruthenium, rhodium, and iridium nanoparticles that were supported on silica and we tested these silica-supported metals for the decomposition of hydrazine. To study the catalytic activity, we designed and constructed a continuous flow reactor. The results show that nano-nickel supported on silica is the most active and selective catalyst with 100% conversion of hydrazine and 94±3% yield of ammonia.

## CHAPTER 1: INTRODUCTION

Sustainability has become an essential concept in chemical manufacturing as well as in research and development in academia, industry, and governmental laboratories. Our society is focusing on conserving resources, minimizing energy usage, and reducing the anthropological impact on the planet. Figure 1.1 reflects the increases in the number of scientific publications focusing on sustainability; a three orders of magnitude increase in publications over the last three decades is an indicator of the recent scientific interest and efforts focused on sustainability. It is important to understand the philosophy of sustainability: it embodies both the economics of the process and the environmental impact, with concomitant social responsibility, as reflected in Figure 1.2 [1]. It provides a broad discipline that encompasses green chemistry and green engineering. Green chemistry is guided by the principles outlined by Anastas and Warren [2] and focuses on developing benign chemical reactions but may not consider the overall process waste generations and increase in energy demand. For example, a reaction could be carried out in water—which is a green solvent—but the energy required for separation may result in a significant increase in process cost. On the other hand, green engineering focuses on designing and commercializing manufacturing processes that are economical and that minimize pollution at the source, as defined by the Environmental Protection Agency.

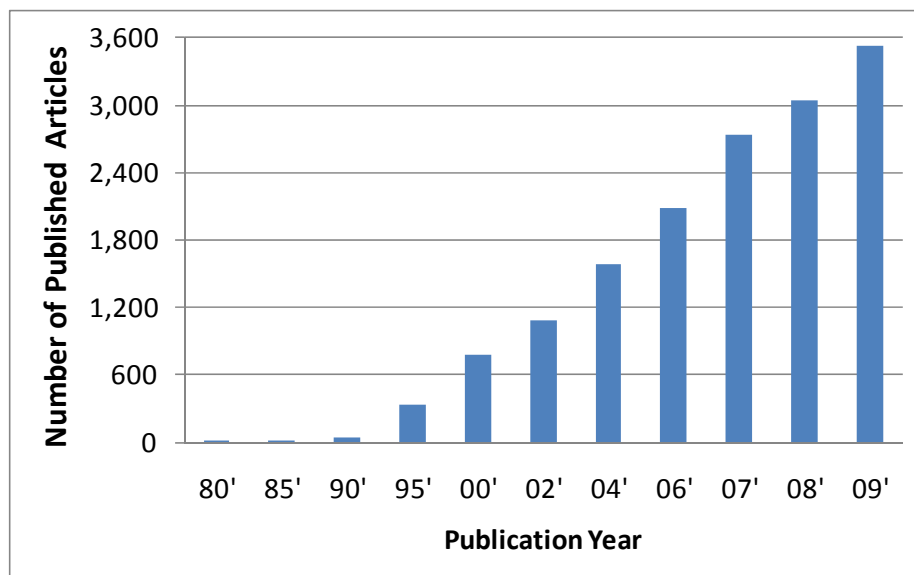


Figure 1.1: Growth in the number of research articles containing the word “sustainable” based on a SciFinder® search (accessed August, 2010).

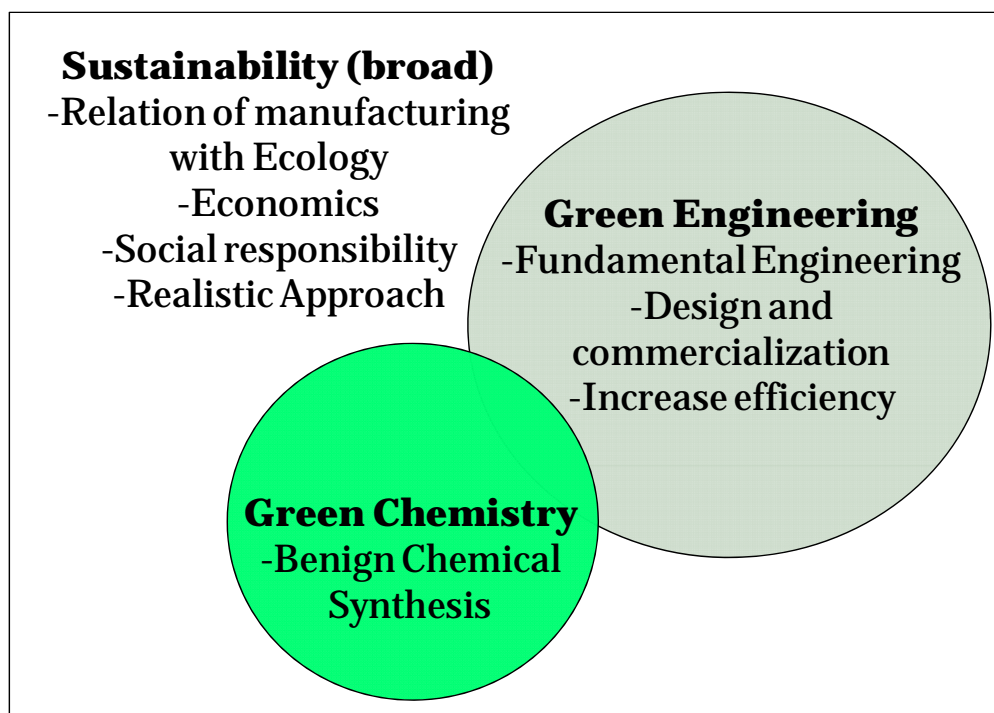


Figure 1.2: Relationship of sustainability, green engineering, and green chemistry.

In this research, we focus on improving the sustainability of three chemical processes:

1. Production of lipophilic pharmaceutical with hydrophilic catalysts
2. Synthesis of nanoparticles
3. Use of hydrazine fuel for space shuttles' propulsion

In Chapter 2, we develop and apply tunable solvents to rhodium catalyzed hydroformylations and enzyme catalyzed hydrolysis for production of pharmaceuticals and fine chemicals. Tunable solvents couple homogeneous reactions with heterogeneous separations through phase manipulation—as depicted in Figure 1.3—to enable removal of products and reuse of catalysts and solvents. Additionally, this process eliminates the need for large amounts of organic solvents that are generally used in liquid-liquid extractions [3]. Tunable solvents can improve chemical processing, reduce process related waste, and reduce process cost. In a typical pharmaceutical/fine chemicals (non-polymer) batch operation, solvent usage accounts for 80 - 90% of mass utilization and often plays the dominant role in the overall toxicity profile of any given process [4]. Also, solvent use consumes about 60% of the overall process energy and accounts for about 50% of post-treatment greenhouse gas emissions in the production of active pharmaceutical ingredients [5]. Therefore, it is essential to develop processing strategies that reduce solvent use and improve the environmental footprint of pharmaceuticals [6, 7]. In the tunable solvent process, we use benign and cheap solvents such as water and CO<sub>2</sub>, which mitigates process cost and pollution. For example, reduction of tetrahydrofuran from 1 kg to 0.75 kg avoids approximately 4 kg of green house gas emissions if one accounts for avoided disposal or recovery emissions [4].

In Chapter 3, we develop and test reversible capping agents to combine synthesis with separation and deposition of metal nanoparticles. This research provides a simple, efficient, and environmental method for the preparation and deposition of metal nanoparticles. The reversible capping agents—also known as reversible ionic liquids—undergo a step change in properties, for example going from non-polar to highly polar, upon a reversible reaction—Figure 1.3. Reversible ionic liquids have been applied to coupling reactions and separations for Heck and Claisen-Schmidt reactions [8], gas separations [9], and oil extractions [10]. In this research, we focus on using these reversible ionic species as templates for synthesis of monodisperse gold nanoparticles followed by a simple and environmental separation and deposition of these particles.

Nanotechnology has gained significant interest in academic research, governmental spending, and industry. For example, the United States government spent more than \$1 billion in nanotechnology funding in 2006 [11]. Globally, similar trends are observed with about \$9 billion for nanotechnology spending in 2005 [12]. The applications of nanomaterial are being investigated for various research areas including biotechnology, energy applications, and catalysis. Unfortunately, the common synthesis methods of nanomaterials generate significant amounts of waste. In terms of *E*-factors, which is the ratio of the amount of materials employed in a process to the amount of product(s) formed, nanomaterials have the highest *E*-factors. For example, bulk chemicals have an *E*-factor of about 1, pharmaceutical have an *E*-factor of around 100, while nanomaterials have an *E*-factor range of 100-100,000 [11]. Generally, the large *E*-factors for nanomaterials result from the use of substantial amounts of organic solvents to remove excess surfactants and capping agents and post-synthesis washes. For example,

the thiol-stabilized liquid-liquid synthesis of gold nanoparticles required 638 grams of organic solvents to purify 0.21 grams of gold nanoparticles [13]. This synthesis has an *E*-factor of 3,320. In this research, we develop a method to remove surfactants/capping agents by simply heating the solution.

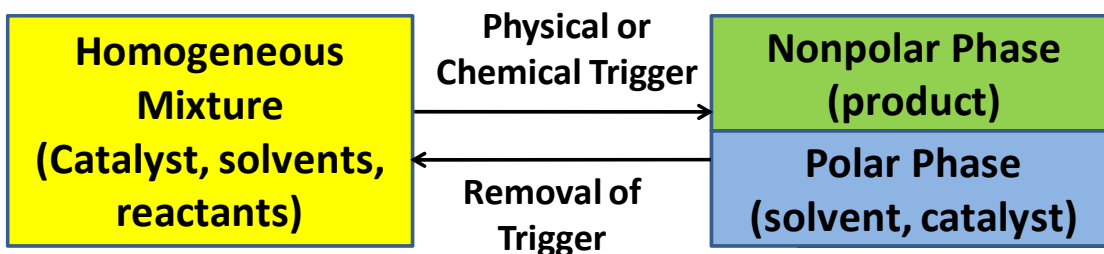


Figure 1.3: General schematic of a process using tunable and smart solvents.

In Chapter 4, we design, synthesize, and test nano-metal based catalysts for controlled decomposition of hydrazine to enable the addition of electric propulsion capabilities to space shuttles that currently utilize only chemical propulsion. In chemical propulsion, the fuel is decomposed or combusted to produce a large quantity of high pressure and high velocity gases that are focused through a nozzle to provides the thrust and lift for the rocket [14]. However, chemical propulsion requires large amounts of fuel making it less attractive for missions that need long lifetime. On the other hand, electric propulsion—defined as the propellant technology that use electricity to increase exhaust velocity [15]—consumes much less energy but provides low thrust. The objective of this research is to develop a catalyst that enables the use of chemical propulsion fuel to enable electric propulsion.

A dual propulsion mode thruster combines the fuel intensive high thrust operation of a chemical system with the energy efficient low thrust operation of an electric propulsion system. This gives a flexibility not currently seen in spacecraft, as a single engine will now be able to efficiently fulfill both short term needs of a system such as rapid high thrust maneuvers to put a satellite into orbit and long term needs such as the minor course corrections required to keep that satellite in orbit over a several year lifespan. Current systems use one engine type or the other, based on what is most beneficial for the mission, which leads to sacrifices being made either in power, speed, propellant weight or cost. The flexibility of our system should lead to a decrease in the amount of propellant needed, allowing for either a larger mission payload or a longer duration of individual missions.

Recommendations for future research related to these projects are discussed in Chapter 5. We discuss relevant reactions for additional pharmaceutical and specialty chemicals that may benefit from tunable and switchable solvents, with a focus on enzymatic reactions and metal catalyzed chiral transformations. Moreover, the utilization of nanoparticles discussed in Chapters 2 and 3 will also be discussed.

# CHAPTER 2: COUPLING HOMOGENEOUS REACTIONS AND HETEROGENEOUS SEPARATIONS WITH ORGANIC-AQUEOUS TUNABLE SOLVENTS

## 2.1: Background

The foremost advantage of tunable solvents is to provide simple and efficient vehicles for conducting both reactions and separations. Tunable solvents are defined as solvents that change properties rapidly but continuously upon the application of an external physical stimulus. This is a distinct advantage over conventional solvent systems. Our group developed various methods to achieve processing advantages with alternative solvents; these solvents include tunable solvents such as supercritical fluids [16-42], nearcritical fluids (gas-expanded liquids [22, 43-49] and nearcritical water [50-61]), and switchable solvents such as reversible ionic liquids [9, 10, 62-64] and piperylene sulfone [65-68]. Figure 2.1 qualitatively relates the “solvent power” (in terms of the Kamlet-Taft polarizability/dipolarity,  $\pi^*$ ) and transport ability (in terms of diffusion coefficient,  $D_A$ ) for the relevant solvents. Liquids are strong solvents but have low diffusion coefficients (about  $10^5$  smaller than gases [69, 70]). Gases have excellent transport properties but are weak solvents. Supercritical fluids such as  $\text{CO}_2$  (SC- $\text{CO}_2$ ) are much stronger solvents than gaseous  $\text{CO}_2$  and have much higher diffusion coefficients than liquids. Therefore, SC- $\text{CO}_2$  is used for many chemical extraction processes (e.g. oils) from solids on industrial scale [71]. For example, Korean based UMAX Co. utilizes

SC-CO<sub>2</sub> (pressure range 32.5-55 MPa) to extract sesame oil from sesame seeds, producing 8,000 liters of oil per day.

Gas-expanded liquids (GXLs), which are mixtures of dissolved gases in organics or ionic-liquids, are better solvents than supercritical fluids and have better diffusion coefficients than liquids. For example, GXLs have shown efficient removal of polyhydroxystyrene-based films and post-plasma-etch residue in small integrated circuits [72], where transport limitations of conventional organics may impose limitations. For any given process, the choice of solvent system depends on the physical and chemical properties of the reactants and products, the processing requirements, environmental considerations, and cost.

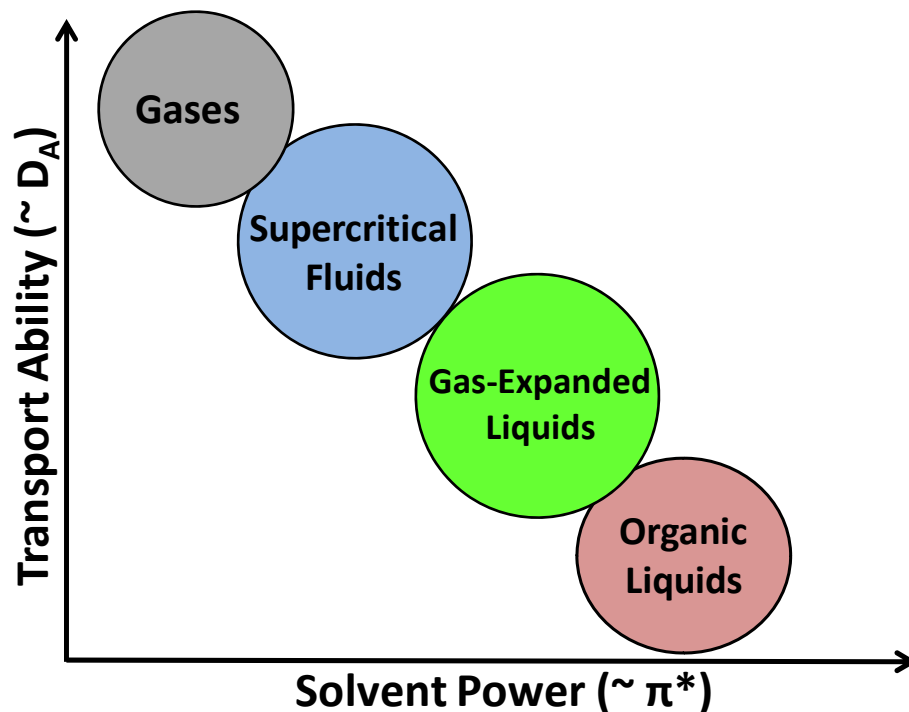


Figure 2.1: Solvent power and transport ability of various solvents.

It is important to develop chemical reaction processes in an holistic manner. Realistically, having a high yield reaction is not enough; separation of the desired product from the reaction system is also of paramount importance. For example, homogeneous reactions are usually superior to heterogeneous reactions in terms of reaction rates and selectivity, especially for chiral catalytic processes like those involving enzymes. However, the difficulty of separating and recycling the catalyst results in serious limitations in applications of homogeneous catalysis. The alternative solvent systems discussed here—which are based on GXLs—offer an efficient, simple, and sustainable method for coupling homogeneous reactions with heterogeneous separations.

In this chapter, we characterize and apply tunable solvents to a variety of reactions. The results include phase behavior, homogeneous reactions yields, and phase manipulation to obtain heterogeneous separation for products removal and catalyst recycle. The introduction part of this chapter provides the relevant background information for this work and includes the definition of tunable solvents with a focus on Organic Aqueous Tunable Solvents (OATS). The reported applications of tunable solvent to the following reactions are also discussed; we use similar reactions to demonstrate the benefits of tunable solvents.

1. Rhodium catalyzed hydroformylation of 1-octene in OATS
2. Enzyme catalyzed hydrolysis in OATS

### 2.1.1: Tunable Solvents

Tunable solvents are defined as solvents with physical properties that are continuously adjustable and can be controlled precisely. The tunable solvents that we investigated are OATS, which are homogeneous mixtures of relatively nonpolar organics (examples are acetonitrile (ACN), tetrahydrofuran (THF), and 1,4-dioxane (Diox)) and water. These homogeneous solvents undergo a phase split to form biphasic liquid-liquid mixtures upon the addition of an antisolvent gas [47]. The phase splitting—from monophasic to biphasic—results from the difference in the antisolvent gas solubility between the aprotic organic solvent and the water. For example, CO<sub>2</sub> is completely miscible with most organics but has limited solubility in aqueous media. Therefore, CO<sub>2</sub> is an effective antisolvent in promoting phase splitting. The resulting biphasic system consists of an organic-rich GXL and an aqueous phase. Physical properties—such as polarity—of GXLs are readily tuned by pressure. Ford *et al.* [46] reported the Kamlet-Taft polarity/polarizability ( $\pi^*$ ) of CO<sub>2</sub>-expanded acetonitrile as a function of CO<sub>2</sub> mole fraction as shown in Figure 2.2. The  $\pi^*$  value decreases gradually from 0.75 for pure acetonitrile to about 0.6 (similar to methanol) at  $x_{\text{CO}_2} = 0.4$  to near zero (similar to cyclohexane) at  $x_{\text{CO}_2} = 0.85$ . GXLs are used as reaction media for improved mass transfer and solubility of gaseous reactants in homogeneous catalysis but may require the use of a membrane or other methods to retain the catalyst for recycle [73-78]. GXLs are also used for separations. The Roberts group at Auburn University utilizes the tunability of GXLs to fractionate polydisperse gold nanoparticles suspended in hexane (sample size of 4.38±1.63 nm) into monodisperse fractions (4.14±1.04 nm at about 4.4 MPa of CO<sub>2</sub>) [79-83].

OATS can be superior to GXLs alone by providing an efficient method for catalyst recovery and recycle in the case of hydrophilic catalysts and organophilic substrates. In OATS, the reaction is carried out homogeneously in a mixed organic/water solvent. Once the reaction is complete, the antisolvent gas is added to yield a biphasic system where the product partitions in the organic-rich phase and the catalyst is retained in the aqueous-rich phase, as demonstrated in Figure 2.3. OATS offer improved rates, yields, and selectivities (characteristic of homogeneous systems) as well as simple catalyst separation and recycle (characteristic of heterogeneous separations).

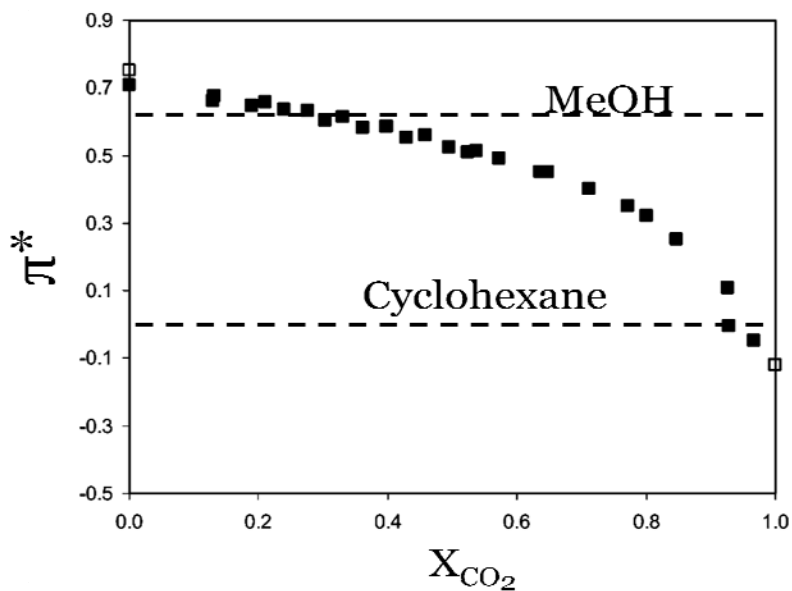


Figure 2.2: Kamlet-Taft dipolarity and polarizability ( $\pi^*$ ) of acetonitrile/ $\text{CO}_2$  mixture as a function of  $\text{CO}_2$  mole fraction.

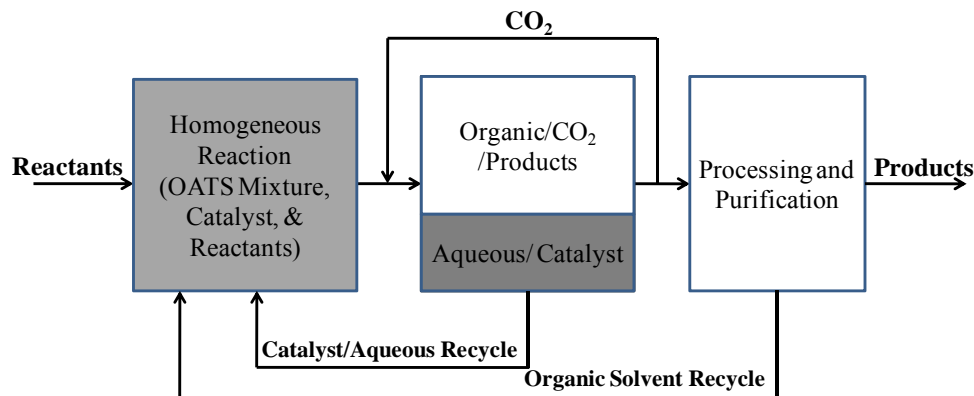


Figure 2.3: Schematic of catalyzed reaction with CO<sub>2</sub>-OATS mediated separation.

### 2.1.2: Phase Behavior of Tunable Solvents

The applicability of OATS depends strongly on phase equilibria. A successful solvent system should provide a readily attainable phase split with a relatively large liquid-liquid region and asymmetric composition distribution to allow for facile separation of the products and recycle of the catalyst [44]. Thus the measurement and modeling of the thermodynamics of phase behavior is an essential part in determining the range of applications of a given tunable system.

Lazzaroni *et al.* reported the high pressure phase behavior of various CO<sub>2</sub>-OATS mixtures [33]. An example of the ternary phase behavior of the liquid-liquid system under CO<sub>2</sub> pressure as shown in Table 2.1. Prior to the addition of CO<sub>2</sub>, a homogeneous mixture acetonitrile (ACN) and water (H<sub>2</sub>O) is introduced into a pressure cell and then CO<sub>2</sub>—in the form of a pressurized gas—is added to induce a phase split. After

equilibrium, the composition of the two liquid phases is measured. The mole fraction of CO<sub>2</sub> does not exceed 4% in the aqueous-rich phase at pressures up to 5.2 MPa. At 4.1 MPa, the aqueous-rich phase consists of more than 90 mol% H<sub>2</sub>O and the organic phase is mostly CO<sub>2</sub> (41 mol%) and acetonitrile (53 mol%). As more CO<sub>2</sub> pressure is applied to the systems, the separation improves; less water is present in the organic-rich phase, and there is less organic in the aqueous phase.

Table 2.1: Liquid-liquid equilibria composition of H<sub>2</sub>O(1)/CO<sub>2</sub>(2)/ACN(3) OATS at 40°C.

P (MPa)	H <sub>2</sub> O-Rich Phase			ACN-Rich Phase		
	x <sub>1</sub>	x <sub>2</sub>	x <sub>3</sub>	x <sub>1</sub>	x <sub>2</sub>	x <sub>3</sub>
1.9	0.73	0.04	0.23	0.49	0.08	0.44
2.4	0.85	0.02	0.14	0.24	0.17	0.59
3.1	0.92	0.01	0.07	0.12	0.26	0.62
4.1	0.91	0.01	0.08	0.07	0.41	0.53
5.2	0.92	0.03	0.06	0.07	0.5	0.43

### 2.1.3: Reported Reactions and Separations in Tunable Solvents

#### 2.1.3.1: Rhodium Catalyzed Hydroformylation of 1-octene in OATS

The hydroformylation of hydrophobic aliphatic alkenes was reported in OATS. Hydroformylation is one of the most important homogeneously catalyzed reaction on industrial scale [84] that utilizes biphasic liquid-organic processing [3]. This is exemplified by the Ruhrchemie/Rhône-Poulenc's process, in which the hydroformylation of propene is carried out in a water-organic biphasic system with the hydrophilic catalyst

rhodium (Rh) - trisulfonated triphenyl phosphine (TPPTS) [84]. The Rh-TPPTS catalytic complex is water-soluble and the reaction takes place predominantly in the aqueous phase. Indeed, in this particular case reactants diffuse into the aqueous phase where the reaction takes place. The products are then extracted into the organic phase and removed for further processing. The biphasic hydroformylation scheme works well for C3-C4 alkenes as their water solubility is sufficient [3, 85] however; hydroformylation of longer chain aliphatic and aromatic alkenes is not possible due to their limited solubility in water [3]. For example, the solubility of propene in water is 200 ppm while the solubility of 1-octene in water is only 2.7 ppm [86, 87]. Although the low solubility is often seen as a limitation, we see it as an opportunity where tunable solvents are obviously superior as they enable homogenous reaction **and** heterogeneous separation (with catalyst recycling).

Hallett *et al.* [45] reported the Rh catalyzed hydroformylation of 1-octene to produce the desired linear aldehyde 1-nonanal—as shown in Figure 2.4—in tetrahydrofuran (THF)-H<sub>2</sub>O OATS (70 vol% organic) under 3 MPa of syngas (CO:H<sub>2</sub> mole ratio of 1:1) pressure. The hydrophilic ligands monosulfonated triphenylphosphine (TPPMS) and trisulfonated triphenylphosphine (TPPTS)—shown in Figure 2.5—were compared. Overall, TPPMS-Rh showed higher catalyst activity (turnover frequency of 350) and comparable selectivity (linear to branched ratio of 2.3) to TPPTS-Rh (turnover frequency of 115 and linear to branched ratio of 2.8).

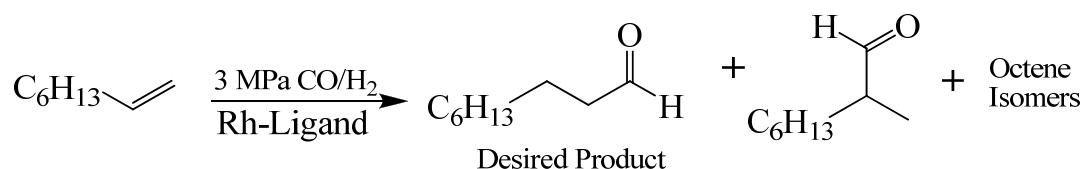


Figure 2.4: Hydroformylation of 1-octene to 1-nonanal and Side Products.

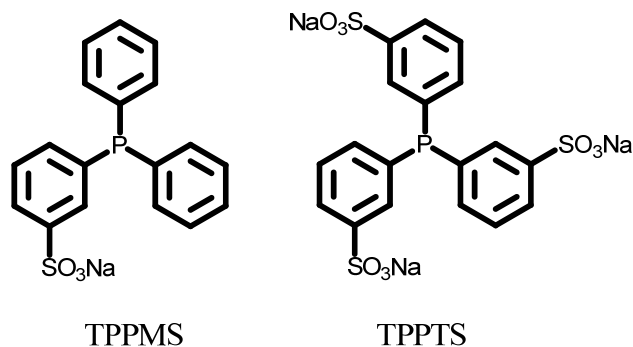


Figure 2.5: Hydrophilic ligands for hydroformylation reactions.

Once the 1-octene hydroformylation is complete, pressurized  $\text{CO}_2$  is introduced into the system for product separation and catalyst recycling. Partition coefficients of the products and the ligands directly portray the efficiency of the  $\text{CO}_2$  induced biphasic separation. We define partition coefficient as the concentration of the reactants, products, ligands or catalysts in their respective desired phase (e.g. aqueous phase for the ligand; organic phase for the products) divided by their concentration in the undesired phase. Figure 2.6 shows the partition coefficients of TPPTS and TPPMS as a function of  $\text{CO}_2$  pressure in the range of 1 to 7 MPa. Partitioning of both ligands increases as a function of increasing  $\text{CO}_2$  pressure due to the improved phase separation at higher pressures, as

discussed above. The hydrophilicity of TPPMS and TPPTS is essentially conferred by the sulfonate groups. Although TPPTS partitions better in the aqueous phase when compared to TPPMS, more than 99.5% of both compounds remain in the aqueous phase with CO<sub>2</sub> pressures of 3 MPa. The partitioning behavior of 1-Nonanal was also efficient as 99% partition in the expanded organic phase at 3 MPa of CO<sub>2</sub>.

In addition, the recycle of the TPPMS-Rh catalyst for three consecutive hydroformylations was demonstrated. After the homogeneous reaction, 3.2 MPa of CO<sub>2</sub> was added to the reactor to obtain phase separation and the organic phase was removed by decantation under pressure. THF and 1-octene were added afterwards to start the next reaction. The results reflect consistent catalytic activity and turnover frequencies (TOF) of 51±3 h<sup>-1</sup> for the three consecutive reactions. The leaching of rhodium in the organic-phase was less than 1ppm as determined by atomic absorption spectroscopy.

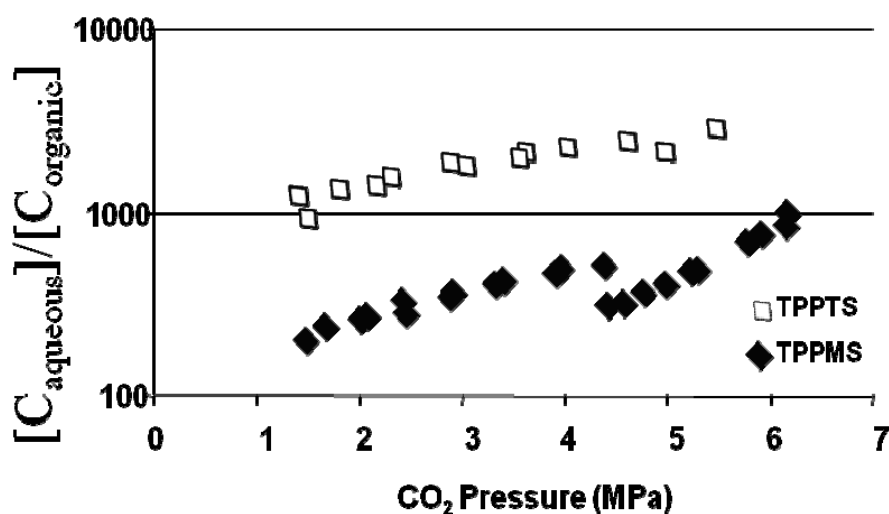


Figure 2.6: Partitioning of hydrophilic TPPMS and TPPTS in the aqueous phase as a function of CO<sub>2</sub> pressure in THF/H<sub>2</sub>O (70:30 v:v) at 25°C.

### 2.1.3.2: Enzyme Catalyzed Reactions in OATS

OATS systems have been used for enzyme-catalyzed reactions. Enzymes function at moderate temperatures and provide synthetic strategies that may otherwise require multiple steps using less selective and active metal-catalysts. However, their applications are largely limited to aqueous media, which constrains the possibility of using them for hydrophobic substrates [43]. OATS provide a suitable medium for enzymatic transformations of hydrophobic substrates and eliminate the need for enzyme immobilization since heterogeneous separation and recovery can be readily achieved.

To carry out enzymatic reactions in CO<sub>2</sub>-OATS one must be aware of two limitations: (1) CO<sub>2</sub> forms carbonic acid with water demanding the use of a buffer to maintain a pH-friendly environment and (2) only some enzymes tolerate organic environments. Therefore, a cautious balance must be achieved to maintain activity in the mixed solvent. The pH of buffered and unbuffered water/dioxane solutions as a function of CO<sub>2</sub> pressures was reported [43]; the pH of unbuffered dioxane/H<sub>2</sub>O (30/70 v/v) was 3 with less than 1 MPa of CO<sub>2</sub>. However; the presence of a sodium phosphate monobasic monohydrate (referred as phosphate afterward) buffer maintains the solution pH above 6 for CO<sub>2</sub> pressures of up to 4 MPa. Hill *et al.* [48] reported the effect of phosphate and (2-hydroxyethyl)-1-piperazineethanesulfonic acid (HEPES) buffers on the phase behavior of 1,4-dioxane/H<sub>2</sub>O/CO<sub>2</sub>. In both cases, an increase of the amount of water in the CO<sub>2</sub>-expanded dioxane was observed. For example, the dioxane-expanded phase contains about 10% water at 3.7 MPa. In the presence of 150 mM phosphate or hepes, the water content in the dioxane-rich phase increases to 15% and 50 %, respectively (at 3.8 MPa). The need for buffer can be avoided by using unreactive gases such as propane, which we

utilize to as antisolvent gas for phase separation as discussed in the results section. The use of flammable propane comes with its procedural limitations and thus; a balance of benefits and limitations must be carefully studied.

Broering *et al.* [43] reported the use of phosphate buffered aqueous/1,4-dioxane tunable solvents for the CAL B catalyzed hydrolysis of 2-phenylethyl acetate (2PEA) to 2-phenylethanol (2PE), as shown in Figure 2.7. The reaction rates with two concentrations of 2PEA—8mM and near-saturation—as a function of increased dioxane volume fraction are shown in Figure 2.8. In aqueous media, the limited solubility of 2PEA in water results in a slow reaction with negligible conversion to products. The addition of dioxane reduces the reaction rate of the 8mM PEA solution from 0.2 mM/min at 10 vol% dioxane and to 0.05 mM/min at 30 vol% dioxane. The reduction in enzyme activity could have resulted from enzyme deactivation by 1,4-dioxane. However, the solubility of 2PEA improves drastically in the presence of dioxane, which compensates for the deactivation of the enzyme and causes the near-saturated 2PEA reaction rate to improve from 0.15 mM/min at 10% dioxane to 0.22 mM/min at 40% dioxane. The 40% dioxane mixture was chosen to recycle the enzyme because it provided the highest specific rate for the reaction and because the volume of the organic layer is larger, which is favorable for product removal. The enzyme was recycled for six consecutive reactions with an average conversion of 61% over two hours. CO<sub>2</sub> was applied after each reaction to induce heterogeneous separation of the product; 80% of the 2PE was removed by decanting. The enzymes maintained catalytic activity of about 85% after six cycles, as shown in Figure 2.9. The decrease in enzymatic activity is explained by dilution of the mixture due to sampling, which accounts for 11% activity loss, as well as enzyme

deactivation due to reduction in solution pH resulting from *in-situ* carbonic acid formation during CO<sub>2</sub> induced phase separation and accumulation of acetate in the aqueous phase despite the use of 150mM phosphate buffer.

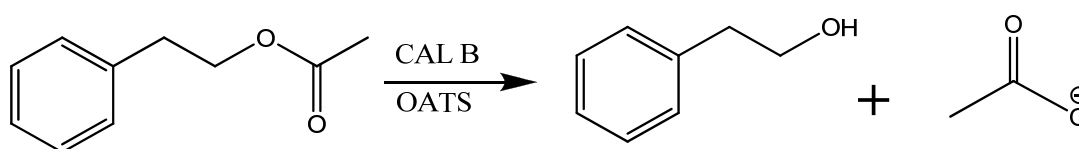


Figure 2.7: Hydrolysis of 2-phenylethyl acetate to 2-phenylethanol using CAL B.

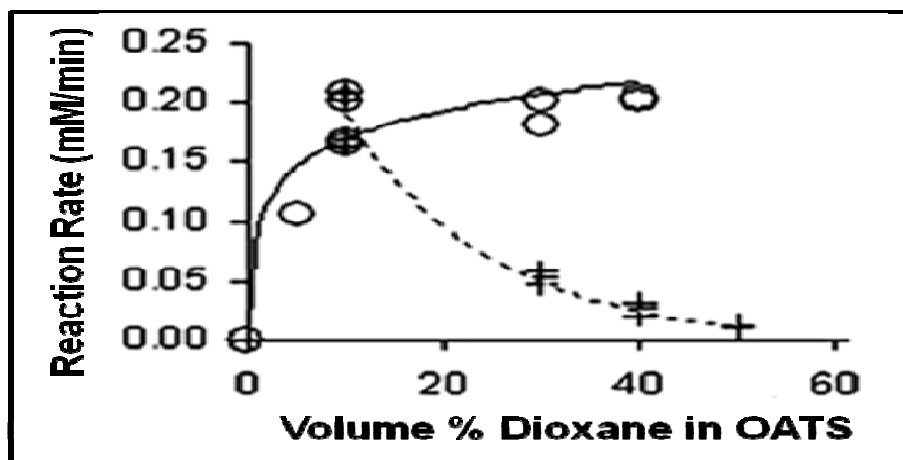


Figure 2.8: Monophasic ester hydrolysis reaction rates for 8mM (+) and near-saturation (O) of 2PEA solutions as a function of 1,4-dioxane fraction in dioxane/H<sub>2</sub>O at room temperature.

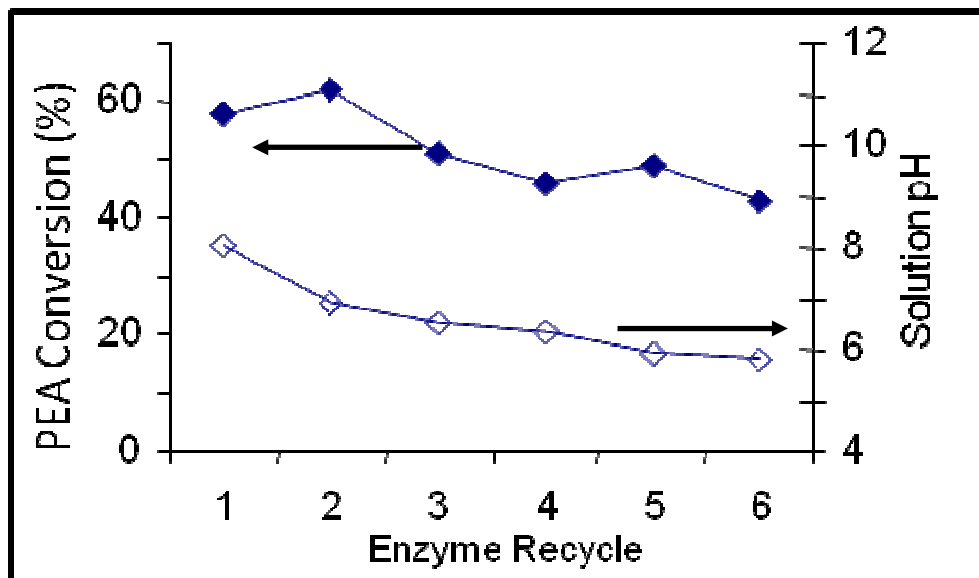


Figure 2.9: CAL B recycles for ester hydrolysis in dioxane/H<sub>2</sub>O (40:60 v:v) (conversion  $\blacklozenge$  and measured solution pH  $\diamond$ ).

## 2.2: Materials and Experimental Methods

### 2.2.1: Materials

The following solvents were degassed by the freeze-pump-thaw method for hydroformylation reactions: HPLC grade acetonitrile (Sigma-Aldrich,  $\geq 99.9\%$ ), 1,4-dioxane (Fischer Scientific, 99.9%), HPLC grade tetrahydrofuran (THF, Sigma-Aldrich,  $\geq 99.9\%$ , inhibitor free), BHT Stabilized THF (Sigma-Aldrich,  $\geq 99.9\%$ , 250 ppm BHT) HPLC grade water (Sigma-Aldrich), and *p*-methylstyrene (Alfa Aesar,  $> 98\%$ ). The following HPLC grade solvents were used as received from Sigma Aldrich: acetone (99.9%), acetonitrile (99.9%), dimethylformamide (99%), 1,4-dioxane (99%), 1-methyl-2-pyrrolidone (99%), tetrahydrofuran (99.9%), and water (99.9%). Carbon dioxide with supercritical fluid chromatography grade (SFC grade, Air Gas, 99.999%) was purified via a Matheson gas purifier and filter cartridge (Model 450B, Type 451 filter). Synthesis gas (syngas, Air Gas, 1:1 molar ratio of  $\text{H}_2:\text{CO}$ ) and instrument grade propane (99.5%, Air Gas) were used as received. The following materials were used as received from the suppliers and stored in a nitrogen filled glove box: triphenylphosphine-3-sulfonic acid sodium salt (TPPMS, TCI America,  $> 90\%$ ) and rhodium (I) dicarbonyl acetylacetonate (Rh(acac), Sigma-Aldrich, 98%). *Candida Rugosa* (Sigma Aldrich) was stored in the refrigerator.

### 2.2.2: Experimental Methods

#### 2.2.2.1: Propane-OATS Phase Behavior

Phase equilibria for the water/propane/organic ternary systems were determined by direct sampling from the different phases in a fixed volume Jerguson sight gauge (a

level meter with quartz sight glass). The Jerguson cell was evacuated for 30 minutes to remove trace solvents and air and then the cell was loaded with a weighed amount (Denver Instrument M-300, analytical balance  $\pm 0.001$  g) of water and organic through the injection port. A constant temperature air bath was maintained by a heater and fan system connected to a temperature controller (DiGi-Sense Temperature Controller – Model 68900-01). The temperature in the cell was monitored using a thermocouple (Omega type K) in contact with the liquid phase. The thermocouple was calibrated against a platinum RTD (Omega PRP-4) with DP251 Precision RTD Benchtop Thermometer (DP251 Omega), providing an accuracy of  $\pm 0.2^\circ\text{C}$ . The cell was allowed to reach temperature equilibrium for 2 hours before pressurizing the cell. Liquid propane was added from a piston pump (ISCO – Model 260D Syringe Pump) while constantly shaking the cell until the desired pressure was reached. Pressure in the cell was measured using a Druck pressure transducer (PDCR 910) and read-out box (DPI 260) that were calibrated against a hydraulic piston pressure gauge (Ruska) to an uncertainty of  $\pm 0.01$  MPa. The cell is mounted to a rotating shaft allowing the cell to be manually shaken. Once the desired pressure is sustained, the system is allowed to equilibrate for a minimum of 3 hours. Samples from each of the phases were obtained by sampling with constant volume sample loop connected to a six-way valve—schematic in Figure 2.10—to enable consistent sample volumes. Constant volume sampling is essential in these experiments since the samples contain significant amounts of dissolved gas. The samples were collected into methanol (a capture solvent) and analyzed for water content via Karl-Fischer titration (Metler Toledo – Karl-Fischer DL31) and for organic content via gas chromatography – mass spectrometry (Agilent GC-HP 6890 with a GCMS-HP 5973 and

HP-5MS column) and quantified using a calibration curve ( $R^2 = 0.995$ ). Propane content was determined by measuring the volume displaced while expanding samples into the headspace of an inverted burette filled with water. The mass of propane was calculated from the displaced volume via the ideal gas equation at STP after allowing the temperature to reach equilibrium. All samples were taken in triplicate and averaged to calculate experimental error and verify repeatability.

#### 2.2.2.2: Enzymatic Reactions in OATS

Stock solutions of 2-phenylethyl acetate (2PEA) in organic solvents (~200mM) and the *Candida Rugosa* in water (0.01g/ml) were prepared. Stock solutions along with additional organic and water were combined to produce a total reaction volume of 6 ml. Aliquots of the reaction were taken at the beginning of the reactions, after 1 hour, and after 2 hours to measure the conversion of the reaction. These aliquots were quenched with a solution of acetic acid and organic (1:1 volume ratio) in a 3:1 volume ratio. The quenched solutions were analyzed using GC and LC using calibration curves to calculate conversion.

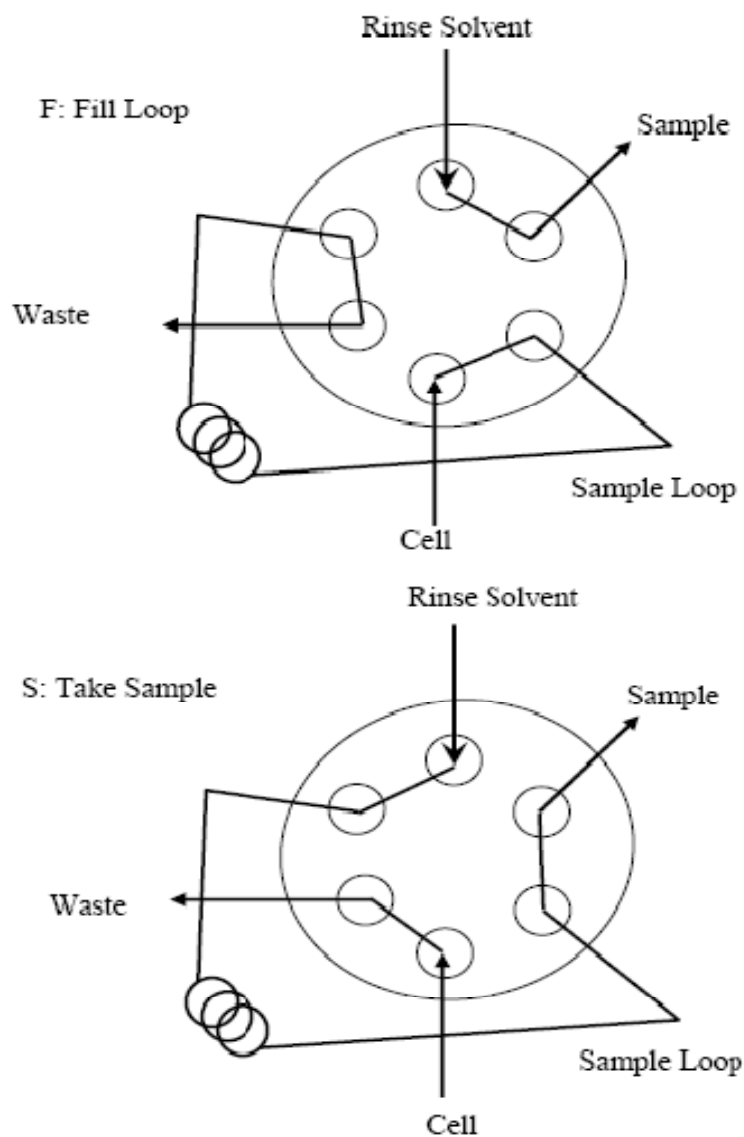


Figure 2.10: Sample loop internal mechanism.

### 2.2.2.3: *p*-Methylstyrene hydroformylation in OATS

Hydroformylations were carried out in a 300 mL stainless steel Parr autoclave (Parr Instrument Company, model 4561). The reaction pressure was monitored with a calibrated digital pressure transducer (Heise, model 901B) providing a precision of  $\pm 0.07$

MPa. A proportional-integral-derivative (PID) temperature controller and tachometer (Parr Instrument Company, model 4842) were used to control the temperature of the reactor to  $\pm 2^\circ\text{C}$  and the stirring speed to  $\pm 5$  rpm. The temperature inside the reactor was monitored with a type J thermocouple and heat was provided by an electric heating mantle. The catalyst solution was prepared by weighing the desired amounts of Rh(acac) and TPPMS in the glove box, adding degassed solution of OATS, and then stirring for at least 20 minutes and visually confirming complete solubility of the catalyst. The reactions were started by evacuating the Parr autoclave and flushing it with 0.3 MPa of syngas. The degassed *p*-methylstyrene, the catalyst solution, and OATS solvents were added using gas-tight syringes (SGE Analytical Science). The total volume of the reaction mixture was 50 mL with a *p*-methylstyrene concentration of 0.15 M. The concentration equivalences of Rh(acac) and TPPMS are 0.0016 and 0.017, respectively. The reactor was heated to temperature, stirred at 300 rpm, and subsequently pressurized with 3.1 MPa of syngas. After the desired reaction period, a liquid phase sample was withdrawn, captured in acetone or methanol, and analyzed with an Agilent gas chromatography-flame ionization detector (GC-FID, model 6890) with an Agilent column (model HP-5MS). External standards of known concentrations were used to calibrate the FID response.

#### 2.2.2.4: Separation of Hydroformylation Substrates in OATS

The separation experiments of hydroformylation substrates were conducted by adding a homogeneous OATS mixture with the desired substrates (2.0 mL of *p*-methylstyrene or 2.3 mL of 2-(*p*-tolyl) propanal—0.15M concentration of both—and 98 mL of 70/30 v/v organic/water OATS solution) to the Parr autoclave described above. CO<sub>2</sub> was added to

the cell using an ISCO syringe pump until the desired pressure was reached. After equilibrium (we determined independently that equilibrium was reached in 15 minutes of stirring and 30 minutes of settling), three samples of the organic-rich and of the aqueous-rich phases were taken using dip tubes, as depicted in Figure 2.11. The dip tubes' length was designed to be within the intended layer and away from the interface to prevent cross contamination of the samples. Each dip tube was connected to a six-way constant volume sample loop—Figure 2.10. We compared stock solutions of starting material in OATS mixture directly charged to the reactor to ones passed through the sample loop and verified that no substrate sticking occurred. Before and after sampling, the sample loop was flushed with at least three times its volume to rinse out any contaminants. The samples were analyzed using the Agilent GC-FID described above. We used a similar procedure for the separation experiments of TPPMS except that the samples were analyzed with UV-Vis spectroscopy to measure the concentrations of the ligand.

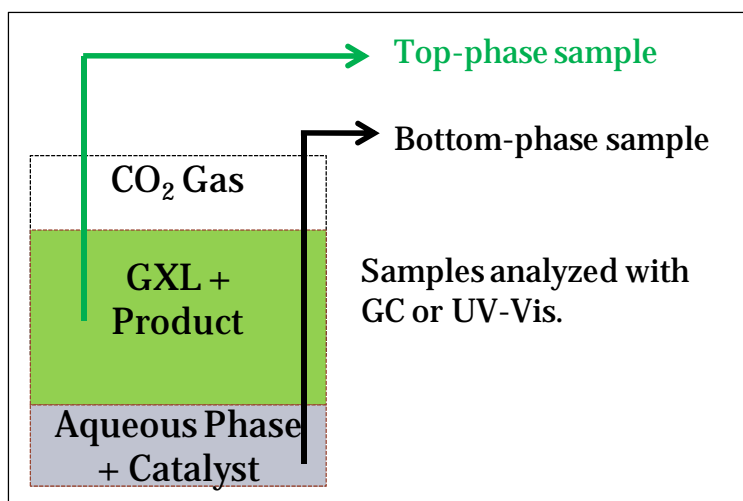


Figure 2.11: Experimental set-up for phase separation experiments under CO<sub>2</sub>-pressure.

#### 2.2.2.5: Catalyst Recycle Experiments in OATS

To demonstrate catalyst recycle, we carried out homogeneous hydroformylation reactions in ACN/H<sub>2</sub>O OATS. The reaction was carried out with *p*-methylstyrene initial concentration of 0.15 M and with Rh:TPPMS:substrate of 1:10:600 at 60°C for one hour and 3.1 MPa syngas. Samples from the homogeneous reaction mixture were collected to analyze for conversion and selectivity. After an ice quench of the reaction, the syngas was vented and the reactor was flushed with CO<sub>2</sub> to remove any syngas and pressurized to 3.1 MPa of CO<sub>2</sub>. We were able to remove 85% of the organic-rich layer with the top phase dip-tube so that fresh *p*-methylstyrene and organic solvent could be added and the next reaction cycle started. Make-up catalyst was added to compensate for catalyst removed during sampling to maintain constant catalyst to substrate ratio.

### 2.3: Results and Discussion

The results include phase behavior of propane-OATS and their application to enzymatic reactions and hydroformylation reactions. However, the majority of the results are focused on the application of CO<sub>2</sub>-OATS to the hydroformylation of a pharmaceutically relevant reactions—the hydroformylation of *p*-methylstyrene. We chose *p*-methylstyrene as model compound since the branched aldehyde product structurally mimics *p*-isobutylstyrene, a key synthetic precursor to ibuprofen [88, 89]. This is particularly important as ibuprofen is a widely used nonsteroidal anti-inflammatory drug with annual production of more than 12 million kg per annum [90]. *p*-methylstyrene reacts with syngas (CO and H<sub>2</sub>, 3MPa) to produce the branched (2-*p*-tolyl-propanal) and linear aldehyde as shown in Figure 2.12; the branched aldehyde is the desired product. In some instances, we compare our results to heterogeneously reported hydroformylations using solid supports because we believe that method is common in industrial applications. However, it is also reported that this type of reaction is carried out in homogeneous organic solvents. In such industrial schemes, the separation of the catalyst—which is hydrophilic to a certain extent—is achieved with multiple aqueous washes. The latter method is waste and energy intensive since the catalyst must be recovered by distilling off the water [3].

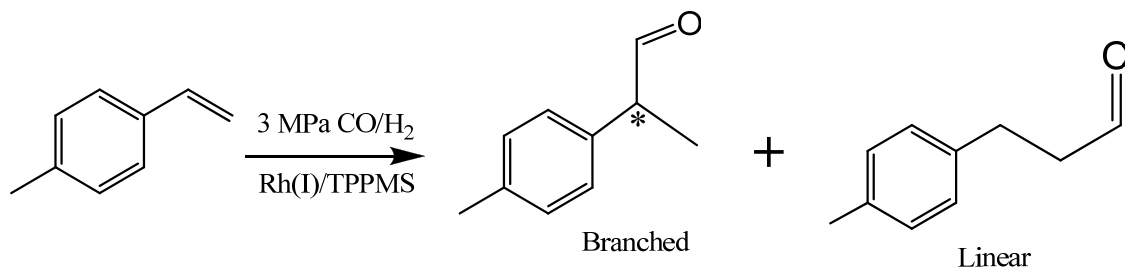


Figure 2.12: Hydroformylation of p-methylstyrene with Rh/TPPMS to produce branched (desired) and linear aldehydes.

### 2.3.1: Phase Behavior of propane-OATS

We investigated the ability of propane to act as an antisolvent for homogeneous organic-aqueous solutions that are miscible at ambient conditions. Solutions of water with the following organics were screened: acetone, acetonitrile, dimethylformamide (DMF), 1,4-dioxane, 1-methyl-2-pyrrolidone, and tetrahydrofuran. The phase separation of these mixtures was tested at 30°C and/or 40°C and with 55 wt% and/or 33 wt% water. Increasing the temperature may improve phase separation due to decrease/weakening of hydrogen bonding. Also, changing the composition of the system may change interactions of the organic with the water. For example, acetone/H<sub>2</sub>O stays miscible under propane pressures when 55 wt% water is used but phase separation is obtained with composition of 33 wt% H<sub>2</sub>O at 40°C; the liquid-liquid equilibria (LLE) data for this system is summarized in Table 2.2. In the experimental pressures of 1.22-1.58 MPa propane, the acetone-rich phase consists of about 5 wt% water. However, the aqueous-rich phase consists of large amounts of acetone up to 50 wt%. The formation of

heterogeneous biphasic systems was also observed in systems consisting of THF/H<sub>2</sub>O (55 wt% H<sub>2</sub>O, 58 vol% H<sub>2</sub>O) at 30°C and 40°C. The LLE data for these systems is summarized in Tables 2.3 and 2.4. Propane caused phase-splitting of this system at relatively low pressures (when compared to CO<sub>2</sub>) and good phases purity is observed. The water in propane-expanded THF is 3 wt% at 0.8MPa at 30°C. The use of propane for phase separation eliminates the *in-situ* carbonic acid formation from the reaction of CO<sub>2</sub> with water, and so may be more suitable when using acid-sensitive catalysts like enzymes.

Phase separation was not observed in systems consisting of organics that are polar with hydrogen bond accepting capabilities such as DMF and 1-methyl-2-pyrrolidone. Also, 1,4-dioxane/H<sub>2</sub>O systems stay miscible probably due to strong interactions of dioxane with water [91]. Finally, acetonitrile/H<sub>2</sub>O systems (33 wt% H<sub>2</sub>O) existed in liquid-liquid region in propane pressure range of 0.97-1.05 MPa at 30°C. Due to the the small operating window in terms of propane pressure, we chose not to characterize this system further.

Table 2.2: Mass Composition of H<sub>2</sub>O(1)/propane(2)/ acetone(3) OATS at 40°C.

P (Mpa)	H <sub>2</sub> O-rich phase			Acetone-rich phase		
	x <sub>1</sub>	x <sub>2</sub>	x <sub>3</sub>	x <sub>1</sub>	x <sub>2</sub>	x <sub>3</sub>
1.22	0.48	0.01	0.50	0.09	0.33	0.58
1.37	0.55	0.01	0.44	0.08	0.45	0.47
1.49	0.58	0.01	0.41	0.06	0.49	0.45
1.58	0.58	0.02	0.40	0.04	0.53	0.43

Table 2.3: Mass Composition of H<sub>2</sub>O(1)/propane(2)/ THF(3) OATS at 30°C.

P (MPa)	H <sub>2</sub> O-rich phase			THF-rich phase		
	x <sub>1</sub>	x <sub>2</sub>	x <sub>3</sub>	x <sub>1</sub>	x <sub>2</sub>	x <sub>3</sub>
0.43	0.71	0.01	0.29	0.06	0.08	0.86
0.56	0.71	0.01	0.28	0.04	0.18	0.79
0.80	0.78	0.02	0.21	0.03	0.31	0.66
0.92	0.82	0.02	0.16	0.03	0.45	0.52

Table 2.4: Mass Composition of H<sub>2</sub>O(1)/propane(2)/ THF(3) OATS at 40°C.

P (Mpa)	H <sub>2</sub> O-rich phase			THF-rich phase		
	x <sub>1</sub>	x <sub>2</sub>	x <sub>3</sub>	x <sub>1</sub>	x <sub>2</sub>	x <sub>3</sub>
0.64	0.75	0.00	0.25	0.06	0.13	0.82
0.85	0.77	0.00	0.23	0.03	0.24	0.72
1.12	0.83	0.01	0.16	0.04	0.29	0.67
1.35	0.84	0.01	0.16	0.02	0.45	0.53

### 2.3.2: Application of propane-OATS to Enzymatic Reactions

We investigated the use of propane-OATS for candida rugosa (*C. rugosa*) catalyzed hydrolysis of 2-phenylethyl acetate (2PEA) to 2-phenylethanol (2PE)—Figure 2.7. *C. rugosa* is a robust enzyme with comparative activities to the industrially used CAL B [92]. We carried out the hydrolysis reaction in propane-OATS systems consisting of acetone/H<sub>2</sub>O (61 vol% acetone) and THF/H<sub>2</sub>O (42 vol% THF). Low or no activity was observed with these compositions. Therefore, we investigated the effect of organic solvent composition on the enzyme activity and the results are summarized in Table 2.5.

The conversion of 2PEA in 25 vol% dioxane OATS reaches about 50% after two hours, which is comparable with CAL B hydrolysis of 2PEA [43]. Reactions in acetone (25 vol%)/H<sub>2</sub>O show lower yield than those in Diox(25 vol% dioxane)/H<sub>2</sub>O. The conversion of 2PEA decreases as the acetone fraction increases with 10% conversion of 2PEA after 39 hours at 70 vol% acetone. In THF-H<sub>2</sub>O (42 vol% THF), no conversion of 2PEA was observed after 48 hours. The large amount of organic component deactivates the enzyme; organics affect enzymes in various ways including dehydration and/or denaturation [93]. The propane-OATS system is not suitable for the above mentioned enzymatic reactions due to the large amount of organic solvent, which caused enzyme deactivation. We shall discuss other potential application that could benefit from this system in the recommendations chapter.

Table 2.5: Phenylethyl acetate hydrolysis in organic-aqueous OATS mixtures.

Organic Component	Volume % Organic	2PEA Fractional Conversion (after 2 hrs)	Initial 2PEA Concentration (mmol/L)
Dioxane	25	0.50	30
Acetone	25	0.23	39
Acetone	40	0.06	41
Acetone	70	0.1* at 39hr	118

### 2.3.3: Application of propane-OATS to Hydroformylation Reactions

We evaluated the application of propane-OATS systems for hydroformylations by checking the solubility of the reactants *p*-methylstyrene and 1-octene. These hydrophobic substrates—at relatively low concentrations—induced spontaneous phase separation at

ambient pressure. This occurs due to the smaller amount of organic component in propane-OATS systems compared to CO<sub>2</sub>-OATS (70 vol% organic). For example, the homogeneous THF-H<sub>2</sub>O solution with 42 vol% THF phase separates with *p*-methylstyrene molarity of 0.015 and with 1-octene molarity of 0.01. These values are about a tenth of the concentrations used in CO<sub>2</sub>-OATS discussed later. The finite solubility of these hydrophobic substrates renders propane-OATS systems impractical for the model hydroformylations. We did not consider the acetone-H<sub>2</sub>O (61 vol% acetone) system for hydroformylation since it has a narrow pressure range of immiscibility (1.22-1.58 MPa propane).

#### **2.3.4: Application of CO<sub>2</sub>-OATS to Hydroformylation of *p*-methylstyrene**

In these reactions, we chose to use 70 vol% organic in the CO<sub>2</sub>-OATS to obtain a practical solubility of the hydrophobic *p*-methylstyrene (0.15M) and to have a sufficient amount of the aqueous media to retain the catalyst in the separations step.

##### 2.3.4.1: Homogeneous *p*-methylstyrene Hydroformylations in CO<sub>2</sub>-OATS

The hydroformylation of *p*-methylstyrene was carried out in ACN/H<sub>2</sub>O, Diox/H<sub>2</sub>O, and THF/H<sub>2</sub>O. The *p*-methylstyrene conversion (referred to as **conversion** from here on) and the selectivity to the 2-(*p*-tolyl)-propanal as a percentage of total aldehydes formed (referred to as **selectivity** from here on) are used to compare the different solvents. The conversion and selectivity after one hour of reaction time and different temperatures of 40, 60, 80, and 120°C are summarized in Table 2.6.

The conversion in ACN/H<sub>2</sub>O and in Diox/H<sub>2</sub>O are similar. The reactions proceed slowly at 40°C with *p*-methylstyrene conversion of less than 20% after one hour. The

conversion shows a strong dependence on the reaction temperature with complete conversion of the starting materials after one hour at 80°C. The strong dependence of reaction rate on temperature is expected since the reaction rate is a logarithmic function of the temperature in the absence of mass transfer limitations.

Early on in this research, we observed that the hydroformylation of *p*-methylstyrene did not work in non-stabilized THF/H<sub>2</sub>O OATS mixtures. Also, a color change of the catalyst solution from yellow (for freshly prepared Rh/TPPMS) to dark gray was observed. In contrast, the hydroformylation progressed in 2,6-Di-*tert*-butyl-*p*-cresol (BHT, free radical scavenger) stabilized THF/H<sub>2</sub>O OATS. We speculate that the peroxides present in non-stabilized THF [94] may cause catalyst poisoning and deactivation. In stabilized THF/H<sub>2</sub>O, the reaction proceeds but conversion rates remain lower than those measured for ACN/H<sub>2</sub>O (Diox/H<sub>2</sub>O OATS yield similar results to ACN/H<sub>2</sub>O) as portrayed in Figure 2.13. We concluded that THF is not a suitable solvent for this reaction and chose to further investigate Diox/H<sub>2</sub>O and ACN/H<sub>2</sub>O systems for separations.

Table 2.6: *p*-methylstyrene conversion and branched product selectivity after 1 hour reaction time in different homogeneous solvents systems.

<b>OATS Mixture (70 vol% Organic)</b>	<b>Reaction Temperature (°C)</b>	<b>Conversion (%)</b>	<b>Branched Product Yield (%)</b>
<b>ACN/H<sub>2</sub>O<sup>a</sup></b>	40	17.2 ± 3.7	94.4 ± 0.9
	60	47.6 ± 3.0	95.9 ± 0.5
	80	100.0 ± 0.0	83.9 ± 4.7
	120	99.2 ± 0.9	66.2 ± 3.6
<b>Diox/H<sub>2</sub>O</b>	40	10.0 ± 2.1	97.8 ± 1.3
	80	100.0 ± 0.0	82.0 ± 2.7
	120	99.0 ± 0.3	52.0 ± 1.9
<b>THF/H<sub>2</sub>O</b>	40	10.7 ± 7.6	97.3 ± 2.2
	80	83.7 ± 7.4	87.5 ± 0.7
	120	93.3 ± 0.9	51.0 ± 2.6

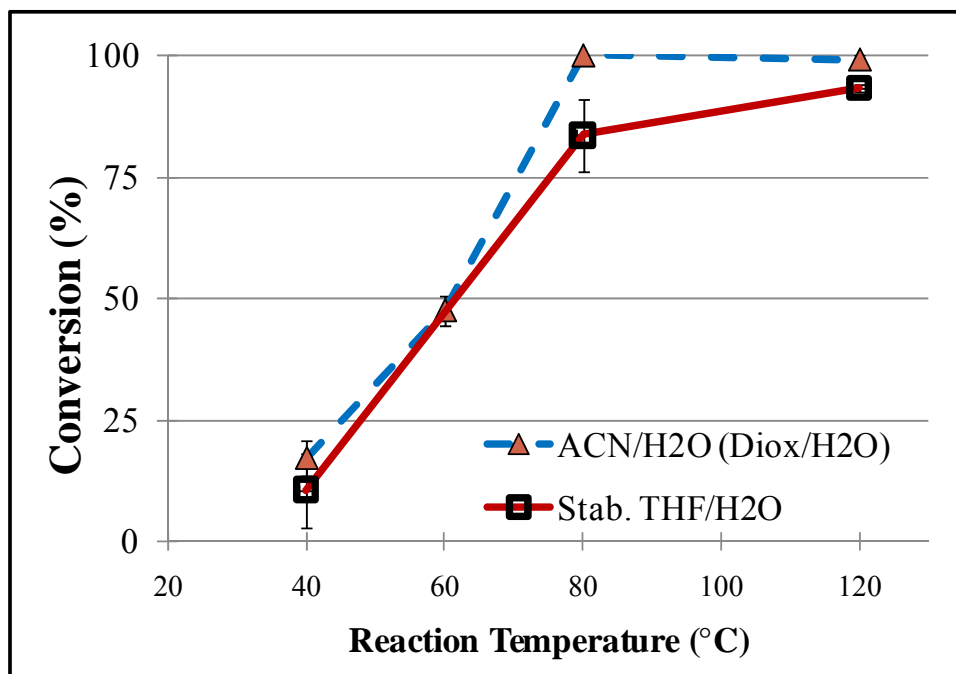


Figure 2.13: *p*-methylstyrene conversion after one hour of reactions time.

The selectivity of *p*-methylstyrene hydroformylation to produce the branched aldehyde was also measured at different temperatures. The selectivity is similar in the three OATS systems at 40°C and 80°C, as demonstrated in Figure 2.14. At 40°C, the selectivity is about 95% and it decreases to about 84% at 80°C. At 120°C, the selectivity in ACN/H<sub>2</sub>O is higher (66.2±3.6) when compared to THF/H<sub>2</sub>O and Diox/H<sub>2</sub>O (about 50%). The difference in selectivity at higher temperatures may be caused by solvent-catalyst interactions. We speculate that interactions between the oxygen in THF and dioxane with the catalyst are causing this difference. Solvent interactions with the catalyst are reported to induce changes in rate and selectivity of hydroformylation reactions; increasing the electron density on the metal enhances the linear aldehyde yield [95, 96]. Furthermore, the decrease in selectivity as a function of increasing temperature

is attributed to  $\beta$ -hydride elimination [97]. The intermediate complex of the branched product with the rhodium catalyst reverts to the starting material at increasing reaction temperatures. By examining the yield in ACN/H<sub>2</sub>O reactions, it seems that  $\beta$ -hydride elimination rate increases significantly at reaction temperatures greater than 60°C.

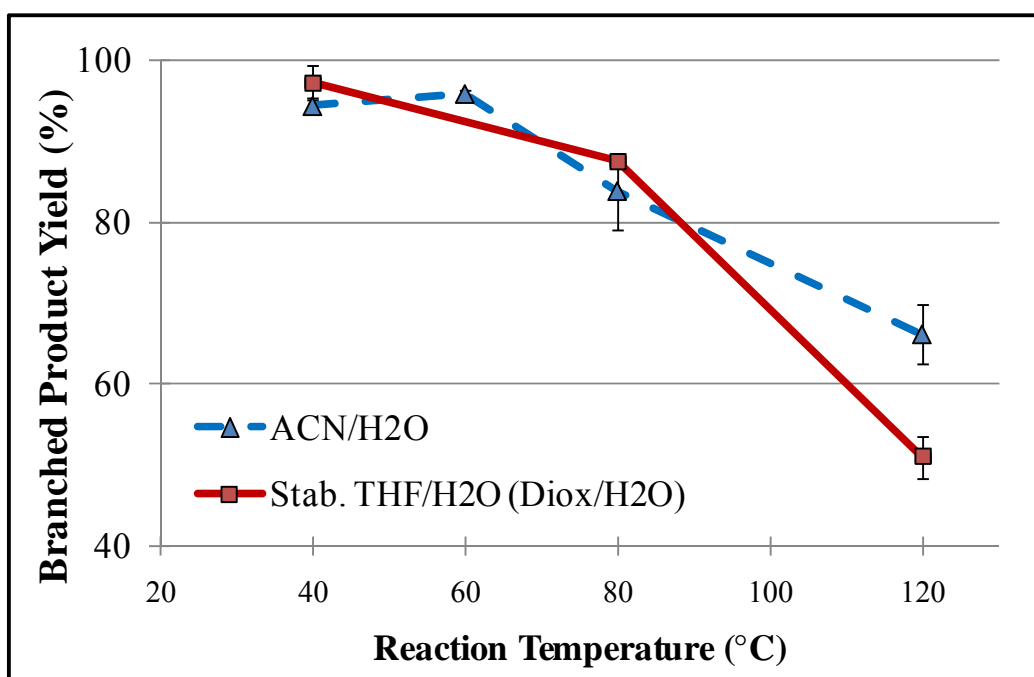


Figure 2.14: 2-(*p*-tolyl)-propanal selectivity after one hour of reaction time.

To characterize further the  $\beta$ -hydride elimination and optimize the reaction, we ran the hydroformylation of *p*-methylstyrene in ACN/H<sub>2</sub>O at 60°C and monitored the conversion and selectivity as a function of time, as shown in Figure 2.15. The conversion reaches 73% after 60 minutes and progresses at a declining rate to 89% after 90 minutes and 99% after 180 minutes. The observed conversion in this experiment

is slightly higher than in ones measured earlier, probably due to higher catalyst loading and/or temperature variations during the reaction. The 2-(*p*-tolyl)-propanal yield is  $95.6 \pm 4.0$  throughout the experiment and remain constant after 24 hours at 60°C and 3.1 MPa of syngas. The constant selectivity confirms that  $\beta$ -hydride elimination reaction is very slow at temperatures up to 60°C. Because of the OATS homogeneous characteristic, the selectivity towards the desired product increases by more than 30% and the conversion rate of starting material is 2-10 times greater than heterogeneously reported reactions using zeolites [98], hydrotalcite clays [99], or ionic liquid modified silica sol-gel [100]. OATS reduces waste providing economical and environmental benefits.

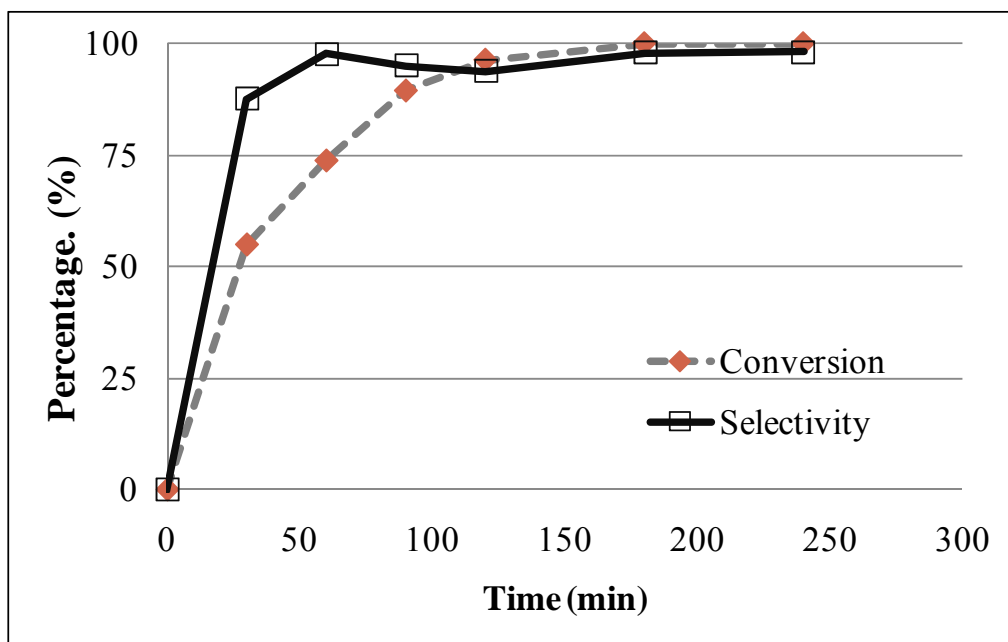


Figure 2.15: *p*-methylstyrene conversion and branched product yield as a function of time at 60°C and 3.1 MPa of syngas.

For *p*-methylstyrene hydroformylations, we chose to use excess TPPMS to utilize fully the rhodium metal and to have efficient post-reaction rhodium recovery, since the ligand constitutes the water soluble part of the catalyst. In this reaction's catalytic cycle, the initial catalytic species are HRh(CO)(TPPMS)<sub>3</sub>. The reaction starts by ejecting a ligand and complexing with the alkene [84]. Early in this work, we conducted a series of reactions with different ligand to catalyst ratios in ACN/H<sub>2</sub>O to ensure that excess ligand did not impose a problem due to competition with CO or the alkene. The conversion and selectivity of *p*-methylstyrene hydroformylation with different ligand to catalyst ratios are summarized in Table 2.7; the reactions were carried out at 80°C for one hour. The conversion and selectivity of reactions with ligand to catalyst ratio of 5 and 10 are similar with quantitative conversion of the *p*-methylstyrene and selectivity of about 85%. At a ligand to catalyst ratio of 2, the conversion decreases to about 90% and the selectivity is about 83%. Overall, the higher ligand to catalyst ratio does not negatively impact the reaction and the data are in agreement with published literature using Rh-TPP catalysts [101, 102], where the reaction rate is maximal for a ligand:catalyst ratio of six or greater, though this may not be the case for all ligands. For example, in hydroformylations with phosphites as ligands, the selectivity of the reaction is a strong function of the ligand to catalyst ratio. In the case of phosphites, it is speculated that highly phosphorylated complexes are formed which causes the isomerisation of  $\alpha$ -olefins [102].

Table 2.7: Effect of TPPMS:Rh on the conversion and selectivity of *p*-methylstyrene hydroformylation in ACN:H<sub>2</sub>O (70 vol% ACN).

Ligand:Catalyst Ratio	Conversion (%)	Branched Aldehyde Yield (%)
2	90.4 ± 2.8	87.3 ± 0.5
5	99.4 ± 0.1	85.4 ± 1.1
10	100 ± 0.0	83.4 ± 3.2

#### 2.3.4.2: CO<sub>2</sub>-induced Heterogeneous Separations for Hydroformylation of *p*-methylstyrene

The efficiency of product separation and catalyst recovery is evaluated by measuring the concentrations of these substrates in the organic-rich phase and the aqueous-rich phase. The ratio of the branched product concentration in the organic phase to that in the aqueous phase (partition coefficient) is shown in Figure 2.16 for Diox/H<sub>2</sub>O and ACN/H<sub>2</sub>O OATS at 20°C. The partition coefficient of *p*-(2-toly)-propanal in ACN/H<sub>2</sub>O OATS increases exponentially as CO<sub>2</sub> pressure increases and more than 99% of the desired product is separated in the organic phase at 2.5 MPa of CO<sub>2</sub>. The partition coefficient in Diox/H<sub>2</sub>O shows a similar trend but more CO<sub>2</sub> pressure (about twice) is required to achieve comparable efficiency to that of ACN/H<sub>2</sub>O system. At 4 MPa of CO<sub>2</sub>, 99% of the branched product is separated in the dioxane rich-phase. The difference in separation efficiency between ACN/H<sub>2</sub>O and Diox/H<sub>2</sub>O OATS can be explained by examining the molecular interactions between H<sub>2</sub>O with dioxane and H<sub>2</sub>O with ACN. Goats *et al.* [91] investigated interactions between dioxane and water and reported the possibility of H-bonded complexes ranging from 1C<sub>4</sub>H<sub>8</sub>O<sub>2</sub>:3H<sub>2</sub>O to 2C<sub>4</sub>H<sub>8</sub>O<sub>2</sub>:1H<sub>2</sub>O in dioxane mole fraction range of 0.25-0.60 (the Diox/H<sub>2</sub>O OATS system has a dioxane

mole fraction of 0.33). The favorable interactions between dioxane and water can explain the need for greater amounts of CO<sub>2</sub> to achieve efficient phase separation. In ACN/H<sub>2</sub>O binary mixture and in the range of water mole fraction of 0.2-0.7 (the ACN/H<sub>2</sub>O OATS system has a water mole fraction of 0.55), water-water interactions are dominant [103] and separation of acetonitrile from water with CO<sub>2</sub> is achieved with relatively low pressures.

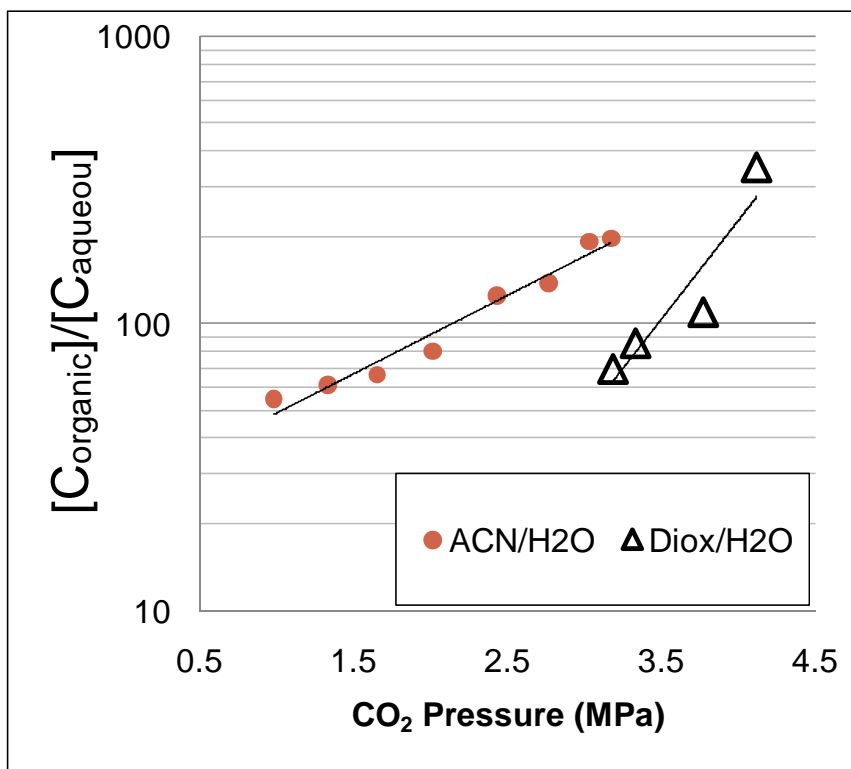


Figure 2.16: Differences in OATS on the separation of 2-(p-tolyl)-propanal in the organic Phase as a function of CO<sub>2</sub> pressure.

The temperature for phase separation is one of the variables that we studied in ACN/H<sub>2</sub>O systems. Increasing the temperature could result in improved separation due to reduction of hydrogen bonding of the water with the acetonitrile and the products. However, the increase in temperature also results in solubility enhancement of the products in the water phase. Overall, these competing effects must be balanced. For example, lower partitioning was obtained at 40°C than at 20°C, as shown in Figure 2.17.

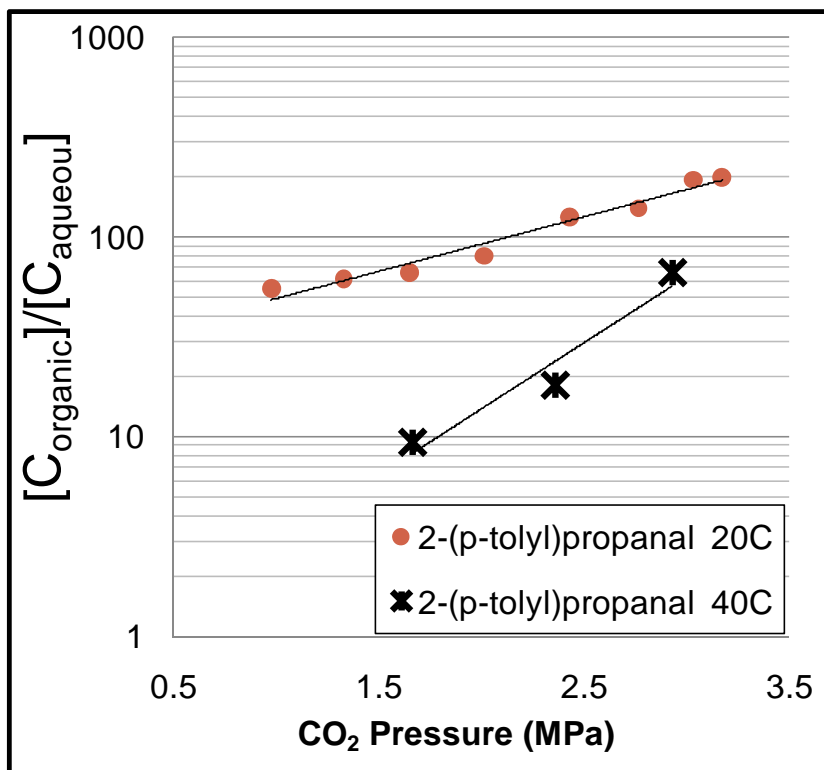


Figure 2.17: Effect of temperature on the separation of 2-(p-tolyl)-propanal in the organic-rich phase in ACN/H<sub>2</sub>O OATS.

The separation of the starting material was also measured and compared to that of the branched product in Figure 2.18; the separation of both compounds increases exponentially as CO<sub>2</sub> pressure is increased. The partition coefficient of *p*-methylstyrene is larger than the partition coefficient of 2-(*p*-tolyl)-propanal. For example, at 1.5 MPa of CO<sub>2</sub> *p*-methylstyrene has a partition coefficient of about 100 while the branched product has a partition coefficient of about 65. This was anticipated as the more hydrophobic nature of *p*-methylstyrene results in lower water solubility than the aldehyde product. The carbonyl oxygen in the product may result in hydrogen-bonding with the water to make this compound more water soluble than the styrene molecule. These partitioning results are in agreement with reported partitioning results for 1-octene and 1-nonanal in THF/H<sub>2</sub>O OATS [45]. In a commercial process, we would recommend taking the reaction to completion and avoiding carryover of the starting material.

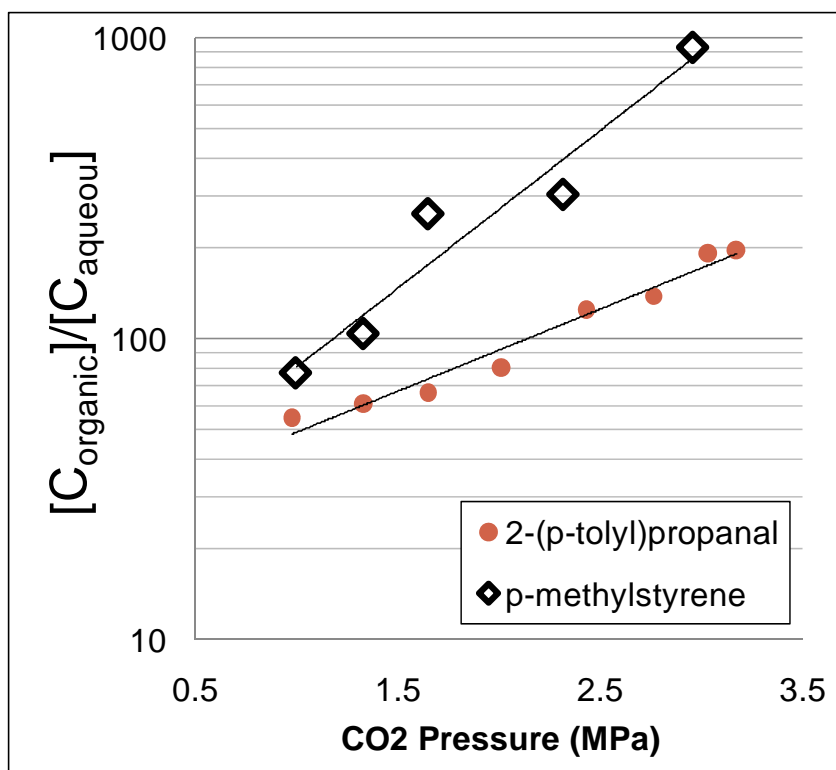


Figure 2.18: Separation of branched product (2-(*p*-tolyl)-propanal) and *p*-methylstyrene in ACN/H<sub>2</sub>O OATS as a function of CO<sub>2</sub> pressure.

The separation efficiency of TPPMS in the aqueous phase is represented in Figure 2.19. We measured the concentration of the TPPMS in both the aqueous-rich and the acetonitrile-rich phases. The partitioning of TPPMS in the aqueous phase increases exponentially with CO<sub>2</sub> pressure. At 4 MPa of CO<sub>2</sub>, 99.9% of the TPPMS is in the aqueous phase and the concentration of TPPMS in acetonitrile phase is below 1 ppm at 3.5 MPa of CO<sub>2</sub>. At the same pressure, the calculated amount of the maximum possible rhodium leaching is around 100 ppb (rhodium leaching is calculated by assuming that

one rhodium atom coordinates with three molecules of TPPMS—we use excess TPPMS in these reactions). The measured quantity of TPPMS retention and calculated Rh leaching are similar in magnitude to those reported by Hallett *et al.* in THF/H<sub>2</sub>O OATS [45]. Also, the catalyst leaching is similar or better than heterogeneously reported systems using Y-zeolites (Rh leaching <0.01%) [98], hydrotalcites (Rh leaching ~ 1.5%) [99]. Also, compared to schemes that utilize temperature as a phase separation switch (thermomorphic, Rh leaching > 2.8%) [104], CO<sub>2</sub>-OATS provides a significant reduction in the amount of rhodium leaching.

The recycling of the Rh-TPPMS catalyst for five consecutive hydroformylations was carried out in ACN/H<sub>2</sub>O OATS and the results are summarized in Figure 2.20. After carrying out the reaction for 1 hour at 60°C, 3.1 MPa of CO<sub>2</sub> (same as reaction pressure) was used to cause phase separation and 85% of the organic-rich layer was decanted under pressure. Fresh starting material and acetonitrile were added to start the next reaction. The average conversion of the five recycle experiments is 47.6±3.0% and the selectivity is 95.9±0.5%. The recycle experiments reflect constant catalytic activity with an average turnover frequency of 193.2±12.3 h<sup>-1</sup> per reaction.

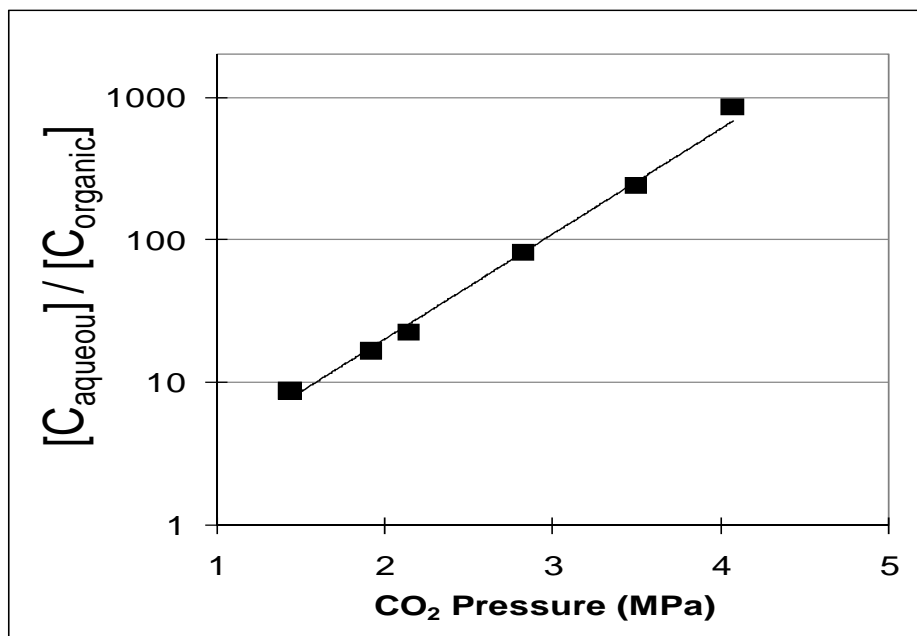


Figure 2.19: Retention of the ligand TPPMS in the aqueous phase in ACN/H<sub>2</sub>O OATS as a function of CO<sub>2</sub> pressure.

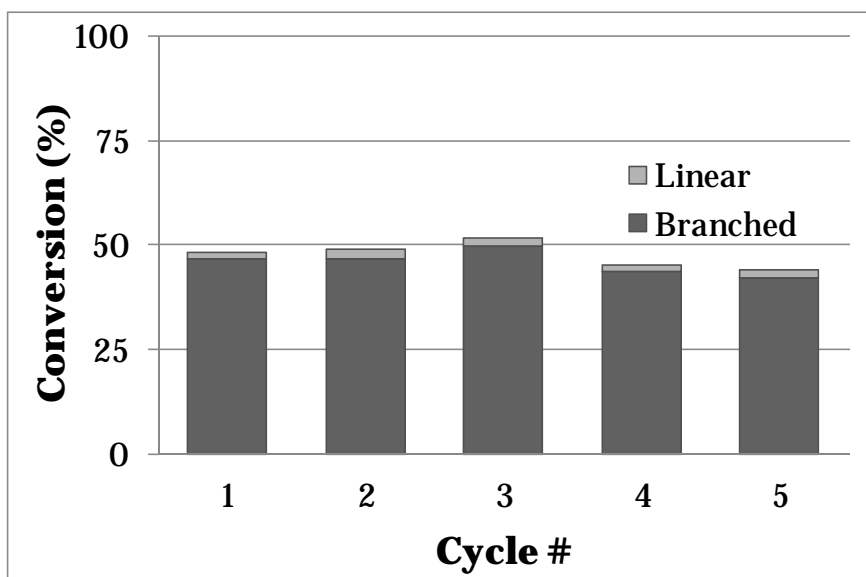


Figure 2.20: Hydroformylation catalyst recycles in ACN/H<sub>2</sub>O OATS with 3.1 MPa of CO<sub>2</sub>.

## 2.4: Conclusions

We have developed and used tunable solvents to couple homogeneous reactions with heterogeneous separations. We report the use of propane to induce phase separation of homogeneous THF/H<sub>2</sub>O and acetone/H<sub>2</sub>O at relatively low pressures of about 1 MPa. Also, we extend the use of organic-aqueous tunable solvents to a pharmaceutically relevant reactions—the hydroformylation of *p*-methylstyrene. The homogeneous reactions provide fast reactions with excellent yields. At 60°C, the reaction reaches completion after 180 minutes with 95% branched aldehyde yield. The CO<sub>2</sub>-induced heterogeneous separation of the product from the catalyst provides an efficient and simple way to remove 99% of the product, to retain 99.9% of catalyst, and to recycle the Rh-TPPMS catalyst for five consecutive reactions.

## **CHAPTER 3: REVERSIBLE CAPPING AGENTS FOR THE SYNTHESIS AND DEPOSITION OF GOLD NANOPARTICLES**

### **3.1: Background**

In this chapter, we discuss the use of amine-based liquids as reversible capping agent for nanoparticles synthesis. Capping agents are employed in the preparation of metallic nanoparticles to avoid particles aggregation and control their size and shape [105-110]. When these metallic particles are used as catalysts, the major challenge is to obtain particles that are clean and free from capping agent. One possible method of removing excess capping agent consists of introducing a large excess of a solvent in the colloidal suspension, such as acetone or methanol, which provokes the extraction of the capping agent and the flocculation of the nanoparticles. Then, the precipitated nanoparticles are separated and re-dispersed in a selected solvent [111-115]. However, capping agents still remain adsorbed on the nanoparticles, depending on the affinity between the metal and the functional group of the capping agent [112, 113]. Therefore, capping agents could still compete with reactants and products for the adsorption sites or hamper their accessibility and which may result in altering the catalytic activity of these particles. As an example, the activity of nano-gold catalysts is affected detrimentally when strong covalent binding capping agents, such as thiol or phosphine complexes are present, in minute amounts [116, 117].

We develop alternative methods to prepare nanoparticles. Recently, our group in collaboration with the Roberts Group at Auburn University reported the capping-agent

free synthesis of monodisperse palladium (Pd) nanoparticles in dimethylsulfoxide (DMSO) ( $3.5\pm 0.49$  nm) [118]. The synthesized Pd nanoparticles were shown to be stable in DMSO for long periods of time (more than 9 months). Infrared spectroscopy revealed that interactions of both the sulfur and the oxygen in DMSO with the Pd and hence, DMSO is acting as a solvent and a stabilizing/capping agent. The separation of the Pd particles was achieved by freeze-drying to remove DMSO; the separated particles can be redispersed in DMSO without aggregating. This method provides an environmental and efficient way to prepare and separate Pd particles.

In this research, we develop systems that utilize microemulsions for gold nanoparticles synthesis. Microemulsions are described as homogeneous-like combinations of water, oils and/or surfactants. Reverse micelles, a class of microemulsions, is an interesting method for the preparation of metal nanoparticles. This method allows the impregnation of solid supports such as porous silica by first wetting the solid support with solvents containing metal particles and then removing the solvent via evaporation. Metal nanoparticles obtained with reverse micelles have a controllable and narrow size distribution, which is attributed to the confined space of the micellar structures and the limited amount of metal salt in the micelles [119, 120]. The methods of solvent removal and particle deposition are limited when it comes to nanoparticles synthesis in microemulsions [121]. Generally, the solvent is removed by evaporation, which is energy-intensive for systems using oils with elevated boiling temperatures. Moreover, Sarkar *et al.* [122] reported the use of ultracentrifugations (31,250 rpm) to separate silver nanoparticles from reverse micelles of water and AOT (sodium bis (2-ethyl hexyl)sulfosuccinate) in heptane. The separated particles showed a polydisperse

size distribution in the range of 5nm to >30 nm with an average of 18.7 nm; only 36% of the separated silver particles are in the 15-20 nm size range.

There are various possible combinations of components to form micelles or reverse micelles in a variety of solvents but the ones we are interested in are those utilizing ionic liquids. Liu *et al.* [123] reported the use of reverse micelles consisting of room temperature ionic liquids (ILs) cores in compressed CO<sub>2</sub> for the synthesis of gold nanoparticles (referred to as NPs from here after). The three ionic liquids examined consisted of 1,1,3,3-tetramethylguanidinium cation and acetate, lactate, or trifluoroacetate anions as shown in Figure 3.1. The reverse micelles were formed by the hydrogen bonding of a sulfonated surfactant—*N*-ethyl perfluorooctylsulfonamide (C<sub>2</sub>H<sub>5</sub>NHSO<sub>2</sub>C<sub>8</sub>F<sub>17</sub>, *N*-EtFOSA)—which has good solubility in liquid CO<sub>2</sub> due to fluorine substitution, with the ILs described above. It was proposed that the protonated guanidinium cation of the ionic liquid was able to participate in hydrogen bonding with the polar head of the sulfonamide surfactant, thus stabilizing the micellar structure. These microemulsions are stable in compressed CO<sub>2</sub> at pressures between 6 – 30 MPa depending on the molar ratio ( $w$ ) of IL to surfactant. For example at 25°C, the system pressure to suspend the micelles is about 6 MPa of CO<sub>2</sub> with  $w=0.15$  and 20 MPa of CO<sub>2</sub> with  $w=0.8$ . The greater amount of IL requires a denser solvent, i.e. higher pressure of CO<sub>2</sub>. The IL-microemulsions were shown to solubilize salts such as chloroauric acid (HAuCl<sub>4</sub>). Furthermore, the reduction of HAuCl<sub>4</sub> to form gold nanoparticles was achieved via rapid expansion of the compressed system into a solution of sodium borohydride in ethanol. Semi-spherical gold nanoparticles were successfully synthesized—Figure 3.2—when the weight ratio of gold salt to ionic liquid ( $W_{\text{HAuCl}_4}/W_{\text{IL}}$ ,

ionic liquid 1,1,3,3-tetramethylguanidinium trifluoroacetate (TMGT)) was 0.01 and Au networks were formed at higher concentrations of gold as shown in Figure 3.3. This work is interesting but there are two limitations to this procedure. First, the reduction step was not controlled and requires the use of additional solvent—ethanol in this case, which requires further processing to purify the nanoparticles. An alternative reduction could be achieved using hydrogen gas but introducing hydrogen at 10 MPa may not be a trivial task. Second, the use of high pressures may impose difficulty in employing this technique.

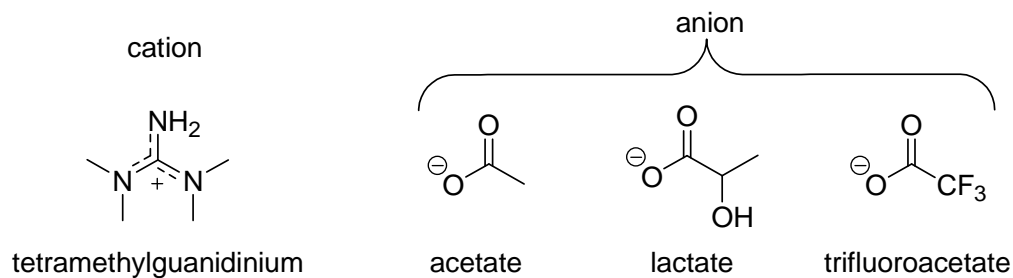


Figure 3.1: Room temperature ionic liquids that form microemulsions with *N*-EtFOSA surfactant in compressed CO<sub>2</sub>.

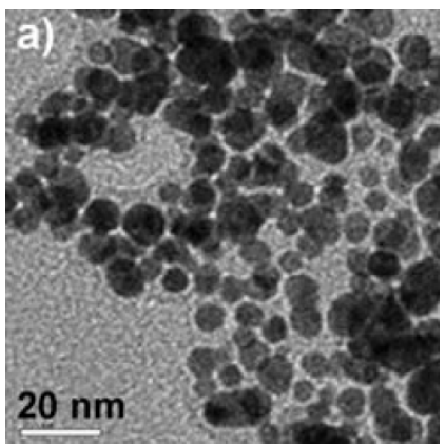


Figure 3.2: TEM Image of gold nanoparticles synthesized with *N*-EtFOSA (0.06 g/ml) and TMGT ( $w = 0.41$ ) in compressed  $\text{CO}_2$  (35°C, 20MPa) with  $W_{\text{HAuCl}_4}/W_{\text{IL}}=0.01$

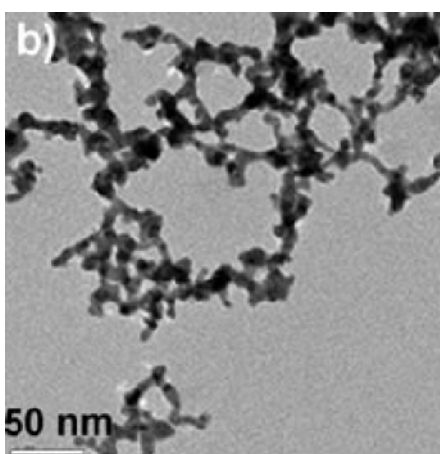


Figure 3.3: TEM Image of gold nanoparticles synthesized with *N*-EtFOSA (0.06 g/ml) and TMGT ( $w = 0.41$ ) in compressed  $\text{CO}_2$  (35°C, 20MPa) with  $W_{\text{HAuCl}_4}/W_{\text{IL}}=0.04$

In our research, we develop systems that use reversible ionic liquids (RevILs) for simple and environmentally benign synthesis of metal nanoparticles. We demonstrate that the microemulsions consisting of RevILs are formed in organic solvents and the RevIL microemulsions can be switched-on to solubilize polar salts and act as a template for NPs synthesis and then switched-off to deposit the NPs.

RevILs are formed by the reversible reaction of compounds with basic nitrogen functionalities (molecular liquid) with CO<sub>2</sub> at ambient pressure to form a liquid salt (ionic liquid). The process results in a step change in properties such as polarity or viscosity. RevILs exhibit negligible vapor pressures and their physical properties are tuned by modifying the structure of the molecular liquid precursor. There are two major classes of reversible ionic liquids (RevILs): two-component and one-component. Two-component RevILs are based on an equimolar reaction of a neutral alcohol and a neutral molecule containing at least one basic nitrogen functionality with CO<sub>2</sub>. One-component systems employ solely a neutral molecule containing at least one basic nitrogen functionality.

Our group, in collaboration with the Jessop group at Queens University, reported the first reversible ionic liquid [63]; an equimolar mixture of liquid 1,8-diazabicyclo[5.4.0]undec-7-ene (DBU) and an alcohol (2-component RevILs) reacts with CO<sub>2</sub> at ambient pressure to form ionic species. The RevIL readily reverses back to the neutral (molecular) liquid by bubbling N<sub>2</sub> or argon and/or applying heat. Other examples of such systems include N,N,N',N'-tetramethyl-N''-butylguanidine and alcohols [64] as shown in Figure 3.4. The RevILs that require the use of alcohols are known as two-component systems. Other systems that eliminate the need of an alcohol, hence named “one-component” systems, were reported shortly after. These systems utilized solely silylated amines like trialkoxy- or trialkyl- silylpropylamines as molecular liquid. Upon reaction with CO<sub>2</sub>, the amine precursors form ionic liquids composed of the corresponding carbamate anion and ammonium cation pairs as shown in Figure 3.5 [10, 62].

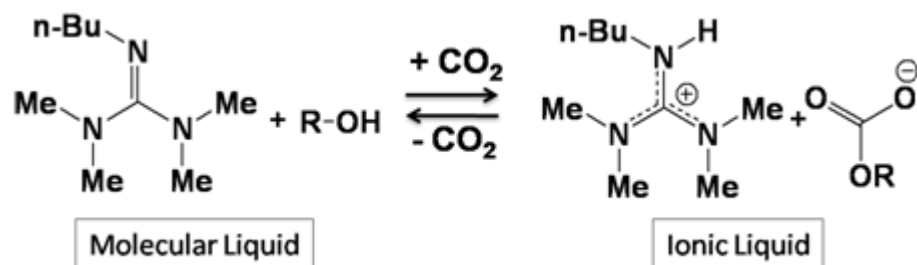
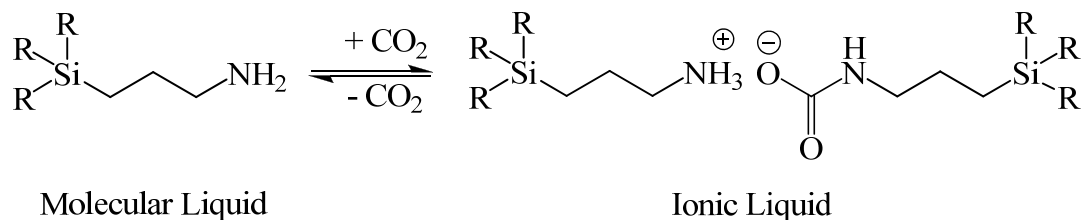


Figure 3.4: 2-component reversible ionic liquids formed by a switch from a molecular liquid mixture of N,N,N',N'-tetramethyl-N''-butylguanidine (TMBG) and alcohol (ROH) to the ionic liquid [TMBGH]<sup>+</sup>[O<sub>2</sub>COR]<sup>-</sup> upon addition of CO<sub>2</sub>. R= C<sub>1</sub> to C<sub>12</sub>.



where R = OMe, OEt, Et, Pr, Hex, etc.

Figure 3.5: 1-component reversible ionic liquids formed by a switch from a molecular liquid trialkoxysilylpropylamine to its corresponding ionic liquid upon addition of CO<sub>2</sub>

## 3.2: Materials and Experimental Methods

### 3.2.1: Materials.

Choloauric acid (Sigma Aldrich, 99.99%) and anhydrous methanol were used as received and kept in the glove box. Hexane (Sigma Aldrich, 95%), heptane (Sigma Aldrich, 99%), dodecane (Sigma Aldrich, 98%), 1-dodecanethiol (Sigma Aldrich, 98%), 1-

octanesulfonyl chloride (Sigma Aldrich, 97%), 1,2-dichloroethane (Sigma Aldrich, 99.8%), propylamine (Sigma Aldrich, 99%) were used as received. Hydrazine (Sigma Aldrich, 98%) was used as received and kept in the refrigerator. Precursor molecules for RevIL were prepared as discussed in literature [10, 124]. TEM grids (Ted Pella) were used as received.

### 3.2.2: Experimental Methods

#### 3.2.2.1: Synthesis of Surfactant

The desired surfactant, *N*-propyl-octylsulfonamide, is not commercially available and was synthesized via analogy with published reactions [125, 126] according to the method shown in Figure 3.6 **Error! Reference source not found.** A 1.7 M solution of 1-octanesulfonyl chloride in 1,2-dichloroethane was added drop wise to an equimolar amount of propylamine in 1,2-dichloroethane at 0°C under argon. The solution was allowed to warm to room temperature and stirred for 24 hours. The product salt was washed with a solution of saturated sodium carbonate and dried with magnesium sulfate; the yield was 79% and characterized using <sup>13</sup>C and <sup>1</sup>H NMR and elemental analysis.

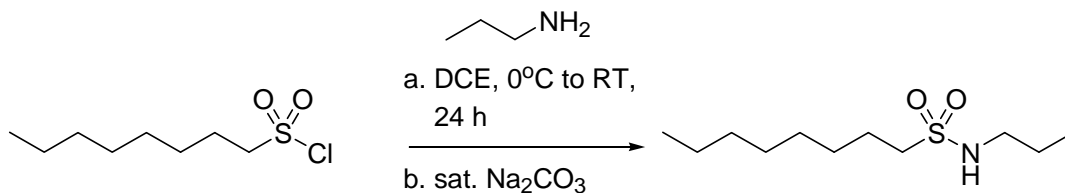


Figure 3.6: Synthesis of surfactant molecule *N*-propyl octylsulfonamide.

#### 3.2.2.4: Gold nanoparticles synthesis

In the experiments with 2-component RevIL, one gram of  $[\text{TMBGH}]^+[\text{O}_2\text{COCH}_3]^-$  was prepared by weighing 0.7975 gram of 2-butyl-1,1,3,3-tetramethylguanidin and 0.161 gram of anhydrous methanol and then bubbling  $\text{CO}_2$  at atmospheric pressure for 15-30 minutes. A stock solution of gold was then prepared by adding 0.084 g of chloroauric acid in 1 ml anhydrous methanol (weight ratio of gold salt/Rev-IL = 0.01); 0.16 g of the gold/methanol solution was then added to the RevIL and the mixture is sparged with  $\text{CO}_2$  for mixing and evaporating the excess methanol. The surfactant, *N*-propyl octylsulfonamide, was then added to the organic solvent (dodecane, heptane, or hexane as specified in results sections) and 0.05 g of RevIL/gold mixture is added. The reducing agent hydrazine was dissolved in 10 ml tetrahydrofuran (5  $\mu\text{L}$  of this solution is 1 equivalent to gold) and 10  $\mu\text{L}$  of this solution is added to the organic/RevIL/gold salt mixture to reduce the  $\text{HAuCl}_4$  to  $\text{Au}^0$  nanoparticles. A sample was withdrawn and 3-5 drops were deposited on a TEM grid. To recycle the solvent system, the solution was heated to  $60^\circ\text{C}$  to reverse the RevIL and the mixture is centrifuged to deposit the particles. The solvent mixture was then decanted and 0.16 g of MeOH/gold solution is added and the solution was sparged with  $\text{CO}_2$  for 30 minutes to reform the microemulsions. 10  $\mu\text{L}$  THF/ $\text{N}_2\text{H}_4$  were added under stirring (solution color changes to blue). A sample was withdrawn and deposit on TEM grid.

In the experiments with 1-component RevIL, the molecular liquid (TPSA, THSA) was sparged with  $\text{CO}_2$  and  $\text{HAuCl}_4$  was added while continuing to bubble  $\text{CO}_2$  (the specific amount of RevIL and gold vary depending on the experiment as discussed below). A given amount (0.02-0.07 g) of the RevIL/gold mixture was added to 1.8ml of

hexane. The reduction was achieved with hydrazine and samples are deposited on TEM grids.

### 3.3: Results and Discussions

#### 3.3.1: Two-component Reversible Ionic Liquid Systems

##### 3.3.1.1: Micelles Formations and Reversal

The formation and reversal of microemulsions with 2-component RevILs core were demonstrated using ionic dye methyl orange (MO)—Figure 3.7—as a mimic for metallic salts. MO is highly UV active and has a maximum absorption around 400 nm. First, the molecular liquid 2-butyl-1,1,3,3-tetramethylguanidin (TMBG) and methanol (slightly in excess) were mixed and CO<sub>2</sub> was bubbled at low rate (about a bubble per second) for 15 minutes to form the ionic liquid 1,1,3,3-tetramethylbutyl guanidinium methylcarbonate ([TMBGH]<sup>+</sup>[O<sub>2</sub>COCH<sub>3</sub>]<sup>-</sup>) shown in Figure 3.4. Afterwards, we checked the solubility of MO in dodecane alone and the UV absorption band was not detected. Also, the UV absorption was not detected MO/surfactant/dodecane and MO/[TMBGH]<sup>+</sup>[O<sub>2</sub>COCH<sub>3</sub>]<sup>-</sup>/dodecane solutions.

The methyl orange UV absorption band was detected at around 410 nm when [TMBGH]<sup>+</sup>[O<sub>2</sub>COCH<sub>3</sub>]<sup>-</sup>, the N-propyl-octylsulfonamide surfactant, and MO were mixed in dodecane, as shown in Figure 3.8. The molar ratio IL/surfactant was 0.5 while the concentration of the surfactant was 0.03 g/ml. The solution color changes to orange indicating the dispersion of MO; the system was allowed to reach equilibrium for an hour. Reversal of the solution was achieved at 150°C after two hours to revert the ionic liquid and hence, switch-off the reverse micelles. The color disappeared and the UV absorption was consistent with the breakdown of the methyl orange dispersion. The reformation of the micellar structures and recyclability of the solvents was achieved by adding methanol—which was lost during the heating—and bubbling CO<sub>2</sub> for an hour.

The orange color reappeared and the UV spectrum confirmed the reappearance of the methyl orange peak—Figure 3.8. With these experiments, we demonstrate that microemulsions with RevIL core are formed and can be switched-on by bubbling CO<sub>2</sub> and switched-off by heating.

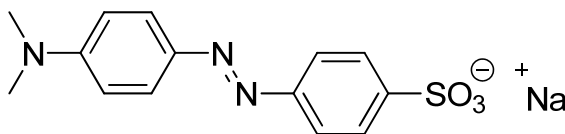


Figure 3.7: Chemical structure of ionic dye methyl orange (4-dimethylaminoazobenzene-4'-sulfonic acid sodium salt).

### 3.3.1.2: Gold Nanoparticles Synthesis

Similar to the experiment discussed above, the system components [TMBGH]<sup>+</sup>[O<sub>2</sub>COCH<sub>3</sub>], *N*-propyl-octylsulfonamide surfactant, and chloroauric acid (HAuCl<sub>4</sub>) were mixed in dodecane. The solution has a clear orange color, which is characteristic of the chloroauric acid. The gold salt was then reduced with hydrazine; the resulting solution has a grey-blue color as shown in Figure 3.9. Samples from the solution were imaged with transmission electron microscopy (TEM)—Figure 3.10—and analyzed for size with ImageJ. In TEM images, the gold particles (NPs) are seen as dark spots while the light grey background is the carbon film. The average size of the NPs formed is 9.5±1.5 nm. It must be noted that only a small number of particles was obtained from the TEM images and therefore, the size may not be representative due to the small sample size. However, we were able to demonstrate that microemulsions with RevIL cores can solubilize the gold salt and can be used to synthesize gold nanoparticles.

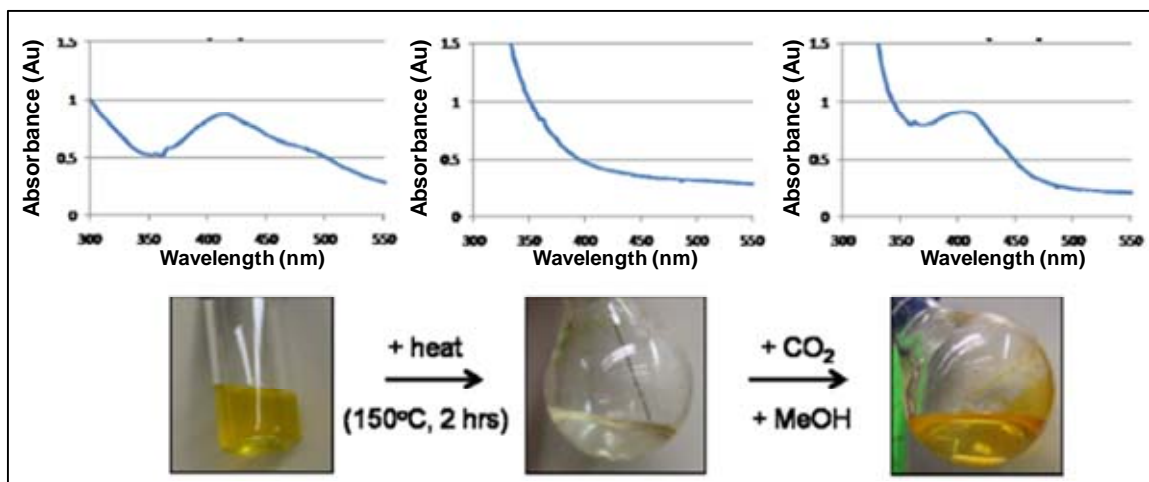


Figure 3.8: UV-Vis experiments demonstrating the formation, reversal, and reformation of micellar structure consisting of  $[\text{TMBGH}]^+[\text{O}_2\text{COCH}_3]^-$ / *N*-propyl-octylsulfonamide/dodecane and polar dye methyl orange.

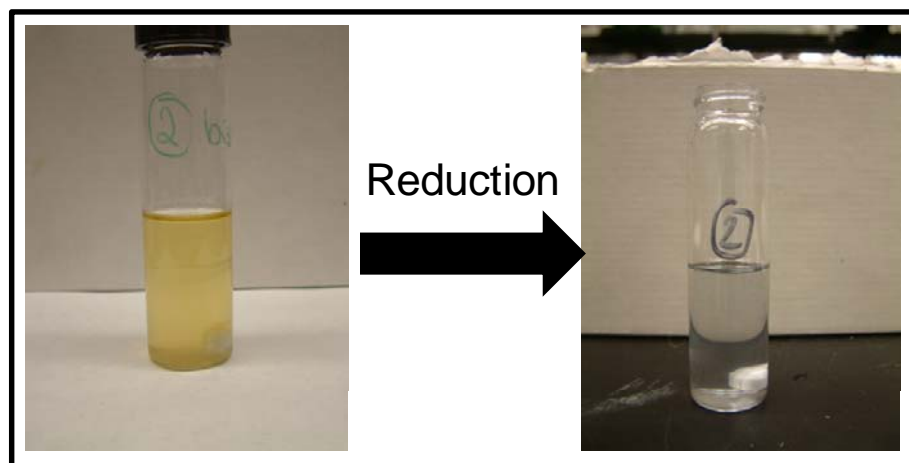


Figure 3.9: Dissolution of chloroauric acid in  $[\text{TMBGH}]^+[\text{O}_2\text{COCH}_3]^-$ / *N*-propyl-octylsulfonamide/dodecane (left) and gold nanoparticles formed after reduction with hydrazine (right).

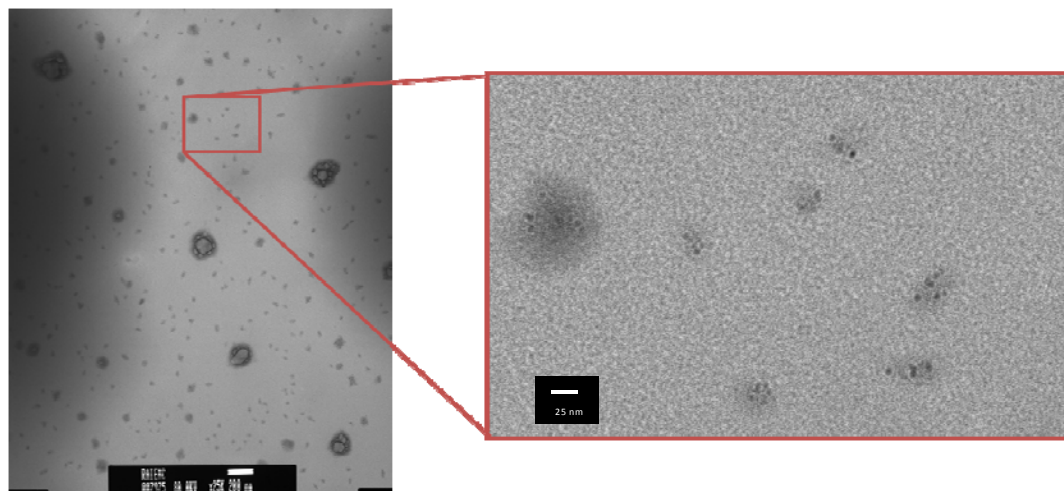


Figure 3.10: TEM image of  $\text{Au}^0$  prepared in  $[\text{TMBGH}]^+[\text{O}_2\text{COCH}_3]^-$ / *N*-propyl-octylsulfon amide/dodecane.

We also studied the effect of organic solvent on this process. We used hexane instead of dodecane and observed that the reversal of the micelles and deposition of the NPs was achieved at  $60^\circ\text{C}$  at 30 minutes, which provides a significant improvement in terms of reversal temperature and duration when compared to the dodecane system discussed above. The RevIL  $[\text{TMBGH}]^+[\text{O}_2\text{COCH}_3]^-$  (0.021 g) and *N*-propyl-octylsulfonamide (0.066 g) were dissolved in hexane (15 ml) and  $\text{HAuCl}_4$  ( $W_{\text{HAuCl}_4}/W_{\text{RevIL}} = 0.123$ ) was added to yield a clear orange solution. The gold salt was reduced to gold particles with hydrazine, and dodecanethiol was added to prevent particle agglomeration during deposition. A representative TEM image of the NPs is shown in Figure 3.11. After depositing a sample, the remaining solution was heated to separate the particles. Then, we recycled the solvent system for a consecutive synthesis of NPs. First,  $\text{CO}_2$  was bubbled through the liquid. The gold salt was added and the solution turned orange. The reduction was carried out using hydrazine and the sample was imaged with TEM and analyzed with

ImageJ. A summary of the particles analyzed in both cycles is shown in Figure 3.12. Both samples show particles in the size range of 6-20 nm with an average particles size of  $11.4 \pm 3.3$  nm for the first cycle and  $12.6 \pm 2.5$  nm for the second cycle. It is beneficial to demonstrate solvent recycle for successive preparation of particles however, it is not essential to recycle the solvent since the amount of RevIL in the system is relatively small ( $\sim 0.002$  g/ml) and it may not be economical or environmental to attempt the recover the RevIL. The important features of  $[\text{TMBGH}]^+[\text{O}_2\text{COCH}_3]^-$  /*N*-propyl-octylsulfonamide/organic that we developed is its ability to form microemulsions and the fact that these micelles solubilize gold salt and are used for the synthesis of gold nanoparticles. The true advantage of this system is the ease of separating the particles and the ability to switch-off the micellar structure by simply heating. The system also offers a number of variables that could be adjusted to gain processing advantages. Some of these variables include the structure of the 2-component RevIL and of the surfactant, the weight ratio of various system components, and the type of organic solvent employed.

It is important to discuss the limitations and challenges to the use of 2-component RevIL/surfactant solvent systems, which we overcame by using 1-component RevILs as discussed in the next section. First, it is challenging to maintain stoichiometric amounts of the molecular liquid and the alcohol, especially after the reversal step where the alcohol is lost. Second, there is a solubility limit of the RevIL in hexane. The microemulsions become unstable, i.e. the system becomes heterogeneous, if the amount of  $[\text{TMBGH}]^+[\text{O}_2\text{COCH}_3]^-$  in hexane exceeds 0.01 g/ml in the presence of 0.006 g/ml surfactant. By using 1-component RevILs, we were able to overcome these limitations.

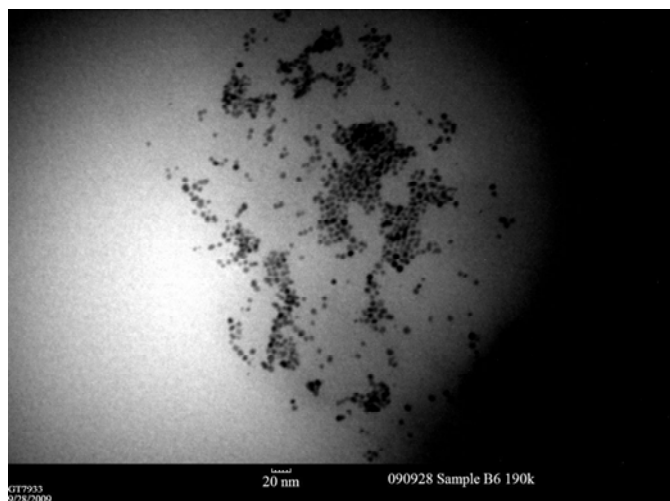


Figure 3.11: TEM image of Au<sup>0</sup> prepared in [TMBGH]<sup>+</sup>[O<sub>2</sub>COCH<sub>3</sub>]<sup>-</sup>/ *N*-propyl-octylsulfon amide/hexane.

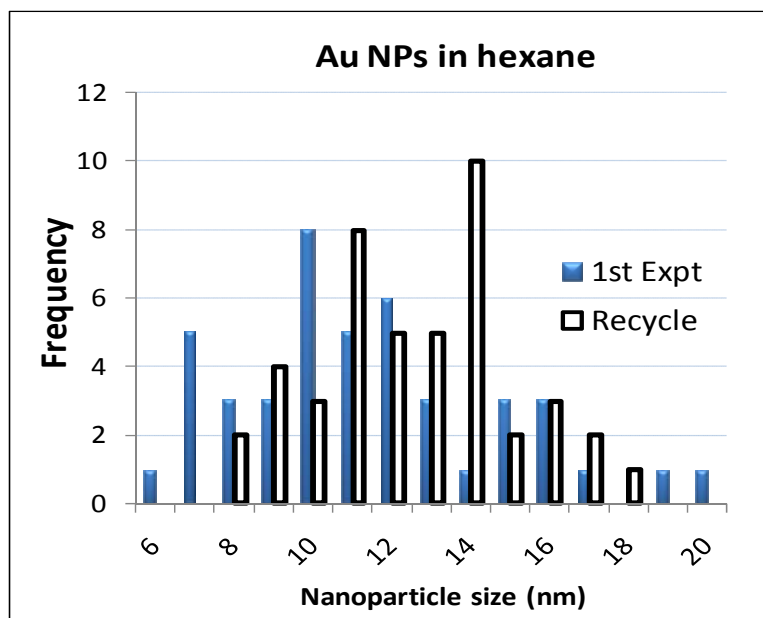


Figure 3.12: Size distribution of Au<sup>0</sup> particle prepared in fresh and recycled [TMBGH]<sup>+</sup>[O<sub>2</sub>COCH<sub>3</sub>]<sup>-</sup> / *N*-propyl-octylsulfon amide/hexane solvent system.

### 3.3.2: One-component Reversible Ionic Liquid Systems

The use of 1-component RevILs to form microemulsions is simpler than the microemulsion system using the 2-component RevIL. The 1-component RevILs form microemulsions in hexane without the need for a surfactant or an alcohol; the trialkylsilyl amine reacts with CO<sub>2</sub> to form the ionic species—Figure 3.5—which forms microemulsions in nonpolar organics.

#### 3.3.2.1: Micelles Formations and Reversal

The formation and reversal of microemulsions with 1-component RevILs microemulsions in hexane was demonstrated using ionic dye methyl orange (MO). First, the molecular liquid (3-aminopropyl)-tripropylsilane (TPSA) was sparged with CO<sub>2</sub> for 30 minutes to form the ionic liquid with the ammonium carbamate (TPSAC) polar species—shown in Figure 3.5. Afterwards, 3-5 mg of MO and 0.1 g of TPSAC were mixed in hexane. We checked the UV-Vis spectra for hexane/TPSA, hexane/TPSAC, and hexane/MO and the UV absorption band around 400 nm was not detected. The methyl orange UV absorption band was detected at 400 nm when TPSAC/MO/hexane were mixed; the solution had a clear orange color as reflected in Figure 3.13. The switching-off of the microemulsions was achieved by heating the solution to 69°C (boiling point of hexane) and stirring for 5-10 minutes; the disappearance of the absorption band around 400 nm was consistent with the reversal of micellar structures as shown in Figure 3.14. Switching on the microemulsions and resuspension of the MO was achieved by adding hexane to a total solution volume of 10 ml and bubbling CO<sub>2</sub> for 30 minutes; no make-up MO or TPSAC were added. The orange color reappeared and the UV spectrum confirmed the reappearance of the methyl orange peak. We carried out similar experiments with 1-

component RevIL (3-aminopropyl)-triethylsilane (TEtSA) and (3-aminopropyl)-trihexylsilane (THSA) and the results were similar. With these experiments, we were able to demonstrate the formation, reversal, and reformation of microemulsions consisting of 1-component RevIL only—without the need for a surfactant. The micellar structures are able to solubilize the polar dye methyl orange in hexane.

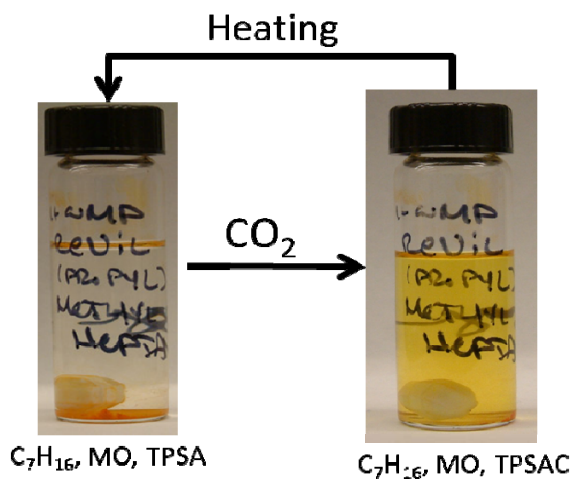


Figure 3.13: Formation, reversal, and reformation of micellar structure consisting of TPSAC RevIL indicated by color change due to dissolution of methyl orange.

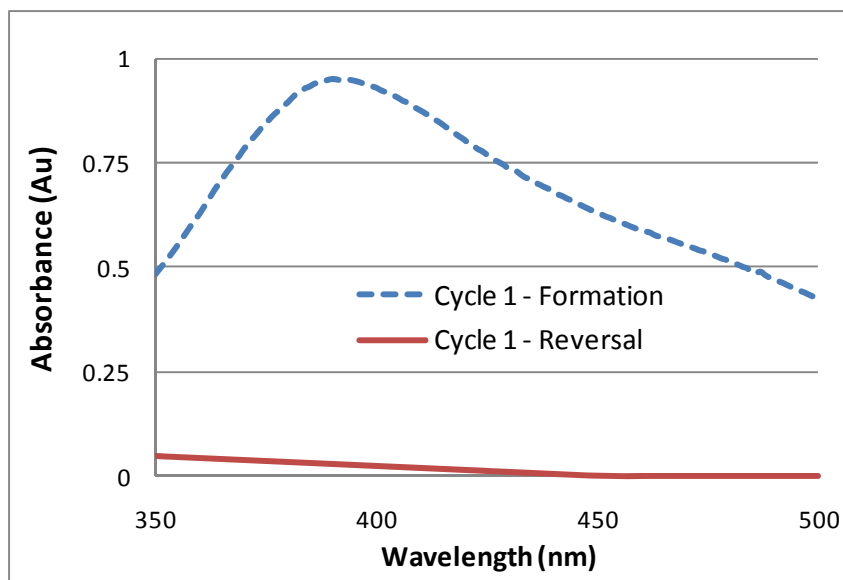


Figure 3.14: UV-Vis spectra demonstrating the formation, reversal, and reformation of micellar structure consisting of TPSAC in hexane as evident by methyl orange absorption peak around 400 nm.

### 3.3.2.2: Gold Nanoparticles Synthesis

The synthesis of gold nanoparticles was carried out in 1-component RevIL solvent systems. The chloroauric acid (0.038g) was mixed with THSA (0.7g) and CO<sub>2</sub> was bubbled in the mixture for 30-60 minutes; sparging CO<sub>2</sub> forms the ionic species and serves for mixing as well. A sample of 0.07 g was then transferred into 1.8 ml of hexane and a few drops of a hydrazine stock solution (0.1 ml hydrazine in 100 ml acetonitrile) were added to form gold particles. The solution color changes from light-orange to violet-blue indicating the reduction of the gold salt to the gold metal particles. Samples from the solution were imaged with transmission electron microscopy (TEM)—Figure 3.15; in The TEM images NPs are seen in dark color and the carbon film is the light grey background. With these concentrations, the particles are forming networks and

agglomerating with or without the use of dodecanethiol capping agent. This observation is in agreement with the work reported by Liu *et al.* (Figure 3.3) [123]. Based on the findings from Liu's work, we reduced the amount of H<sub>AuCl</sub><sub>4</sub>. Experiments with 0.005g chloroauric acid in 0.7g TPSA were carried out. A sample of 0.025g of H<sub>AuCl</sub><sub>4</sub>/TPSAC was then added to 1.8 ml hexane followed by reduction with hydrazine. A TEM image of the sample is shown in Figure 3.16; the particles show minimal agglomeration without the use of a capping agent. The imaged particles are semi-spherical with an average size of about 20 nm. Further optimization of these systems is underway by students in our group.

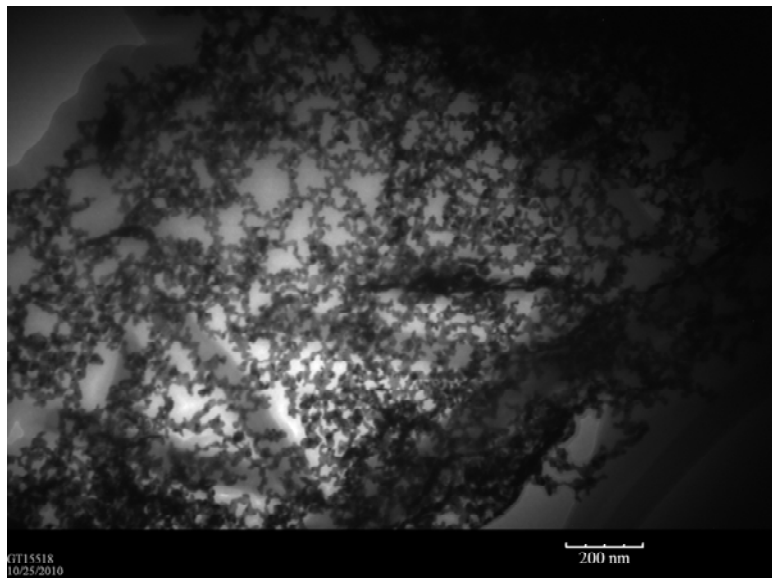


Figure 3.15: TEM Image of gold nanoparticles synthesized with THSAC in hexane (0.035 g/ml) with  $W_{\text{HAuCl}_4}/W_{\text{IL}}=0.054$ .

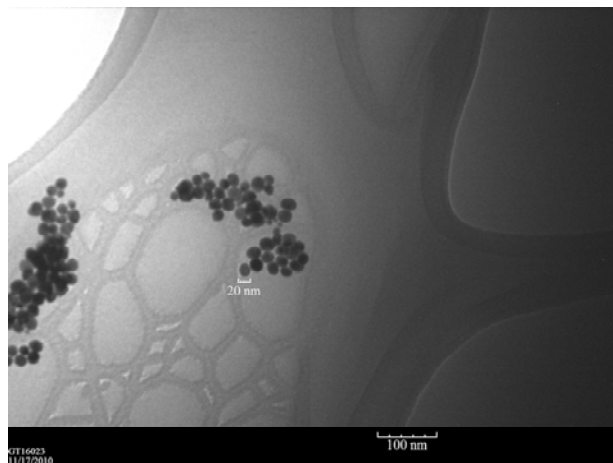


Figure 3.16: TEM Image of gold nanoparticles synthesized with TPSAC in hexane (0.012 g/ml) with  $W_{\text{HAuCl}_4}/W_{\text{IL}}=0.007$ .

### 3.4: Conclusions

In this research, we demonstrated that reversible ionic liquids form microemulsions that can be switched-on by bubbling  $\text{CO}_2$  and switched-off by heating. These microemulsions solubilize ionic compounds such as methyl orange and chloroauric acid. We utilized these microemulsions as a template for controlled synthesis of gold nanoparticles as well as simple and environmental separation and deposition of these particles. With 2-component RevIL,  $[\text{TMBGH}]^+[\text{O}_2\text{COCH}_3]^-/N$ -propyloctylsulfonamide/hexane were used to form particles in the size range of 6-20 nm with an average particles size of  $11.4 \pm 3.3$ . With 1-component RevIL, (3-aminopropyl)-tripropylsilane was used to prepare semi-spherical gold particles with an average size of about 20nm. The 1-component RevILs systems provide a simpler method to form microemulsions when compared to the 2-component RevILs systems since they eliminate the need for alcohols and surfactants and further work with this project will focus on optimizing these systems to prepare nanoparticles.

## **CHAPTER 4: CATALYST SYNTHESIS AND TESTING FOR A DUAL PURPOSE HYDRAZINE THRUSTER**

### **4.1: Background**

Hydrazine is used as a liquid propellant in military orbital and deep space rockets as well as in commercial satellites. Hydrazine decomposes at high temperatures of up to 800°C over a heterogeneous catalyst bed—mainly iridium metal—to produce hydrogen, nitrogen, and ammonia [127]. This reaction yields a large quantity of high pressure and high velocity gases, which are focused through a nozzle to provide the thrust and lift for the rocket. This type of propulsion—known as chemical propulsion—generates high thrust and is suitable for rapid space shuttle maneuvers [14]. However, this type of propulsion provides low specific impulse of 230-250 seconds (change in momentum per unit weight of propellant) making it less attractive for long term missions.

The other type of propulsion employed in space shuttles is electric propulsion. Electric propulsion uses electricity to increase exhaust velocity [15] and provides high specific impulse with low thrust. Therefore, the amount of propellant necessary is greatly decreased compared to standard chemical propulsion. Electric propulsion is ideal for long term space missions where small course corrections and changes are needed over time. Hydrazine is not suitable for electric propulsion because it fragments into nitrogen and hydrogen ions but only the nitrogen ions can be used for acceleration [128]. On the other hand, ammonia—a product of controlled hydrazine decomposition—has been shown to ionize and can be used for electric propulsion [129]. Combining both electric and

chemical propulsion from a sole propellant is an attractive avenue for satellite technology as it provides high thrust (for take-off) with flexible and precise maneuvering (for trajectory adjustment). This directly translates into significant cost gain by increasing a satellite's lifetime while requiring only minor changes in its overall weight and existing components.

The objective of this multidisciplinary project is to design and test catalysts in a continuous flow reactor for the controlled decomposition of hydrazine to maximize the yield of ammonia. The outcome of this research allows the use of chemical propulsion fuel—hydrazine—to be utilized for electric propulsion as well. Ammonia is ionized by passing through helicon plasma generator that employs radio frequency waves to deposit energy into the gas. The energized electrons break free from the atom and can be accelerated with electrostatic gradients [130, 131]. By selectively controlling the decomposition of hydrazine to produce ammonia, the electric propulsion unit can be added to the space shuttle.

Controlling the decomposition of hydrazine is a key challenge in developing a dual propulsion system that uses hydrazine as the sole propellant for electric and chemical propulsion. There are three major pathways in which hydrazine can decompose, as shown in Figure 4.1. Hydrazine exothermically decomposes into ammonia and nitrogen (Pathway 1) or into nitrogen and hydrogen (Pathway 2). However, at elevated temperatures the reaction mainly produces nitrogen and hydrogen (Pathway 3). The catalysts being developed in this work are designed to provide an optimal balance between efficiency and chemoselectivity to yield primarily ammonia and that the

exothermicity of the reaction should be limited to minimize the occurrence of the undesired pathways (Pathways 2 and 3) [132].



Figure 4.1: Decomposition pathways of hydrazine.

The yield of hydrazine decomposition products depends on the metal catalyst and the temperature of the reaction [133]. As a decomposition mechanism, the literature suggests no scrambling of nitrogen atoms as shown in Figure 4.2. By this mechanism, hydrazine adsorbs to the catalyst surface by hydrogen abstraction to form an adsorbed  $\text{N}_2\text{H}_2$  molecule (Step 1, Figure 4.2). This reacts by a concerted mechanism with a second hydrazine molecule in the vapor phase to form ammonia and nitrogen (Step 2, Figure 4.2).

Hydrazine decomposition has been studied over metal thin films [134, 135], hot wires [136, 137], metal foils [138-140], on a single metal crystal [141-143], and over metal powders and supported catalysts [144-148]. The behavior of these metal catalysts is defined in terms of their activity, which is the ability to convert hydrazine to products, and selectivity for the formation of ammonia. For the current research, a catalyst with high activity and selectivity is desired. Maurel *et al.* [148] evaluated the activity and selectivity of iridium, rhodium, nickel, platinum, cobalt, ruthenium, palladium, silver and

copper granules supported on alumina at temperatures <180°C. In his work, it was found that these metals decrease in activity in the following order:

$$\text{Ir} > \text{Rh} > \text{Ni} \sim \text{Pt} \sim \text{Co} \sim \text{Ru} > \text{Pd} \sim \text{Ag} \sim \text{Cu}$$

However, in terms of selectivity, a different order is was observed as shown below.

$$\text{Ag} > \text{Co} > \text{Cu} > \text{Ru} \sim \text{Ir} > \text{Ni} > \text{Rh} > \text{Pt} > \text{Pd}$$

From this information, it was decided to focus on Co, Cu, Ni, Ir, Rh, and Ru as they appear to have the best potential in terms of activity and selectivity. In this research, we investigate the use of metal nanoparticles supported on silica. Metal nanoparticles possess unique properties (such as enhanced catalytic activity and chemoselectivity) often different from the bulk metals, due to high surface to mass ratio [149]. A plethora of methods for the preparation of metal nanoparticles are reported in the literature detailing ways to achieve precise control of their size [149-161]. While some methods require the use of specific capping agents in the nanoparticle synthesis [149], other methods use ethylene glycol as both the solvent and the capping agent [160, 161]. For example, Couto *et al.* carried out the synthesis of nickel nanoparticles using nickel chloride hexahydrate reduced by sodium borohydride in ethylene glycol in the presence of the capping agent polyvinylpyrrolidone [149]. In contrast, Wu *et al.* reported the preparation of nickel nanoparticles via the reduction of nickel chloride with hydrazine hydrate in the presence of sodium hydroxide in ethylene glycol, which was both the solvent and capping agent [161].

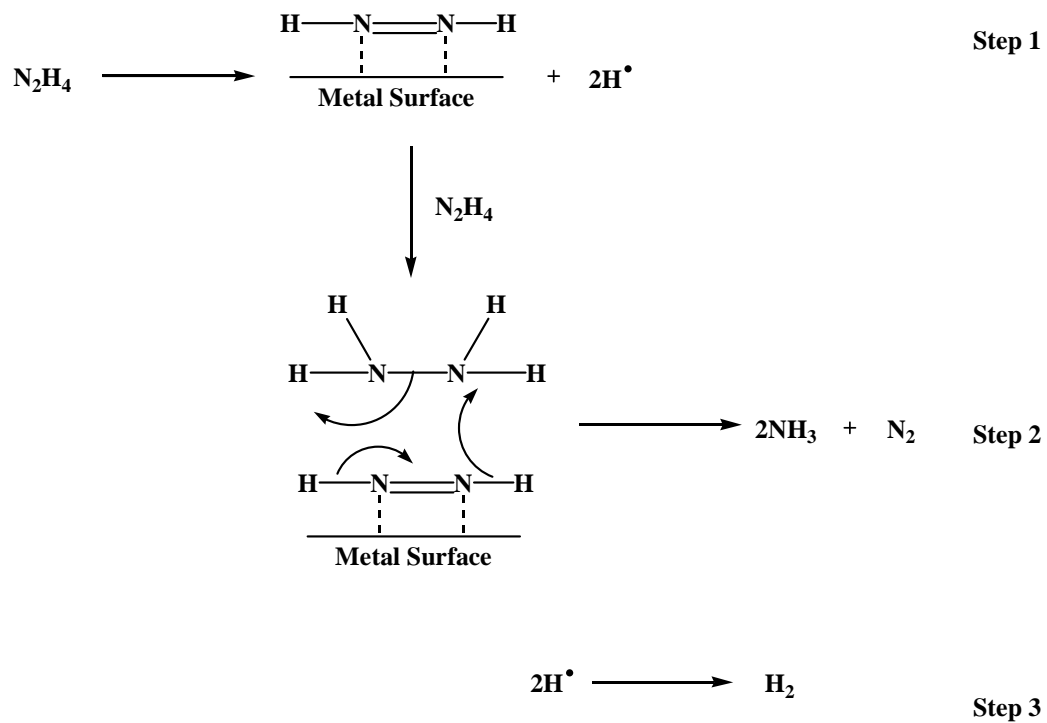


Figure 4.2: Proposed hydrazine decomposition mechanism.

## 4.2: Materials and Experimental Methods

### 4.2.1: Materials

Nickel chloride, copper chloride, ruthenium chloride, rhodium chloride hydrate, iridium chloride hydrate, cobalt chloride, amorphous silica, hydrazine, hydrazine monohydrate, sodium hydroxide, and sodium borohydride were purchased from Sigma Aldrich and used without further purification. Spherical silica was purchased from Sorbent Technologies (Atlanta, GA). Calibrating gas mixtures of ammonia, nitrogen, and hydrogen (2 mol% and 8 mol%  $\text{NH}_3$ ) with argon as the balance gas were purchased from Scott Specialty Gas Corporation (Augusta, GA). All GC-TCD columns were purchased from and packed by Supelco (Bellefonte, PA).

### 4.2.2: Experimental Methods

#### 4.2.2.1: Metal Nanoparticles Synthesis

The desired metal salt (listed above, 0.5 mmol) was added to dry ethylene glycol (25mL) along with sodium hydroxide (0.072g, 1.8 mmol) and the mixture was warmed to 60°C under stirring until complete dissolution of solids. Hydrazine monohydrate (0.3 mL, 6.2 mmol) was added at 60°C—except for cobalt, rhodium, and ruthenium—and the mixture was allowed to react until complete reduction of the metal. For cobalt, the reduction was carried out at 190°C since cobalt forms stable complex with hydrazine [155, 162]. Also, the reductions of ruthenium and rhodium were carried out at 120°C and 190°C, respectively, because the reduction did not progress at 60°C. These reduction temperatures are similar to those reported in literature for rhodium and ruthenium [152, 153, 156-158, 163]. The reaction progress was tracked with UV-Vis spectroscopy and the

results were confirmed with chlorine elemental analysis. Particles were isolated by centrifugation, washed with ethanol, and dried overnight in a vacuum oven at 80°C. Analysis of size distribution was carried out with Transmission Electron Microscopy (TEM) and X-ray Diffraction (XRD).

#### 4.2.2.2: Synthesis of Silica Supported Metal Particles

Initially, we attempted to adsorb the nickel nanoparticles on the silica by solvent evaporation at high temperature after mixing the particles in ethanol with the silica for 12 hours. However, after drying at 100°C for more than 12 hours, we observed no evidence of particles adsorption on the support. XRD analysis showed only the silica peak. Therefore, we modified the method as follows. The metal salt (listed above except for cobalt, 0.5 mmol) and sodium hydroxide (0.072g, 1.8mmol ) were added to dry ethylene glycol (25mL). The solution was warmed to 60°C with stirring until complete dissolution of solid. The desired amount of silica was added (8% loading, 75-200 $\mu$ m, 150 $\text{Å}$  pores). Hydrazine monohydrate (0.3 mL, 6.2 mmol) was added and the mixture was allowed to react to reach complete reduction of the metals. The mixture was then cooled to room temperature and the product was collected by centrifugation, washed with ethanol and dried with vacuum and heat. The supported metal on the silica was characterized with scanning electron microscopy (SEM) and Brunauer, Emmett and Teller analysis (BET).

For the supported cobalt catalyst synthesized with the above method, we observed that the isolated product was a dark brown powder, which is not the expected color, and it was not magnetic. This indicates that metallic cobalt was not formed. In literature, it is known that cobalt can form silicate complexes when reduced in the presence of silica

[164]. To address this, Co particles were formed first and the desired amount of silica was then added to the system and left to stir for three days at room temperature. The product was collected by centrifugation, washed with ethanol, and dried overnight in a vacuum oven at 80°C.

#### 4.2.2.3: Hydrazine decomposition products analysis

The decomposition of hydrazine with the prepared supported catalysts was carried out in a heated packed bed reactor. The continuous flow reactor design and construction is discussed in the results section. Initially, the catalyst was packed in ¼ inch 316 stainless steel tubing (4 inches in length). Into one end, 230 mesh size stainless steel mesh, and glass wool were packed. Catalyst powder was added through a funnel while pulling vacuum on the other end of the tube accompanied by vibration to ensure even packing. After the tube was filled, glass wool was inserted in the other end, as well as another piece of 230 mesh size stainless steel mesh. Later in the project, the catalyst was packed in empty HPLC columns of 4.6mm inner diameter and 30mm in length made of 316 stainless steel. A frit containing 20µm pores was placed at each end of the column. Catalyst powder was added through a funnel while pulling vacuum on the other end of the tube accompanied by vibration to ensure even packing

Hydrazine (1 mL) was loaded into a glass vessel and argon carrier gas was sparged through the system as shown in Figure 4.10 and 4.11. Flow rate was controlled by a flow meter. The concentration of hydrazine in the gas phase was controlled by adjusting the temperature of liquid hydrazine and the pressure of the system. The hydrazine/gas stream was then passed through the temperature controlled catalyst bed

and the product stream is then passed through a sample loop heated to 75°C. Rotation of a six-port valve injected the sample from the sample loop into the GC.

The product stream analysis was carried out with a Gas Chromatography coupled with a Thermal Conductivity detector (GC-TCD) with calibration curves to quantify the amount of hydrazine and ammonia. The product gas stream passes through the injection six port valve, which allows for taking sample from the continuously running reactor as shown in Figure 4.3. Following injection, all products pass over a Carbowax 1500 column (6 ft. long, 1/8 inch outer diameter) at a flow rate of 50mL/min in a GC heated to 130°C and directly to the detector. With this method, hydrogen and nitrogen cannot be separated and they elute as a single peak. However, there is good peak separation between the combined H<sub>2</sub>/N<sub>2</sub> peak, the ammonia peak, and the hydrazine peak, allowing for analysis of products based on yield of ammonia formed.

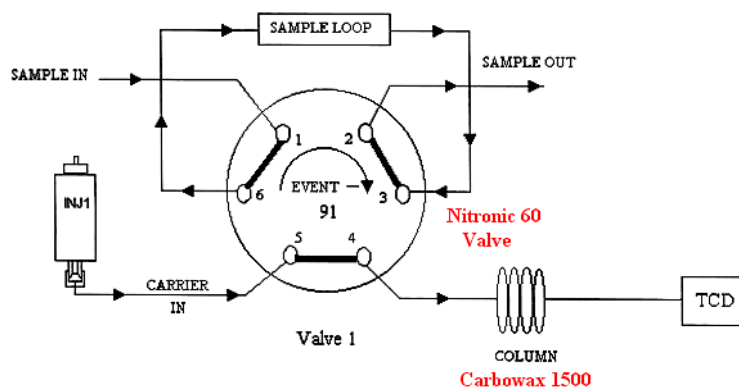


Figure 4.3: Schematic of GC-TCD analysis set-up.

### **4.3: Results and Discussion**

In this section, the results of the synthesis and characterization of metal nanoparticles and characterization of the silica-supported metals are reported. In addition, we discuss the design and development of the continuous flow reactor and the hydrazine decomposition yield and selectivity with various catalysts.

#### **4.3.1: Metal Nanoparticles Synthesis**

Prior to being tested for support on silica, the synthesized metal nanoparticles were characterized and the results are shown in Table 4.1. The conversion of the precursor metal salts is more than 98% as determined by UV-Vis and chlorine elemental analysis. The particles were also analyzed with XRD and the results indicate the absence of metal oxides. Except for nickel, the synthesized particles' size is about two nanometers. The nickel nanoparticles are larger and more polydisperse when compared to other metals with an average size of 6 nm and a standard deviation of 4 nm. This may be explained by agglomeration of nickel nanoparticles as reflected in the TEM image of nickel particles—Figure 4.4. The majority of the particles have a size of 3, 4, 5, or 6 nm with smaller fractions of particles with size 2 nm and 7-11 nm. The size histogram also reflects the formation of larger agglomerates in the 12-20 nm size range. If we consider iridium particles—Figure 4.5—as an example for comparison, the Ir particles synthesized are mostly 0.5, 1, or 2 nm in size with small fractions of particle with 4 and 5 nm size (the TEM images for Cu, Co, Ru, and Rh are similar to that of Ir). However, the size polydispersity of nickel particles was not considered to detriment to our purpose at this time.

Table 4.1: Size of metal nanoparticles as determined by TEM analysis.

Metal Nanoparticles	Precursor Metal Salt	Nanoparticles size (nm)
Ni	NiCl <sub>2</sub>	6.0 ± 4.0
Cu	CuCl	1.4 ± 0.9
Co	CoCl <sub>2</sub>	1.2 ± 0.9
Ru	RuCl <sub>3</sub>	1.3 ± 0.8
Rh	RhCl <sub>3</sub> .3H <sub>2</sub> O	2.0 ± 1.0
Ir	IrCl <sub>3</sub> .3H <sub>2</sub> O	2.0 ± 1.0

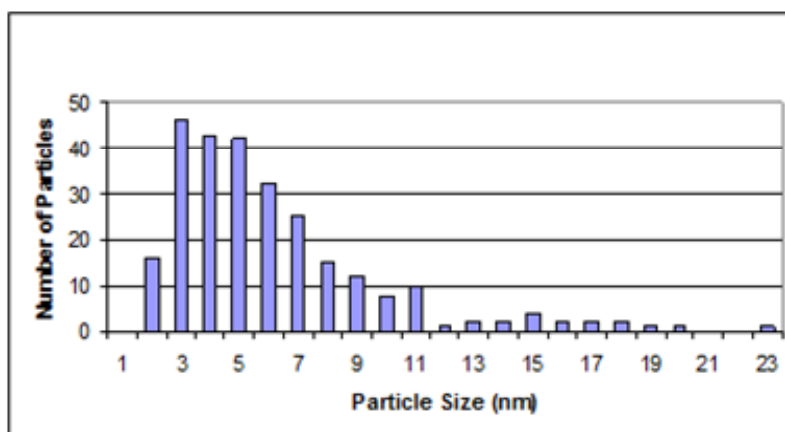
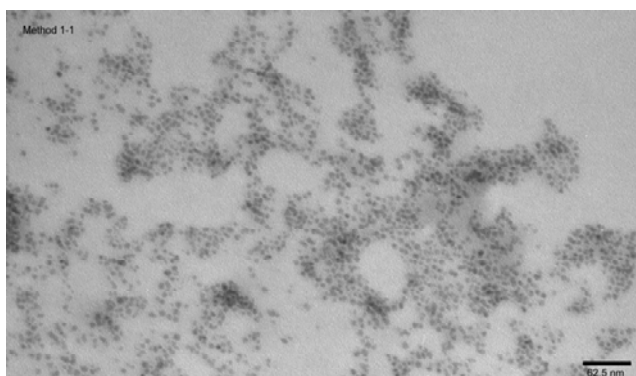


Figure 4.4: TEM images of nickel nanoparticles (top) and the corresponding particle size distribution histogram (bottom).

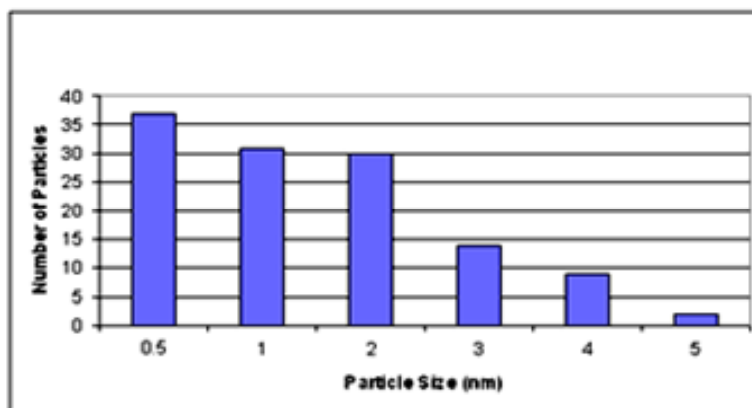
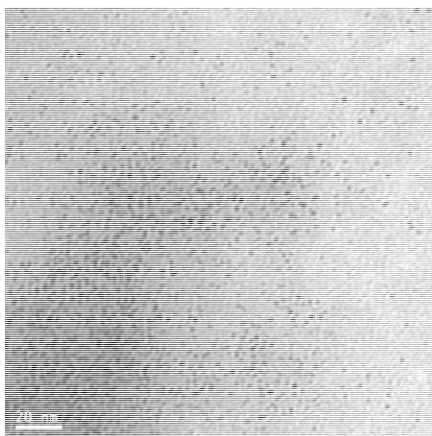


Figure 4.5: TEM images of iridium nanoparticles (top) and the corresponding particle size distribution histogram (bottom).

### 4.3.2 Supported Metal Nanoparticle Synthesis

The silica-supported metals were prepared by the addition of silica prior to reduction of the metal salt, except for cobalt as discussed in the methodology section. Nickel, cobalt, copper, ruthenium, rhodium, and iridium metals were supported on spherical silica and isolated by centrifugation, washed with ethanol, and dried overnight in a vacuum oven at 80°C. The supported samples of each metal were analyzed by CI and metals elemental analysis to determine conversion and actual percent loading, XRD to confirm formation of the desired metal, scanning electron microscopy (SEM) imaging to

look at metal distribution on the surface, and with a Brunauer, Emmett and Teller (BET) equipment to determine surface area and pore volume. Table 4.2 shows a comparison of the values found for a representative sample of each of these different metals. The XRD analysis was consistent with the pure metals and no metal oxides were detected.

The supported samples of each metal were synthesized in a narrow loading range of 2.6%-3.6%. Also, all were found to have complete or near complete conversion as Cu, Ir and Co showed no remaining Cl present in the system and Ni, Ru, and Rh showed only traces (<0.25%). The uncoated silica was analyzed and found to have a BET surface area of  $168 \pm 5 \text{ m}^2/\text{g}$  and a pore volume of  $0.9 \pm 0.1 \text{ cm}^3/\text{g}$ . Compared to this, depositing the nanoparticles on the silica surface did not appear to cause a substantial change in either surface area or pore volume, except in the cases of cobalt and rhodium, where both values decreased. For cobalt, this was a decrease of approximately 50% (57% decrease in surface area, 33% decrease in pore volume) while rhodium showed a decrease of 35% percent in surface area and 33% in pore volume.

Table 4.2: Comparison of conversion, metal loading, surface area and pore volume.

<b>Metal</b>	<b>Metal % Load</b>	<b>% Cl Found<sup>A</sup></b>	<b>BET Surface Area (m<sup>2</sup>/g)</b>	<b>Pore Volume (cm<sup>3</sup>/g)</b>
(Si) <sub>support</sub>	-	-	$168 \pm 5$	$0.9 \pm 0.1$
Ni	3.0%	<0.25%	$167 \pm 5$	$0.9 \pm 0.1$
Cu	2.6%	0%	$141 \pm 4$	$0.8 \pm 0.1$
Co	3.1%	0%	$96 \pm 3$	$0.6 \pm 0.1$
Ru	3.1%	<0.25%	$195 \pm 5$	$0.8 \pm 0.1$
Ir	3.4%	0%	$163 \pm 5$	$0.9 \pm 0.1$
Rh	3.6%	<0.25%	$109 \pm 3$	$0.6 \pm 0.1$

0% - No Cl detected. <0.25% - Trace Cl detected, but below the quantitative analysis limits of the instrument.

In all SEM images, the metals are visible as white or light colored particles on a dark silica support. Nickel—Figure 4.6—and copper—Figure 4.7—showed small amount of clustering although most of the particles retained their nano-scale. Rhodium, ruthenium, cobalt, and iridium showed a large amount of clustering. Most particles have agglomerated to form micrometer size particles; example of iridium on silica is shown in Figure 4.8.

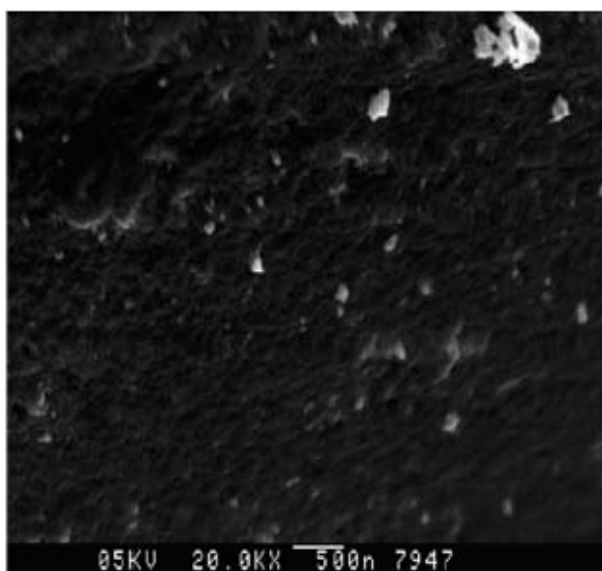


Figure 4.6: SEM images of nickel particles supported on silica surface.

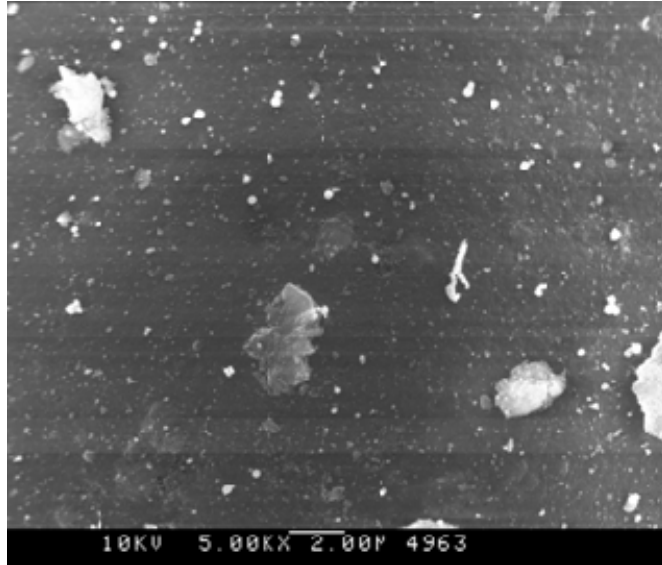


Figure 4.7: SEM images of copper particles supported on silica surface.

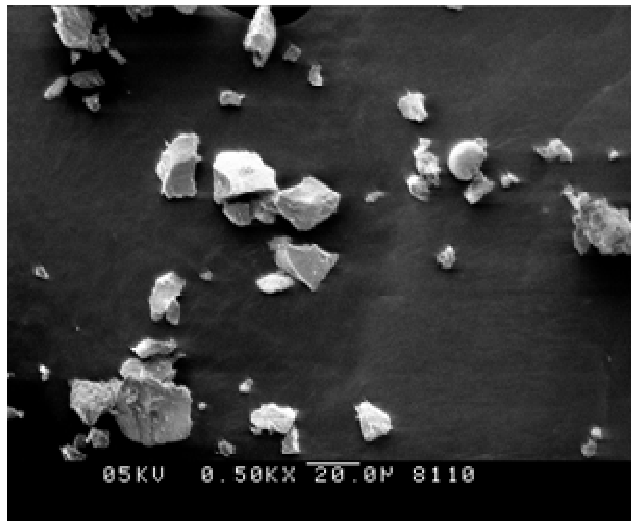


Figure 4.8: SEM image of iridium particles supported on a silica surface.

### 4.3.3: Reactor Environment Safety

Hydrazine is a class 3 explosive and a class 3 health risk chemical, making it a rigorously regulated substance. In coordination with the Environmental Health and Safety department (EHS) at Georgia Tech, a standard operating procedure and an emergency procedure were developed for working with hydrazine. The entire reactor system was placed within a hood and is equipped with pressure sensors and pressure relief valves. The hood ventilation system was adjusted to a flow of 120 ft/min, which is the legal requirement for handling Class 3 chemicals. The level of hydrazine in the laboratory is continuously monitored using a Honeywell® ChemCassette system, shown in Figure 4.9 (left side). The detection limit of this device was set at the conservative level of 5 ppb. This is the level to which an individual can be exposed for 8 hours without suffering from adverse health issues such as irritation of the eyes, nose, and throat, dizziness, nausea, and in extreme cases pulmonary edema and seizures. In addition, each operator is required to wear a monitoring badge that changes color when exposed to hydrazine (Figure 4.9 - right side).

The intensity of the color is a function of the hydrazine level to which it has been exposed. These badges are purchased from DoD Technologies and can be used for 48 hrs before they must be disposed of. Their detection limit is 0.5 ppm. These same badges have been placed within the hood at strategic places as an extra precaution to signal possible hydrazine leaks. If a badge outside the hood or on the body of any operator turns colors, the lab will immediately be evacuated and those involved taken for medical attention.



Figure 4.9: ChemCasette hydrazine monitoring system and hydrazine monitoring badges.

#### 4.3.4: Hydrazine Reactor Design

To study the catalyst activity for the decomposition of hydrazine to ammonia, we designed and built a reactor in our lab. The design and construction of the continuous flow reactor provided a large degree of flexibility. The reactor allows the study the activity of the catalyst as a function of (1) catalyst bed temperature, (2) hydrazine concentration, (3) percent loading of catalyst, (4) amount of catalyst in the catalyst bed, and (5) the flow rate of the system.

The first generation reactor—shown in Figure 4.10—was divided in three sections: (1) hydrazine introduction, (2) a catalyst bed with a water heater, and (3) analysis with a Gas Chromatography coupled with a Thermal Conductivity detector (GC-TCD). In the first section, the argon carrier gas passed through a flow meter and a pressure indicator with a relief valve. The argon gas is then bubbled through the heated

liquid hydrazine in a containment vessel resulting in a combination hydrazine/argon stream.

The concentration of hydrazine in the gas stream is controlled by adjusting the hydrazine container temperature and therefore, the vapor pressure of hydrazine. The hydrazine-containing argon stream was then directed through a valve allowing the stream to pass through the second section of the reactor, the temperature controlled catalyst bed. The catalyst bed was constructed from ¼ inch stainless steel tubing. The catalyst powder was kept in place by a piece of mesh and a small piece of glass wool at each extremity. After passing over the catalyst bed, product stream flowed into the third section, the GC-TCD, for analysis. Before completely exiting the system and being released into the hood, the gas stream was bubbled through a nitric acid solution of pH 1 to neutralize the ammonia and a bleach solution that is 6.15 mol% sodium hypochlorite to neutralize any remaining hydrazine.

This first generation reactor was used for initial decomposition testing with Ni supported on silica. The reactor was designed to allow the argon stream to bypass the hydrazine or the hydrazine/argon stream to bypass the catalyst bed, the analysis, or both if so desired. However, it quickly became clear that the complexity of the system made troubleshooting difficult and time consuming. Also, the system was long as it extended across an entire hood and contained over 20 feet of stainless steel tubing. The prolonged residence time allowed for a great deal of interaction between the hydrazine and the stainless steel, before it even came into contact with the catalyst bed. Also, the many valves and tube connections that were incorporated into the reactor required leak-testing and extensive maintenance due to corrosion and breakage. Therefore, we decided to

redesign the reactor with a simpler system for more accurate results, a better control of the variables of the system, and greater consistency and repeatability.

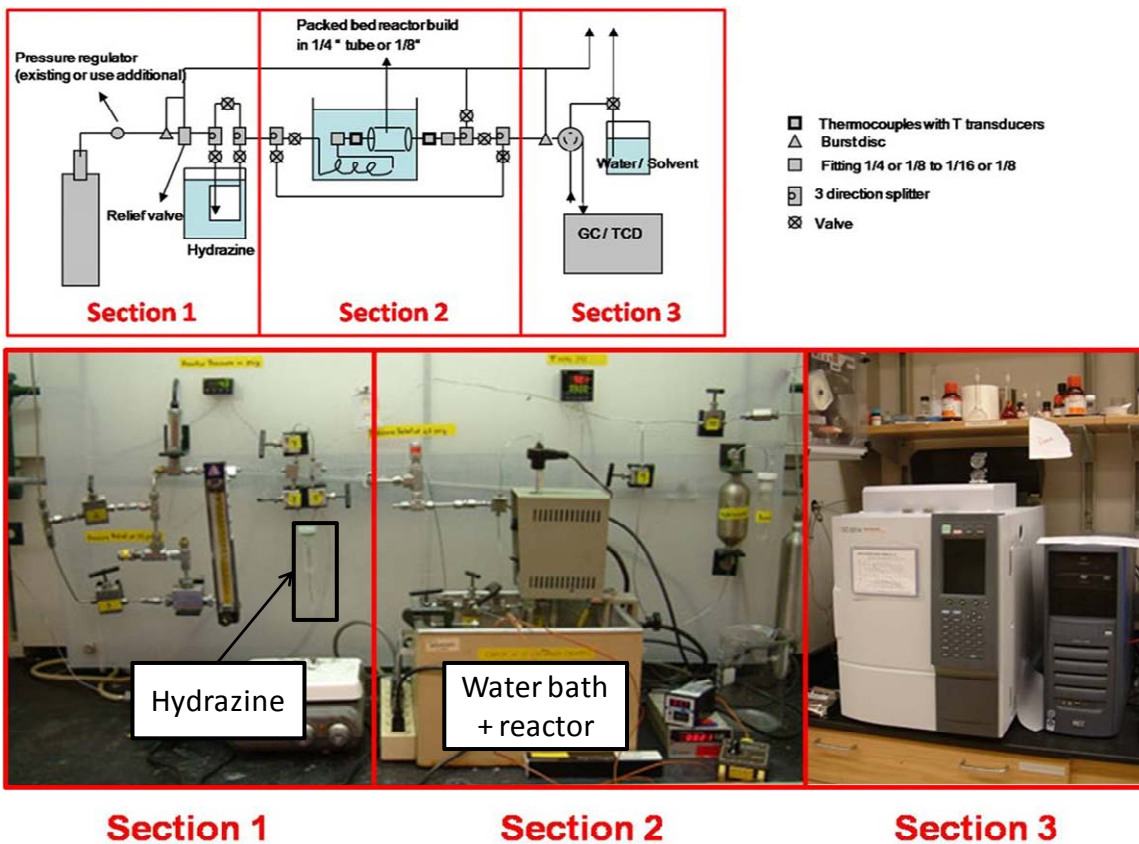


Figure 4.10: Reactor designed and built to test the hydrazine decomposition abilities of metal catalysts supported on silica.

The modified reactor—referred to as the second generation reactor—incorporated several changes as shown in Figure 4.11. First and foremost, the length of tubing between hydrazine introduction and analysis was shortened. The length of tubing between the hydrazine introduction and catalyst bed was shortened to less than one foot and the length of tubing from catalyst bed to GC-TCD was shortened to about two feet. Second, the quarter inch stainless steel tubing being used for catalyst packed beds was replaced by HPLC columns of 4.6mm inner diameter and 30mm in length. As these columns come with filters on either end, they could now be packed completely with catalyst without the need for mesh or glass wool inserts. These columns could be packed with about 0.3g of catalyst, and the packing procedure remained the same, with vacuum and vibration used for consistent packing.

The third change was the removal of a bypass system around the packed catalyst bed. This decreased the number of valves and fittings in the system, again making it simpler and decreasing the number of potential leaks or corrosion points between hydrazine and the reactor itself. Finally, the fourth change was the removal of the water bath to heat the catalyst bed. This was replaced with electric heating using a heating tape and a temperature controller. This allowed for better control of the temperature of the gas stream, as this heating was controlled by a temperature probe inserted into the flow of the gas stream itself, rather than by an external temperature probe.

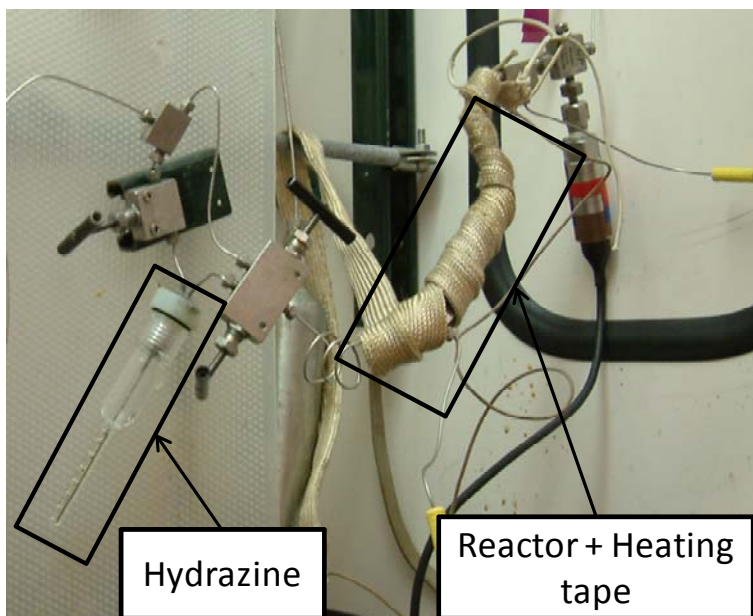
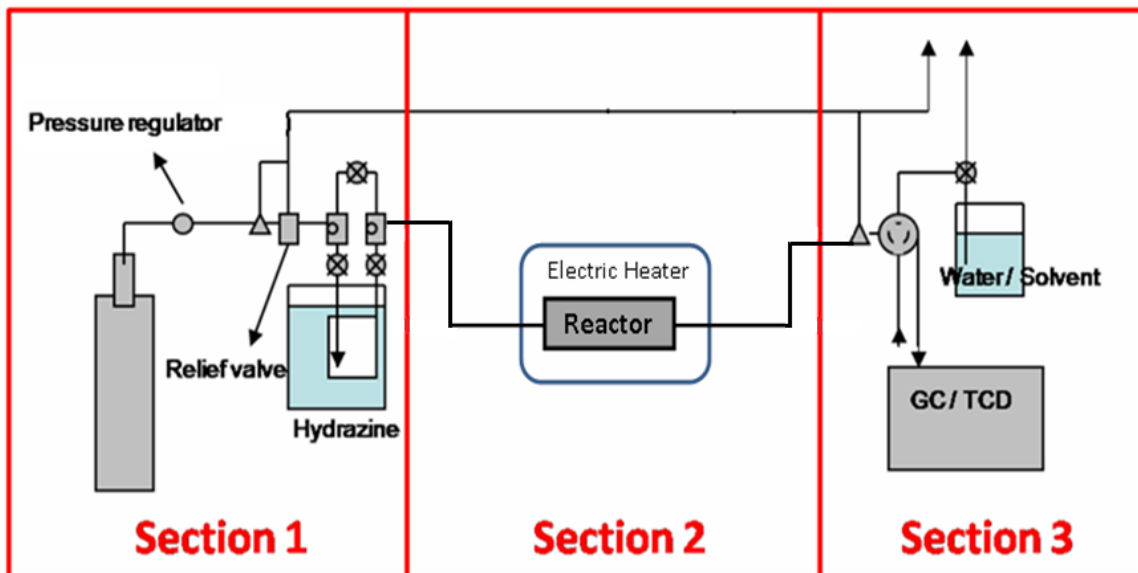


Figure 4.11: Schematic of second generation reactor.

#### 4.3.5: Decomposition of Hydrazine

The initial hydrazine decomposition experiments were carried out with the first generation reactor using 1.06 wt% Ni on silica. Hydrazine was kept at room temperature (~25°C) with a system flow rate of 83.7 mL/min (about 1 mol% hydrazine in the gas stream). The system was tested with the catalyst bed at 25°C, 35°C, 50°C, and 60°C. At each temperature, the experiments were carried out for 40 minutes and two samples were taken. Under these conditions, the system did not reach steady state at each condition but we were able to observe general trends. The areas found for hydrazine, hydrogen and nitrogen were converted to mole percent amounts of the total gas stream using the 83.7 mL/min calibration curve. Under these conditions, at all temperatures, a hydrazine peak was seen. The amount of hydrazine seen was highest at 25°C, with 1.32% and decreased steadily to 0.25% at 60°C indicating 19% of the hydrazine remained unreacted. There was 0% yield of ammonia, but very small quantities of hydrogen and nitrogen were present at all temperatures. Along with the expected peaks for hydrazine, hydrogen and nitrogen, a new peak appeared with a retention time that varied from 8.9 to 10.4 minutes as the temperature was increased. We speculate that diazene was being produced. Diazene is a well-known intermediate in the decomposition of hydrazine to its final product mixture of ammonia, hydrogen and nitrogen [165]. In our system, hydrazine was only undergoing partial decomposition and diazene could be formed by the adsorption of hydrogen onto the nickel catalyst surface. The formation of diazene may result from the incomplete decomposition of hydrazine due to the short exposure time between the hydrazine and the catalyst caused by either high flow rate or small amount of catalyst packed into the catalyst bed, or a combination of the two. To overcome this, the catalyst

bed was packed with 0.7 g of catalyst with 2.90% nickel loading by weight and the argon flow was lowered to 29.4 ml/min. The temperature of the catalyst bed was maintained at 75°C and hydrazine was kept at room temperature (1.35 mol% hydrazine). The reactor was run at these conditions and ammonia, hydrazine, diazene, and hydrogen/nitrogen were all present from the beginning. The hydrazine and diazene amounts decreased, and the ammonia amount increased until equilibrium was reached with 100% conversion of hydrazine, and a total gas stream composed of 1.7% ammonia. This is a 96±2 % yield of ammonia, and it represents 82±3 % of the total product stream. The nano-nickel catalyst supported on silica appeared more active toward the formation of ammonia than the nickel thin film reported in the literature, which produced a product stream containing 76.03% ammonia at 90°C [166].

After re-designing the reactor and analytical method, all supported nanoparticle catalysts (Ni, Cu, Co, Ir, Rh, and Ru) were tested for their activity towards hydrazine decomposition and selectivity for ammonia formation and the results are summarized in Table 4.3. Each catalyst to be tested had between 2.6% and 3.6% actual metal loading (except one of the Ir catalysts which had 1.3% metal loading). For each test, approximately 0.3 g of catalyst was packed into the catalyst bed. The catalyst bed was heated to 90°C with flowing argon for 12 hours prior to the decomposition reaction. During the reaction, the bed was heated to 75°C and the flow rate of the system was kept at 29.4mL/min. The hydrazine was kept at room temperature (~ 25°C).

For each catalyst, based on the mole percent of hydrazine entering the system, the theoretical 100% yield amount of ammonia was calculated. The actual amount of ammonia formed was determined from the ammonia calibrating curve. The percent yield

was determined as the ratio of the two. Each metal was tested twice using fresh catalyst either from the same or a similarly prepared batch of catalyst to confirm reproducibility.

Table 4.3: Results from supported nanoparticle catalyst decomposition tests.

<b>Metal Loading</b>	<b>BET Surface Area (m<sup>2</sup>/g)</b>	<b>NH<sub>3</sub> Yield (% , ± SD)</b>	<b>Conversion (%)</b>
3.0% Ni	167 ± 5	91 ± 3	100
2.9% Ni <sup>A</sup>		96 ± 2	100
2.6% Cu	141 ± 4	NA	0
2.6% Cu		NA	0
3.1% Ru	195 ± 5	67 ± 4	100
3.1% Ru		60 ± 6	100
3.1% Co	96 ± 3	NA	0
3.1% Co		NA	0
3.3% Ir	163 ± 5	67 ± 5	100
1.3% Ir		63 ± 3	100
3.6% Rh	109 ± 3	60 ± 2	100
2.8% Rh		55 ± 4	100

A. Results obtained using first generation reactor system

Ni, Ru, Rh, and Ir showed 100% conversion of the hydrazine to products. In terms of selectivity, nickel provided the highest ammonia yields of 94±3 %. Ruthenium and

iridium both produced similar yields of ammonia with  $67\pm 6\%$  and  $62\pm 6\%$ . Under our conditions, rhodium showed the lowest selectivity with  $57\pm 4\%$  ammonia yield.

Copper and cobalt were found to have no measurable activity for hydrazine decomposition. With cobalt, only un-reacted hydrazine was seen. Interestingly with copper, some products peaks were initially seen. However, after 30 minutes of reaction time, only hydrazine was seen. This could be due to rapid poisoning of the catalyst. Based on its excellent ammonia yields, complete conversion of hydrazine to products, and moderate equilibration times, nickel appears to be the most promising catalyst for further study and optimization.

#### **4.4: Conclusions**

The synthesis of nickel, copper, cobalt, iridium, ruthenium, and rhodium nanoparticles was successfully demonstrated. The nanoparticles were analyzed by elemental analysis, XRD, and TEM imaging. The deposition of the nanoparticles on support (silica) was conducted, producing metal-supported catalyst in the range 2.6-3.6 wt.% loading.

To test these catalysts for the decomposition of hydrazine to produce ammonia, we designed, built, and optimized a continuous flow reactor. Silica-supported catalysts of nickel, copper, cobalt, ruthenium, rhodium and iridium have been tested. Cobalt and copper did not exhibit activity. However, nickel, ruthenium, rhodium, and iridium all showed high activity. Nickel showed the most selectivity for ammonia formation with ammonia yields of  $94\pm 3\%$ . In all cases, nickel is the best catalyst to decompose hydrazine to ammonia.

## CHAPTER 5: CONCLUSIONS AND RECOMMENDATIONS

The focus of this research was to improve the sustainability of various processes by employing tunable solvents, switchable solvents, and catalysis. Sustainability encompasses economics of the process, environmental impact, and social responsibility [1]. In Chapter 2, we report applications of tunable solvents to metal and enzyme catalyzed reactions of hydrophobic substrates. Tunable solvents are defined as solvent that change properties rapidly but continuously upon the application of an external physical stimulus and we utilize these solvents to couple homogeneous reactions with heterogeneous separations. We developed organic-aqueous tunable solvents that utilize propane for efficient phase separation at moderate pressures around 1 MPa; for example the water contents in the in propane-expanded THF is 3 wt% at 0.8MPa at 30°C. Also, we extended the use of CO<sub>2</sub>-organic-aqueous tunable solvents to a pharmaceutically-relevant reaction—the hydroformylation of *p*-methylstyrene. The homogeneous reactions provide fast reactions with excellent yields. At 60°C, the reaction reaches completion after 180 minutes with 95% branched aldehyde yield. The CO<sub>2</sub>-induced heterogeneous separation of the product from the catalyst provides an efficient and simple way to remove 99% of the product, to retain 99.9% of catalyst, and to recycle the Rh-TPPMS catalyst for five consecutive reactions.

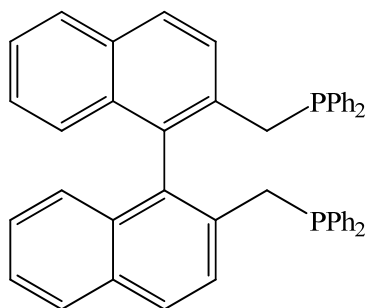
We are currently evaluating the use of organic-ionic liquid tunable solvents to combine homogeneous reactions with heterogeneous separations. Tunable solvents that do not contain water, for example polyethylene glycol (PEG)-organic and ionic liquid-organic, may be beneficial for applications with water sensitive catalysts such as some

version of the Grubbs' catalysts [167]. Our group reported the phase behavior of PEG-dioxane-CO<sub>2</sub> (POTS) phase behavior [168] and applied these systems to the C-O coupling reaction of 1-bromo-3,5-dimethylbenzene and *o*-cresol with potassium hydroxide to produce *o*-tolyl-3,5-xylyl ether and the reaction of 1-bromo-3,5-di-*tert*-butylbenzene and potassium hydroxide yielding 3,5-di-*tert*-butylphenol in PEG tunable solvents [47]. We see tunable ionic liquids-organic systems (TOIS) as a complimentary solvent system to OATS and POTS that may be beneficial for certain reactions. For example, ionic-liquids (ILs) are reported to enhance the catalytic activity for some chemical transformation, especially those including enzymes [169-172]. In addition, homogeneous mixtures of ILs and organics have been reported to phase-separate under CO<sub>2</sub> pressures [173-175] and therefore, they could be beneficial for separating nonpolar products from ionic catalysts. For example, in CO<sub>2</sub>-acetonitrile-[bmim][Tf<sub>2</sub>N] (1-Butyl-3-Methyl-Imidazolium-bis(trifluoromethanesulfonyl) imide) system, the distribution coefficient of the [bmim][Tf<sub>2</sub>N] ( $X_{\text{IL-phase}} / X_{\text{organic-phase}}$ ) is 135 at 7.9 MPa of CO<sub>2</sub> and increases to 965 at 8.1 MPa of CO<sub>2</sub>.

There two advantages to using propane instead of CO<sub>2</sub> in OATS: elimination of *in-situ* acid formation and phase separation at lower pressures. This system is suitable for reactions that employ enzymes as well as those with acid-sensitive catalysts or substrates. For *Candida Rugosa* hydrolysis, we have shown that the amount of organic solvent in these systems was detrimental to the enzyme's activity. However, there are research efforts in the field of enzyme evolution to improve enzyme stability in organic-rich environments [176]. Future application of organic-tolerant enzymes will benefit from the propane-OATS systems that we developed. Also, propane-OATS is suitable for reactions

that include substrates with protecting groups that are cleaved by acids such as tetrahydropyranal protected alcohols [177].

Chiral reactions are another interesting class of reaction that may benefit from OATS. An example is the chiral hydroformylation of styrene with sulfonated 2,2'-Bis-(diplienylphosphinomethyl)-1,1'-binaphthyl-Rh (BINAS-Rh, Figure 5.1). The two variables that should be evaluated are 1) catalyst partitioning in the aqueous phase and 2) starting material conversion and branched product enantioselectivity (*S*-enantiomer is desired in the case of ibuprofen). The homogeneous chiral hydroformylation of styrene with 2,2'-Bis-(diplienyl-phosphinomethyl)-1,1'-binaphthyl-Rh (NAPHOS-Rh) was shown to provide higher enantioselectivity than biphasic H<sub>2</sub>O-toluene chiral hydroformylation of styrene with BINAS-Rh (32% and 18%, respectively) [178]. For this reaction, OATS could provide a method to overcome the limitation of the biphasic system (lower yield and enantioselectivity) while offering simple and efficient catalyst recovery.



In chapter 3, we investigated the use of reversible ionic liquids (RevILs) for synthesis of nanoparticles. RevILs are formed by the reversible reaction of compounds with basic nitrogen functionalities (molecular liquid) with CO<sub>2</sub> at ambient pressure to form a liquid salt (ionic liquid). There are two major classes of reversible ionic liquids: two-component (utilize an amine and an alcohol) and one-component (utilize an amine only). In this research, we demonstrated that RevILs form microemulsions that can be switched-on by bubbling CO<sub>2</sub> and switched-off by heating. These microemulsions solubilize ionic compounds such as methyl orange and chloroauric acid. We utilized these microemulsions as a template for controlled synthesis of gold nanoparticles. With 2-component RevILs, [TMBGH]<sup>+</sup>[O<sub>2</sub>COCH<sub>3</sub>]<sup>-</sup>/*N*-propyl-octylsulfon-amide/hexane were used to form particles in the size range of 6-20 nm with an average particles size of 11.4±3.3. With 1-component RevILs, (3-aminopropyl)-tripropylsilane was used to prepare semi-spherical gold particles with an average size of about 20nm. The 1-component RevILs systems provide a simpler method to form microemulsions when compared to the 2-component RevILs systems since they eliminate the need for alcohols and surfactants. We are currently optimizing synthesis and deposition of gold nanoparticles with 1-component RevILs. We plan to study the effect of the structure of the 1-component RevIL on the size and shape of the synthesized nanoparticles. The physical properties of RevILs, e.g. polarity, can be modified by changing the structure of these compounds [9, 10]. Therefore, we speculate that using different RevILs or mixtures of RevILs may change the size of the prepared nanoparticles. Ultimately, we will compare catalytic activity of the synthesized gold nanoparticles prepared for oxidation

reactions such as the oxidation of glucose to gluconic acid [179] and the oxidation of alcohols [109].

In chapter 4, we developed a catalyst that efficiently decomposes hydrazine to selectively produce ammonia. This enables the use of the chemical propulsion hydrazine for electric propulsion as well. We prepared nickel, copper, cobalt, ruthenium, rhodium, and iridium nanoparticles that were supported on silica and we tested these silica-supported metals for the decomposition of hydrazine. To study the catalytic activity, we designed and constructed a continuous flow reactor. The results show that nano-nickel supported on silica is the most active and selective catalyst with 100% conversion of hydrazine and  $94\pm 3\%$  yield of ammonia. The current and future work for this project focuses on the long-term activity of the catalyst and its activity for the use with liquid hydrazine (as opposed to vapor hydrazine). These tests will be performed at the facilities of our industrial partner American Pacific (AMPAC), as they have the equipment and safety precautions in place necessary for dealing with the decomposition of liquid hydrazine.

## References

1. Lapkin, A. and D. Constable, *Green Chemistry Metrics: Measuring and Monitoring Sustainable Processes*. 2008, New York: Wiley-Blackwell.
2. Anastas, P.T. and J.C. Warner, *Green Chemistry: Theory and Practice*. 1998, New York: Oxford University Press.
3. Herwig, J. and R. Fischer, *Rhodium Catalyzed Hydroformylation - Aqueous Biphasic Hydroformylation*. 2000, Oberhausen, Germany: Kluwer Academic Publishers.
4. Constable, D.J.C., C. Jimenez-Gonzalez, and R.K. Henderson, *Perspective on Solvent Use in the Pharmaceutical Industry*. *Organic Process Research & Development*, 2007. **11**(1): p. 133-137.
5. Jimenez-Gonzalez, C., A.D. Curzons, D.J.C. Constable, and V.L. Cunningham, *Expanding Gsk's Solvent Selection Guide Application of Life Cycle Assessment to Enhance Solvent Selections*. *CLEAN TECHNOLOGIES AND ENVIRONMENTAL POLICY*, 2005. **7**(1): p. 42-50.
6. Sheldon, R.A., *Green Solvents for Sustainable Organic Synthesis: State of the Art*. *Green Chemistry*, 2005. **7**(5): p. 267-278.
7. Anastas, P. and T. Williamson, *Frontiers in Benign Chemical Synthesis and Processes*. 1998, London: University Press.
8. Hart, R., P. Pollet, D.J. Hahne, E. John, V. Llopis-Mestre, V. Blasucci, H. Huttenhower, W. Leitner, C.A. Eckert, and C.L. Liotta, *Benign Coupling of Reactions and Separations with Reversible Ionic Liquids*. *Tetrahedron*, 2010. **66**(5): p. 1082-1090.
9. Blasucci, V.M., R. Hart, P. Pollet, C.L. Liotta, and C.A. Eckert, *Reversible Ionic Liquids Designed for Facile Separations*. *Fluid Phase Equilibria*, 2010. **294**(1-2): p. 1-6.

10. Blasucci, V., R. Hart, V.L. Mestre, D.J. Hahne, M. Burlager, H. Huttenhower, B.J.R. Thio, P. Pollet, C.L. Liotta, and C.A. Eckert, *Single Component, Reversible Ionic Liquids for Energy Applications*. Fuel, 2010. **89**(6): p. 1315-1319.
11. Eckelman, M.J., J.B. Zimmerman, and P.T. Anastas, *Toward Green Nano: E-Factor Analysis of Several Nanomaterial Syntheses*. Journal of Industrial Ecology, 2008. **12**(3): p. 316-328.
12. Allen, G., *The Economic Promise of Nanotechnology*. Issues in Science and Technology, 2005. **21**(4): p. 55-56.
13. Brust, M., M. Walker, D. Bethell, D.J. Schiffrin, and R. Whyman, *Synthesis of Thiol-Derivatized Gold Nanoparticles in a 2-Phase Liquid-Liquid System*. Journal of the Chemical Society-Chemical Communications, 1994(7): p. 801-802.
14. Zheng, M.Y., X.W. Chen, R.H. Cheng, N. Li, J. Sun, X.D. Wang, and T. Zhang, *Catalytic Decomposition of Hydrazine on Iron Nitride Catalysts*. Catalysis Communications, 2006. **7**(3): p. 187-191.
15. Goebel, D.M. and I. Katz, *Fundamentals of Electric Propulsion: Ion and Hall Thrusters* Space Science and Technology Series, ed. J. Yuen. 2003, Hoboken: John Wiley and Sons.
16. Bush, D. and C.A. Eckert, *Estimation of Solid Solubilities in Supercritical Carbon Dioxide from Solute Solvatochromic Parameters*, in *Supercritical Fluids - Extraction and Pollution Prevention*, M.A. Abraham and A.K. Sunol, Editors. 1997. p. 37-50.
17. Dillow, A.K., J.S. Brown, C.L. Liotta, and C.A. Eckert, *Supercritical Fluid Tuning of Reactions Rates: The Cis-Trans Isomerization of 4-4'-Disubstituted Azobenzenes*. Journal of Physical Chemistry A, 1998. **102**(39): p. 7609-7617.
18. Eckert, C.A., D. Bush, J.S. Brown, and C.L. Liotta, *Tuning Solvents for Sustainable Technology*. Industrial & Engineering Chemistry Research, 2000. **39**(12): p. 4615-4621.
19. Eckert, C.A. and K. Chandler, *Tuning Fluid Solvents for Chemical Reactions*. Journal of Supercritical Fluids, 1998. **13**(1-3): p. 187-195.

20. Eckert, C.A., S. Kazarian, B.L. West, and N. Brantley, *Polymer Processing with Supercritical Fluids: Partitioning of Solutes and Cosolvents between Supercritical Fluids and Polymer Materials*. Abstracts of Papers of the American Chemical Society, 1998. **215**: p. 123-IEC.
21. Eckert, C.A., B.L. Knutson, and P.G. Debenedetti, *Supercritical Fluids as Solvents for Chemical and Materials Processing*. Nature, 1996. **383**(6598): p. 313-318.
22. Eckert, C.A., C.L. Liotta, D. Bush, J.S. Brown, and J.P. Hallett, *Sustainable Reactions in Tunable Solvents*. Journal of Physical Chemistry B, 2004. **108**(47): p. 18108-18118.
23. Eckert, C.A., J.G. Vanalsten, and T. Stoicos, *Supercritical Fluid Processing*. Environmental Science & Technology, 1986. **20**(4): p. 319-325.
24. Glaser, R., J. Williardt, D. Bush, M.J. Lazzaroni, and C.A. Eckert, *Application of High-Pressure Phase Equilibria to the Selective Oxidation of Alcohols over Supported Platinum Catalysts in Supercritical Carbon Dioxide*, in *Utilization of Greenhouse Gases*, C.J. Liu, R.G. Mallinson, and M. Aresta, Editors. 2003. p. 352-364.
25. Jayachandran, J.P., C. Wheeler, B.C. Eason, C.L. Liotta, and C.A. Eckert, *Phase Transfer Catalyzed Intramolecular Cycloalkylation of Phenylacetonitrile with Alpha, Omega-Dibromoalkanes in Supercritical Ethane*. Journal of Supercritical Fluids, 2003. **27**(2): p. 179-186.
26. Jessop, P.G., C.A. Eckert, C.L. Liotta, R.J. Bonilla, J.S. Brown, R.A. Brown, P. Pollet, C.A. Thomas, C. Wheeler, and D. Wynne, *Catalysis Using Supercritical or Subcritical Inert Gases under Split-Phase Conditions*, in *Clean Solvents - Alternative Media for Chemical Reactions and Processing*, M.A. Abraham and L. Moens, Editors. 2002. p. 97-112.
27. Jessop, P.G., M.M. Olmstead, C.D. Ablan, M. Grabenauer, D. Sheppard, C.A. Eckert, and C.L. Liotta, *Carbon Dioxide as a Solubility "Switch" for the Reversible Dissolution of Highly Fluorinated Complexes and Reagents in Organic Solvents: Application to Crystallization*. Inorganic Chemistry, 2002. **41**(13): p. 3463-3468.
28. Jessop, P.G., R.R. Stanley, R.A. Brown, C.A. Eckert, C.L. Liotta, T.T. Ngo, and P. Pollet, *Neoteric Solvents for Asymmetric Hydrogenation: Supercritical Fluids*,

- Ionic Liquids, and Expanded Ionic Liquids*. Green Chemistry, 2003. **5**(2): p. 123-128.
29. Johnston, K.P. and C.A. Eckert, *An Analytical Carnahan-Starling-Van Der Waals Model for Solubility of Hydrocarbon Solids in Supercritical Fluids*. Aiche Journal, 1981. **27**(5): p. 773-779.
30. Johnston, K.P., D.H. Ziger, and C.A. Eckert, *Solubilities of Hydrocarbon Solids in Supercritical Fluids - the Augmented Vanderwaals Treatment*. Industrial & Engineering Chemistry Fundamentals, 1982. **21**(3): p. 191-197.
31. Kazarian, S.G., N.H. Brantley, and C.A. Eckert, *Applications of Vibrational Spectroscopy to Characterize Poly(Ethylene Terephthalate) Processed with Supercritical Co<sub>2</sub>*. Vibrational Spectroscopy, 1999. **19**(2): p. 277-283.
32. Kazarian, S.G., N.H. Brantley, B.L. West, M.F. Vincent, and C.A. Eckert, *In Situ Spectroscopy of Polymers Subjected to Supercritical Co<sub>2</sub>: Plasticization and Dye Impregnation*. Applied Spectroscopy, 1997. **51**(4): p. 491-494.
33. Lazzaroni, M.J., D. Bush, R. Jones, J.P. Hallett, C.L. Liotta, and C.A. Eckert, *High-Pressure Phase Equilibria of Some Carbon Dioxide-Organic-Water Systems*. Fluid Phase Equilibria, 2004. **224**(1): p. 143-154.
34. Liotta, C.L., D. Suleiman, D.L. Boatright, A.K. Dillowwilson, and C.A. Eckert, *Phase-Transfer Catalysis in Supercritical Fluids*. Abstracts of Papers of the American Chemical Society, 1995. **209**: p. 56-IEC.
35. Lu, J., E.C. Boughner, C.L. Liotta, and C.A. Eckert, *Nearcritical and Supercritical Ethanol as a Benign Solvent: Polarity and Hydrogen-Bonding*. Fluid Phase Equilibria, 2002. **198**(1): p. 37-49.
36. Ngo, T.T., D. Bush, C.A. Eckert, and C.L. Liotta, *Spectroscopic Measurement of Solid Solubility in Supercritical Fluids*. Aiche Journal, 2001. **47**(11): p. 2566-2572.
37. Nolen, S.A., J. Lu, J.S. Brown, P. Pollet, B.C. Eason, K.N. Griffith, R. Glaser, D. Bush, D.R. Lamb, C.L. Liotta, C.A. Eckert, G.F. Thiele, and K.A. Bartels, *Olefin Epoxidations Using Supercritical Carbon Dioxide and Hydrogen Peroxide without Added Metallic Catalysts or Peroxy Acids*. Industrial & Engineering Chemistry Research, 2002. **41**(3): p. 316-323.

38. Teja, A.S. and C.A. Eckert, *Commentary on Supercritical Fluids: Research and Applications*. Industrial & Engineering Chemistry Research, 2000. **39**(12): p. 4442-4444.
39. Tomasko, D.L., K.J. Hay, G.W. Leman, and C.A. Eckert, *Pilot-Scale Study and Design of a Granular Activated Carbon Regeneration Process Using Supercritical Fluids*. Environmental Progress, 1993. **12**(3): p. 208-217.
40. Tomasko, D.L., S.J. Macnaughton, N.R. Foster, and C.A. Eckert, *Removal of Pollutants from Solid Matrices Using Supercritical Fluids*. Separation Science and Technology, 1995. **30**(7-9): p. 1901-1915.
41. West, K.N., C. Wheeler, J.P. McCarney, K.N. Griffith, D. Bush, C.L. Liotta, and C.A. Eckert, *In Situ Formation of Alkylcarbonic Acids with Co<sub>2</sub>*. Journal of Physical Chemistry A, 2001. **105**(16): p. 3947-3948.
42. Wheeler, C., D.R. Lamb, J.P. Jayachandran, J.P. Hallett, C.L. Liotta, and C.A. Eckert, *Phase-Transfer-Catalyzed Alkylation of Phenylacetonitrile in Supercritical Ethane*. Industrial & Engineering Chemistry Research, 2002. **41**(7): p. 1763-1767.
43. Broering, J.M., E.M. Hill, J.P. Hallett, C.L. Liotta, C.A. Eckert, and A.S. Bommarius, *Biocatalytic Reaction and Recycling by Using Co<sub>2</sub>-Induced Organic-Aqueous Tunable Solvents*. Angewandte Chemie-International Edition, 2006. **45**(28): p. 4670-4673.
44. Lu, J., J. Lazzaroni, J.P. Hallett, A.S. Bommarius, C.L. Liotta, and C.A. Eckert, *Tunable Solvents for Homogeneous Catalyst Recycle*. Industrial & Engineering Chemistry Research, 2004. **43**(7): p. 1586-1590.
45. Hallett, J.P., J.W. Ford, R.S. Jones, P. Pollet, C.A. Thomas, C.L. Liotta, and C.A. Eckert, *Hydroformylation Catalyst Recycle with Gas-Expanded Liquids*. Industrial & Engineering Chemistry Research, 2008. **47**(8): p. 2585-2589.
46. Ford, J.W., M.E. Janakat, J. Lu, C.L. Liotta, and C.A. Eckert, *Local Polarity in Co<sub>2</sub>-Expanded Acetonitrile: A Nucleophilic Substitution Reaction and Solvatochromic Probes*. Journal of Organic Chemistry, 2008. **73**(9): p. 3364-3368.

47. Blasucci, V.M., Z.A. Husain, A.Z. Fadhel, M.E. Donaldson, E. Vyhmeister, P. Pollet, C.L. Liotta, and C.A. Eckert, *Combining Homogeneous Catalysis with Heterogeneous Separation Using Tunable Solvent Systems*. Journal of Physical Chemistry A, 2010. **114**(11): p. 3932-3938.
48. Hill, E.M., J.M. Broering, J.P. Hallett, A.S. Bommarius, C.L. Liotta, and C.A. Eckert, *Coupling Chiral Homogeneous Biocatalytic Reactions with Benign Heterogeneous Separation*. Green Chemistry, 2007. **9**(8): p. 888-893.
49. Pollet, P., R.J. Hart, C.A. Eckert, and C.L. Liotta, *Organic Aqueous Tunable Solvent (Oats): A Vehicle for Coupling Reaction and Separation*. Accounts of Chemical Research, 2010. **43**: p. 1237-1245.
50. Brown, J.S., R. Glaser, C.L. Liotta, and C.A. Eckert, *Acylation of Activated Aromatics without Added Acid Catalyst*. Chemical Communications, 2000(14): p. 1295-1296.
51. Brown, J.S., J.P. Hallett, D. Bush, and C.A. Eckert, *Liquid-Liquid Equilibria for Binary Mixtures of Water Plus Acetophenone, Plus 1-Octanol, Plus Anisole, and Plus Toluene from 370 K to 550 K*. Journal of Chemical and Engineering Data, 2000. **45**(5): p. 846-850.
52. Chandler, K., F.H. Deng, A.K. Dillow, C.L. Liotta, and C.A. Eckert, *Alkylation Reactions in near-Critical Water in the Absence of Acid Catalysts*. Industrial & Engineering Chemistry Research, 1997. **36**(12): p. 5175-5179.
53. Chandler, K., B. Eason, C.L. Liotta, and C.A. Eckert, *Phase Equilibria for Binary Aqueous Systems from a near-Critical Water Reaction Apparatus*. Industrial & Engineering Chemistry Research, 1998. **37**(8): p. 3515-3518.
54. Chandler, K., C.L. Liotta, C.A. Eckert, and D. Schiraldi, *Tuning Alkylation Reactions with Temperature in near-Critical Water*. AIChE Journal, 1998. **44**(9): p. 2080-2087.
55. Cope, E.D., R.J. Hart, P. Pollet, K.M. Croft, M.A. Gantt, K.J. Nicodemus, P.T. Nielsen, M.A. Shaffer, C.L. Liotta, and C.A. Eckert, *Removal of N-Boc Protecting Groups in Nearcritical Water*, in *ACS Spring Meeting*. 2010: San Francisco, CA.

56. Hart, R.J., E.D. Cope, P. Pollet, C.A. Eckert, C.L. Liotta, and D.P. Kjell, *Nearcritical Water for the Benign Removal of N-Boc Protecting Groups*, in *Annual AIChE Meeting*. 2009: Nashville, TN.
57. Lesutis, H.P., R. Glaser, C.L. Liotta, and C.A. Eckert, *Acid/Base-Catalyzed Ester Hydrolysis in near-Critical Water*. *Chemical Communications*, 1999(20): p. 2063-2064.
58. Liotta, C.L., J.P. Hallett, P. Pollet, and C.A. Eckert, *Reactions in Nearcritical Water*, in *Organic Reactions in Water: Principles, Strategies and Applications*, U.M. Lindström, Editor. 2007, Blackwell Publishing Ltd: Oxford, UK. p. 256-297.
59. Lu, J., J.S. Brown, E.C. Boughner, C.L. Liotta, and C.A. Eckert, *Solvatochromic Characterization of near-Critical Water as a Benign Reaction Medium*. *Industrial & Engineering Chemistry Research*, 2002. **41**(12): p. 2835-2841.
60. Nolen, S., C.L. Liotta, C.A. Eckert, and R. Glaser, *The Catalytic Opportunities of near-Critical Water: A Benign Medium for Conventionally Acid and Base Catalyzed Condensations in Organic Synthesis*. *Green Chemistry*, 2003. **5**: p. 663-669.
61. Patrick, H.R., K. Griffith, C.L. Liotta, C.A. Eckert, and R. Glaser, *Near-Critical Water: A Benign Medium for Catalytic Reactions*. *Industrial & Engineering Chemistry Research*, 2001. **40**(26): p. 6063-6067.
62. Blasucci, V., C. Dilek, H. Huttenhower, E. John, V. Llopis-Mestre, P. Pollet, C.A. Eckert, and C.L. Liotta, *One-Component, Switchable Ionic Liquids Derived from Siloxylated Amines*. *Chemical Communications*, 2009(1): p. 116-118.
63. Jessop, P.G., D.J. Heldebrant, X.W. Li, C.A. Eckert, and C.L. Liotta, *Green Chemistry - Reversible Nonpolar-to-Polar Solvent*. *Nature*, 2005. **436**(7054): p. 1102-1102.
64. Phan, L., D. Chiu, D.J. Heldebrant, H. Huttenhower, E. John, X.W. Li, P. Pollet, R.Y. Wang, C.A. Eckert, C.L. Liotta, and P.G. Jessop, *Switchable Solvents Consisting of Amidine/Alcohol or Guanidine/Alcohol Mixtures*. *Industrial & Engineering Chemistry Research*, 2008. **47**(3): p. 539-545.

65. Donaldson, M.E., V.L. Mestre, D. Vinci, C.L. Liotta, and C.A. Eckert, *Switchable Solvents for in-Situ Acid-Catalyzed Hydrolysis of Beta-Pinene*. Industrial & Engineering Chemistry Research, 2009. **48**(5): p. 2542-2547.
66. Jiang, N., D. Vinci, C.L. Liotta, C.A. Eckert, and A.J. Ragauskas, *Piperylene Sulfone: A Recyclable Dimethyl Sulfoxide Substitute for Copper-Catalyzed Aerobic Alcohol Oxidation*. Industrial & Engineering Chemistry Research, 2008. **47**(3): p. 627-631.
67. Marus, G.A., E. Vyhmeister, P. Pollet, M.E. Donaldson, V. Llopis-Mestre, S. Faltermeier, R. Roesel, M. Tribo, L. Gelbaum, C.L. Liotta, and C.A. Eckert, *Sustainable and Scalable Synthesis of Piperylene Sulfone: A "Volatile" and Recyclable DmsO Substitute*. Industrial & Engineering Chemistry Research, 2010. **In Press**.
68. Vinci, D., M. Donaldson, J.P. Hallett, E.A. John, P. Pollet, C.A. Thomas, J.D. Grilly, P.G. Jessop, C.L. Liotta, and C.A. Eckert, *Piperylene Sulfone: A Labile and Recyclable DmsO Substitute*. Chemical Communications, 2007(14): p. 1427-1429.
69. Hines, A.L. and R.N. Maddox, *Mass Transfer Fundamentals and Applications* ed. N.R. Amundson. 1985, New Jersey: Prentice Hall.
70. Bird, R.B., W.E. Stewart, and E.N. Lightfoot, *Transport Phenomena*. Second ed. 2006, New Delhi: Wiley India.
71. Brunner, G., *Applications of Supercritical Fluids*. Annual Review of Chemical and Biomolecular Engineering, ed. J.M. Prausnitz, M.F. Doherty, and R.A. Segalman. Vol. 1. 2010, Palo Alto: Annual Reviews.
72. Song, I., M. Spuller, G. Levitin, and D.W. Hess, *Photoresist and Residue Removal Using Gas-Expanded Liquids*. Journal of the Electrochemical Society, 2006. **153**(4): p. G314-G318.
73. Subramaniam, B., *Gas-Expanded Liquids for Sustainable Catalysis and Novel Materials: Recent Advances*. Coordination Chemistry Reviews, 2010. **254**(15-16): p. 1843-1853.

74. Muldoon, M.J., *Modern Multiphase Catalysis: New Developments in the Separation of Homogeneous Catalysts*. Dalton Transactions, 2010. **39**(2): p. 337-348.
75. Abbott, A.P., E.G. Hope, R. Mistry, and A.M. Stuart, *Controlling Phase Behaviour on Gas Expansion of Fluid Mixtures*. Green Chemistry, 2009. **11**(10): p. 1536-1540.
76. Akien, G.R. and M. Poliakoff, *A Critical Look at Reactions in Class I and II Gas-Expanded Liquids Using CO<sub>2</sub> and Other Gases*. Green Chemistry, 2009. **11**(8): p. 1083-1100.
77. Yin, J.Z., X.R. Ma, X.Z. Zhang, and A.Q. Wang, *Thermodynamic Properties of Carbon Dioxide Expanded Liquids and Applications in Chemical Reactions*. Progress in Chemistry, 2008. **20**(9): p. 1251-1262.
78. Jessop, P.G. and B. Subramaniam, *Gas-Expanded Liquids*. Chemical Reviews, 2007. **107**(6): p. 2666-2694.
79. Anand, M., M.C. McLeod, P.W. Bell, and C.B. Roberts, *Tunable Solvation Effects on the Size-Selective Fractionation of Metal Nanoparticles in CO<sub>2</sub> Gas-Expanded Solvents*. Journal of Physical Chemistry B, 2005. **109**(48): p. 22852-22859.
80. McLeod, M.C., M. Anand, C.L. Kitchens, and C.B. Roberts, *Precise and Rapid Size Selection and Targeted Deposition of Nanoparticle Populations Using CO<sub>2</sub> Gas Expanded Liquids*. Nano Letters, 2005. **5**(3): p. 461-465.
81. Anand, M., L.A. Odom, and C.B. Roberts, *Finely Controlled Size-Selective Precipitation and Separation of CdSe/ZnS Semiconductor Nanocrystals Using CO<sub>2</sub>-Gas-Expanded Liquids*. Langmuir, 2007. **23**(13): p. 7338-7343.
82. Anand, M., S.S. You, K.M. Hurst, S.R. Saunders, C.L. Kitchens, W.R. Ashurst, and C.B. Roberts, *Thermodynamic Analysis of Nanoparticle Size Selective Fractionation Using Gas-Expanded Liquids*. Industrial & Engineering Chemistry Research, 2008. **47**(3): p. 553-559.
83. Saunders, S.R. and C.B. Roberts, *Size-Selective Fractionation of Nanoparticles at an Application Scale Using CO<sub>2</sub> Gas-Expanded Liquids*. Nanotechnology, 2009. **20**(47).

84. Hagen, J., *Industrial Catalysis: A Practical Approach*. 2006, Wiley-VCH: Weinheim. p. 1-14.
85. Herrmann, W.A. and C.W. Kohlpaintner, *Water-Soluble Ligands, Metal-Complexes, and Catalysts - Synergism of Homogeneous and Heterogeneous Catalysts*. *Angewandte Chemie-International Edition in English*, 1993. **32**(11): p. 1524-1544.
86. McAuliff, C., *Solubility in Water of Paraffin Cycloparaffin Olefin Acetylene Cycloolefin and Aromatic Hydrocarbons*. *Journal of Physical Chemistry*, 1966. **70**(4): p. 1267-&.
87. McAuliffe, C., *Solubility in Water of C<sub>1</sub>-C<sub>9</sub> Hydrocarbons*. *Nature*, 1963. **200**(4911): p. 1092-1093.
88. Neibecker, D., R. Reau, and S. Lecolier, *Synthesis of 2-Arylpropionaldehydes through Hydroformylation*. *Journal of Organic Chemistry*, 1989. **54**(22): p. 5208-5210.
89. Riley, D.P., D.P. Getman, G.R. Beck, and R.M. Heintz, *Selective Metal-Catalyzed Autoxidation of 2-Arylpropionaldehydes - an Improved Synthesis of Ibuprofen*. *Journal of Organic Chemistry*, 1987. **52**(2): p. 287-290.
90. Colour Publications Pvt, L., *Ibuprofen*. *Journal of Chemical Business of India*, 99. **13**(5): p. 59.
91. Goates, J.R. and R.J. Sullivan, *Thermodynamic Properties of the System Water-Para-Dioxane*. *Journal of Physical Chemistry*, 1958. **62**(2): p. 188-190.
92. Tsitsimpikou, C., H. Daflos, and F.N. Kolisis, *Comparative Studies on the Sugar Esters Synthesis Catalysed by Candida Antarctica and Candida Rugosa Lipases in Hexane*. *Journal of Molecular Catalysis B-Enzymatic*, 1997. **3**(1-4): p. 189-192.
93. Khmel'nitsky, Y.L., V.V. Mozhaev, A.B. Belova, M.V. Sergeeva, and K. Martinek, *Denaturation Capacity - a New Quantitative Criterion for Selection of Organic-Solvents as Reaction Media in Biocatalysis*. *European Journal of Biochemistry*, 1991. **198**(1): p. 31-41.

94. Schurz, J. and H. Stubchen, *Explosion Beim Destillieren Von Tetrahydrofuran*. Angewandte Chemie-International Edition, 1956. **68**(5): p. 182-182.
95. Deshpande, R.M., S.S. Divekar, B.M. Bhanage, and R.V. Chaudhari, *Effect of Solvent on the Kinetics of Hydroformylation of 1-Hexene Using  $\text{Hrh}(\text{Co})(\text{Pph}_3)_3$  Catalyst*. Journal of Molecular Catalysis, 1992. **77**(2): p. L13-L17.
96. Deshpande, R.M., S.S. Divekar, R.V. Gholap, and R.V. Chaudhari, *Enhancement of Rate and Selectivity in Hydroformylation of Allyl Alcohol through Solvent Effect*. Industrial & Engineering Chemistry Research, 1991. **30**(6): p. 1389-1390.
97. Lazzaroni, R., A. Raffaelli, R. Settambolo, S. Bertozzi, and G. Vitulli, *Regioselectivity in the Rhodium-Catalyzed Hydroformylation of Styrene as a Function of Reaction Temperature and Gas-Pressure*. Journal of Molecular Catalysis, 1989. **50**(1): p. 1-9.
98. Mukhopadhyay, K. and R.V. Chaudhari, *Heterogenized  $\text{Hrh}(\text{Co})(\text{Pph}_3)_3$  on Zeolite Y Using Phosphotungstic Acid as Tethering Agent: A Novel Hydroformylation Catalyst*. Journal of Catalysis, 2003. **213**(1): p. 73-77.
99. Sharma, S.K., P.A. Parikh, and R.V. Jasra, *Hydroformylation of Alkenes Using Heterogeneous Catalyst Prepared by Intercalation of  $\text{Hrh}(\text{Co})(\text{Tppts})(3)$  Complex in Hydrotalcite*. Journal of Molecular Catalysis a-Chemical, 2010. **316**(1-2): p. 153-162.
100. Hamza, K. and J. Blum, *Highly Selective Hydroformylation of Vinylarenes to Branched Aldehydes by  $[\text{Rh}(\text{Cod})\text{Cl}]_2$  Entrapped in Ionic Liquid Modified Silica Sol-Gel*. European Journal of Organic Chemistry, 2007(28): p. 4706-4710.
101. Janecko, H., A.M. Trzeciak, and J.J. Ziolkowski, *New Rhodium Complexes as Low-Pressure Hydroformylation Catalysts - Effect of Ligand on Catalyst Activity and Selectivity*. Journal of Molecular Catalysis, 1984. **26**(3): p. 355-361.
102. Kolesnichenko, N.V., N.A. Markova, A.T. Teleshev, and E.V. Slivinskii, *Modification of Rhodium Carbonyl Catalysts for Hydroformylation of 2-Butenes by Organophosphorus Ligands*. Russian Chemical Bulletin, 1999. **48**(4): p. 698-700.

103. Cringus, D., S. Yeremenko, M.S. Pshenichnikov, and D.A. Wiersma, *Hydrogen Bonding and Vibrational Energy Relaxation in Water-Acetonitrile Mixtures*. Journal of Physical Chemistry B, 2004. **108**(29): p. 10376-10387.
104. Shaharun, M.S., B.K. Dutta, H. Mukhtar, and S. Maitra, *Hydroformylation of 1-Octene Using Rhodium-Phosphite Catalyst in a Thermomorphic Solvent System*. Chemical Engineering Science, 2010. **65**(1): p. 273-281.
105. Bratlie, K.M., H. Lee, K. Komvopoulos, P.D. Yang, and G.A. Somorjai, *Platinum Nanoparticle Shape Effects on Benzene Hydrogenation Selectivity*. Nano Letters, 2007. **7**(10): p. 3097-3101.
106. Borodko, Y., S.E. Habas, M. Koebel, P.D. Yang, H. Frei, and G.A. Somorjai, *Probing the Interaction of Poly(Vinylpyrrolidone) with Platinum Nanocrystals by Uv-Raman and Ftir*. Journal of Physical Chemistry B, 2006. **110**(46): p. 23052-23059.
107. Bonet, F., K. Tekaia-Elhsissen, and K.V. Sarathy, *Study of Interaction of Ethylene Glycol/Pvp Phase on Noble Metal Powders Prepared by Polyol Process*. Bulletin of Materials Science, 2000. **23**(3): p. 165-168.
108. Abad, A., A. Corma, and H. Garcia, *Catalyst Parameters Determining Activity and Selectivity of Supported Gold Nanoparticles for the Aerobic Oxidation of Alcohols: The Molecular Reaction Mechanism*. Chemistry-a European Journal, 2008. **14**(1): p. 212-222.
109. Abad, A., P. Concepcion, A. Corma, and H. Garcia, *A Collaborative Effect between Gold and a Support Induces the Selective Oxidation of Alcohols*. Angewandte Chemie-International Edition, 2005. **44**(26): p. 4066-4069.
110. Quintanilla, A., V.C.L. Butselaar-Orthlieb, C. Kwakernaak, W.G. Sloof, M.T. Kreutzer, and F. Kapteijn, *Weakly Bound Capping Agents on Gold Nanoparticles in Catalysis: Surface Poison?* Journal of Catalysis, 2010. **271**(1): p. 104-114.
111. Fievet, F., J.P. Lagier, B. Blin, B. Beaudoin, and M. Figlarz, *Homogeneous and Heterogeneous Nucleations in the Polyol Process for the Preparation of Micron and Sub-Micron Size Metal Particles*. Solid State Ionics, 1989. **32-3**: p. 198-205.

112. Fierro-Gonzalez, J.C. and B.C. Gates, *Catalysis by Gold Dispersed on Supports: The Importance of Cationic Gold*. Chemical Society Reviews, 2008. **37**(9): p. 2127-2134.
113. Enache, D.I., D. Barker, J.K. Edwards, S.H. Taylor, D.W. Knight, A.F. Carley, and G.J. Hutchings, *Solvent-Free Oxidation of Benzyl Alcohol Using Titanic-Supported Gold-Palladium Catalysts: Effect of Au-Pd Ratio on Catalytic Performance*. Catalysis Today, 2007. **122**(3-4): p. 407-411.
114. Enache, D.I., D.W. Knight, and G.J. Hutchings, *Solvent-Free Oxidation of Primary Alcohols to Aldehydes Using Supported Gold Catalysts*. Catalysis Letters, 2005. **103**(1-2): p. 43-52.
115. Dominguez-Dominguez, S., A. Berenguer-Murcia, D. Cazorla-Amoros, and A. Linares-Solano, *Semihydrogenation of Phenylacetylene Catalyzed by Metallic Nanoparticles Containing Noble Metals*. Journal of Catalysis, 2006. **243**(1): p. 74-81.
116. Chen, J., Q.H. Zhang, Y. Wang, and H.L. Wan, *Size-Dependent Catalytic Activity of Supported Palladium Nanoparticles for Aerobic Oxidation of Alcohols*. Advanced Synthesis & Catalysis, 2008. **350**(3): p. 453-464.
117. Haider, P., B. Kimmerle, F. Krumeich, W. Kleist, J.D. Grunwaldt, and A. Baiker, *Gold-Catalyzed Aerobic Oxidation of Benzyl Alcohol: Effect of Gold Particle Size on Activity and Selectivity in Different Solvents*. Catalysis Letters, 2008. **125**(3-4): p. 169-176.
118. Liu, J., N. Ruffini, P. Pollet, V. Llopis-Mestre, C. Dilek, C.A. Eckert, C.L. Liotta, and C.B. Roberts, *More Benign Synthesis of Palladium Nanoparticles in Dimethyl Sulfoxide and Their Extraction into an Organic Phase*. Industrial & Engineering Chemistry Research, 2010. **49**: p. 8174-8179.
119. Eastoe, J. and B. Warne, *Nanoparticle and Polymer Synthesis in Microemulsions*. Current Opinion in Colloid & Interface Science, 1996. **1**(6): p. 800-805.
120. Eastoe, J., S. Stebbing, J. Dalton, and R.K. Heenan, *Preparation of Colloidal Cobalt Using Reversed Micelles*. Colloids and Surfaces a-Physicochemical and Engineering Aspects, 1996. **119**(2-3): p. 123-131.

121. Campelo, J.M., D. Luna, R. Luque, J.M. Marinas, and A.A. Romero, *Sustainable Preparation of Supported Metal Nanoparticles and Their Applications in Catalysis*. Chemsuschem, 2009. **2**(1): p. 18-45.
122. Sarkar, D., P. Gupta, A. Gautam, and K.C. Khilar, *Reuse of Surfactant/Oil Phase in Nanoparticle Synthesis Using W/O Microemulsions*. Aiche Journal, 2008. **54**(2): p. 582-587.
123. Liu, J.H., S.Q. Cheng, J.L. Zhang, X.Y. Feng, X.G. Fu, and B.X. Han, *Reverse Micelles in Carbon Dioxide with Ionic-Liquid Domains*. Angewandte Chemie-International Edition, 2007. **46**(18): p. 3313-3315.
124. Huttenhower, H.A., *Development of New Chemistry for a Dual Use Hydrazine Thruster, Switchable Room Temperature Ionic Liquids, a Study of Silane Grafting to Model Polyethylene Compounds, and Synthesis of the Novel Hydrazine Replacement Fuel Molecules 1,1-Dimethyl-2-[2-Azidoethyl]Hydrazine and 1,1-Dimethyl-2-[2-Azidoethyl]Hydrazone*, in *School of Chemistry & Biochemistry*. 2010, Georgia Institute of Technology: Atlanta.
125. Burns, M.R., S.A. Jenkins, N.M. Vermeulen, R. Balakrishna, T.B. Nguyen, M.R. Kimbrell, and S.A. David, *Structural Correlation between Lipophilicity and Lipopolysaccharidesequestering Activity in Spermine-Sulfonamide Analogs*. Bioorganic & Medicinal Chemistry Letters, 2006. **16**(24): p. 6209-6212.
126. Deck, P., D. Pendzialek, M. Biel, M. Wagner, B. Popkirova, B. Ludolph, G. Kragol, J. Kuhlmann, A. Giannis, and H. Waldmann, *Development and Biological Evaluation of Acyl Protein Thioesterase 1 (Apt1) Inhibitors*. Angewandte Chemie-International Edition, 2005. **44**(31): p. 4975-4980.
127. Vieira, R., C. Pham-Huu, N. Keller, and M.J. Ledoux, *New Carbon Nanofiber/Graphite Felt Composite for Use as a Catalyst Support for Hydrazine Catalytic Decomposition*. Chemical Communications, 2002(9): p. 954-955.
128. Willis, C., F.P. Lossing, and R.A. Back, *Heat of Formation of N<sub>2</sub>H<sub>2</sub> and Proton Affinity of N<sub>2</sub>*. Canadian Journal of Chemistry-Revue Canadienne De Chimie, 1976. **54**(1): p. 1-3.
129. Esker, D.W., J.C. Kroutil, and R.J. Checkley, *Radiation Cooled Mpd Arc Thruster*. 1969, NASA.

130. Groh, K.H. and H.W. Loebt, *State-of-the-Art of Radiofrequency Ion Thrusters*. Journal of Propulsion and Power, 1991. **7**(4): p. 573-579.
131. Funaki, I., H. Kuninaka, and K. Toki, *Plasma Characterization of a 10-Cm Diameter Microwave Discharge Ion Thruster*. Journal of Propulsion and Power, 2004. **20**(4): p. 718-727.
132. Chen, X.W., T. Zhang, M.Y. Zheng, L.G. Xia, T. Li, W.C. Wu, X.D. Wang, and C. Li, *Catalytic Decomposition of Hydrazine over Alpha-Mo2c/Gamma-Al2o3 Catalysts*. Industrial & Engineering Chemistry Research, 2004. **43**(19): p. 6040-6047.
133. Maurel, R. and J.C. Menezo, *Catalytic Decomposition of N-15-Labeled Hydrazine on Alumina-Supported Metals*. Journal of Catalysis, 1978. **51**(2): p. 293-295.
134. Contamin, R.C. and F.C. Tompkins, *Heterogeneous Decomposition of Hydrazine on Molybdenum Films*. Transactions of the Faraday Society, 1971. **67**(578): p. 545-&.
135. Cosser, R.C. and F.C. Tompkins, *Heterogeneous Decomposition of Hydrazine on Tungsten Films*. Transactions of the Faraday Society, 1971. **67**(578): p. 526-&.
136. WATANABE, K. and K. AZUMA, *Note on the Field Emission Microscopic Observation of Decomposition of Hydrazine on Rhenium*. JOURNAL OF THE RESEARCH INSTITUTE FOR CATALYSIS HOKKAIDO UNIVERSITY, 1967. **14**(3): p. 257-258.
137. Willhoft, E.M. and Robertso.Aj, *Mass-Spectrometric Investigation of Formation of Di-Imide by Catalytic Decomposition of Hydrazine at Low Pressures on Platinum*. Chemical Communications, 1967(8): p. 385-&.
138. Khomenko, A.A. and L.O. Apelbaum, *Kinetics of Catalytic Decomposition of Hydrazine Vapor on Palladium*. Kinetics and Catalysis, 1976. **17**(3): p. 600-607.
139. Smith, O.I. and W.C. Solomon, *Kinetics of Hydrazine Decomposition on Iridium and Alumina Supported Iridium Catalysts*. 1973, AIR FORCE ROCKET PROPULSION LAB. p. 34.

140. Wood, B.J. and H. Wise, *Interaction of Hydrazine with Polycrystalline Iridium Foil*. Journal of Catalysis, 1975. **39**(3): p. 471-480.
141. Block, J., *Chemisorption and Field Ionization of Hydrazine on Platinum Surfaces*. Zeitschrift Fur Physikalische Chemie-Frankfurt, 1972. **82**(1-4): p. 1-10.
142. Grunze, M., *Interaction of Hydrazine with an Fe(111) Surface*. Surface Science, 1979. **81**(2): p. 603-625.
143. Rienaecker, G. and J. Voelter, *Decomposition of Hydrazine Vapor on Copper Single Crystals* Zeitschrift für anorganische und allgemeine Chemie, 1959. **302**: p. 292-298.
144. Contour, J.P., J. Pagniet, and Pannetie.G, *Catalytic Properties of Iridium Deposited on Alumina .3. Application of Thermodesorption to Study of Adsorbed Ammonia*. Bulletin de la Societe Chimique de France, 1970(1): p. 75-&.
145. Contour, J.P. and Pannetie.G, *Hydrazine Decomposition over a Supported Iridium Catalyst*. Journal of Catalysis, 1972. **24**(3): p. 434-&.
146. Escard, J., C. Leclere, and J.P. Contour, *State of Supported Iridium in a Hydrazine Decomposition Catalyst*. Journal of Catalysis, 1973. **29**(1): p. 31-39.
147. Martignoni, P., H.A. Nappier, W.A. Duncan, J.A. Murfree, and W.W. Wharton, *The Thermal and Catalytic Decomposition of Ammonia and Hydrazine*. 1970, U.S. Army.
148. Maurel, R., J.C. Menezo, and J. Barrault, *Hydrazine Decomposition over Groups Viii and Ib Metals*. Journal de Chimie Physique et de Physico-Chimie Biologique, 1973. **70**(9): p. 1221-1226.
149. Couto, G.G., J.J. Klein, W.H. Schreiner, D.H. Mosca, A.J.A. de Oliveira, and A.J.G. Zarbin, *Nickel Nanoparticles Obtained by a Modified Polyol Process: Synthesis, Characterization, and Magnetic Properties*. Journal of Colloid and Interface Science, 2007. **311**(2): p. 461-468.
150. Balela, M.D.L., Z. Lockman, A. Azizan, E. Matsubara, and A.V. Amorsolo, *Protective Agent-Free Synthesis of Colloidal Cobalt Nanoparticles*. Journal of Physical Science, 2008. **19**(1): p. 1-11.

151. Bonet, F., V. Delmas, S. Grugeon, R.H. Urbina, P.Y. Silvert, and K. Tekaiia-Elhsissen, *Synthesis of Monodisperse Au, Pt, Pd, Ru and Ir Nanoparticles in Ethylene Glycol*. *Nanostructured Materials*, 1999. **11**(8): p. 1277-1284.
152. Grass, M.E., S.H. Joo, Y.W. Zhang, and G.A. Somorjai, *Colloidally Synthesized Monodisperse Rh Nanoparticles Supported on Sba-15 for Size- and Pretreatment-Dependent Studies of Co Oxidation*. *Journal of Physical Chemistry C*, 2009. **113**(20): p. 8616-8623.
153. Hoefelmeyer, J.D., K. Niesz, G.A. Somorjai, and T.D. Tilley, *Radial Anisotropic Growth of Rhodium Nanoparticles*. *Nano Letters*, 2005. **5**(3): p. 435-438.
154. Gibson, C.P. and K.J. Putzer, *Synthesis and Characterization of Anisometric Cobalt Nanoclusters*. *Science*, 1995. **267**(5202): p. 1338-1340.
155. Kamal, S.S.K., P.K. Sahoo, M. Premkumar, N.V.R. Rao, T.J. Kumar, B. Sreedhar, A.K. Singh, S. Ram, and K.C. Sekhar, *Synthesis of Cobalt Nanoparticles by a Modified Polyol Process Using Cobalt Hydrazine Complex*. *Journal of Alloys and Compounds*, 2009. **474**(1-2): p. 214-218.
156. Yan, X.P., H.F. Liu, and K.Y. Liew, *Size Control of Polymer-Stabilized Ruthenium Nanoparticles by Polyol Reduction*. *Journal of Materials Chemistry*, 2001. **11**(12): p. 3387-3391.
157. Xiao, J.P., Y. Xie, and W. Luo, *A Rational Low-Temperature Approach to the Synthesis of Gladiate Ruthenium Nanoparticles*. *Chemistry Letters*, 2002(4): p. 462-463.
158. Gao, S., J. Zhang, Y.F. Zhu, and C.M. Che, *A Convenient Solvothermal Route to Ruthenium Nanoparticles*. *New Journal of Chemistry*, 2000. **24**(10): p. 739-740.
159. Kurihara, L.K., G.M. Chow, and P.E. Schoen, *Nanocrystalline Metallic Powders and Films Produced by the Polyol Method*. *Nanostructured Materials*, 1995. **5**(6): p. 607-613.
160. Bai, L.Y., F.L. Yuan, and Q. Tang, *Synthesis of Nickel Nanoparticles with Uniform Size Via a Modified Hydrazine Reduction Route*. *Materials Letters*, 2008. **62**(16): p. 2267-2270.

161. Wu, S.H. and D.H. Chen, *Synthesis and Characterization of Nickel Nanoparticles by Hydrazine Reduction in Ethylene Glycol*. Journal of Colloid and Interface Science, 2003. **259**(2): p. 282-286.
162. Guo, F., H.G. Zheng, Z.P. Yang, and Y.T. Qian, *Synthesis of Cobalt Nanoparticles in Ethanol Hydrazine Alkaline System (Ehas) at Room Temperature*. Materials Letters, 2002. **56**(6): p. 906-909.
163. Viau, G., R. Brayner, L. Poul, N. Chakroune, E. Lacaze, F. Fievet-Vincent, and F. Fievet, *Ruthenium Nanoparticles: Size, Shape, and Self-Assemblies*. Chemistry of Materials, 2003. **15**(2): p. 486-494.
164. Kogelbauer, A., J.C. Weber, and J.G. Goodwin, *The Formation of Cobalt Silicates on Co/SiO<sub>2</sub> under Hydrothermal Conditions*. Catalysis Letters, 1995. **34**(3-4): p. 259-267.
165. Huang, S.X., T.S. Rufael, and J.L. Gland, *Diimide Formation on the Ni(100) Surface*. Surface Science, 1993. **290**(1-2): p. L673-L676.
166. Alhaydari, Y.K., J.M. Saleh, and M.H. Matloob, *Adsorption and Decomposition of Hydrazine on Metal-Films of Iron, Nickel, and Copper*. Journal of Physical Chemistry, 1985. **89**(15): p. 3286-3290.
167. Ackermann, L., A. Furstner, T. Weskamp, F.J. Kohl, and W.A. Herrmann, *Ruthenium Carbene Complexes with Imidazolin-2-Ylidene Ligands Allow the Formation of Tetrasubstituted Cycloalkenes by Rcm*. Tetrahedron Letters, 1999. **40**(26): p. 4787-4790.
168. Donaldson, M.E., L.C. Draucker, V. Blasucci, C.L. Liotta, and C.A. Eckert, *Liquid-Liquid Equilibria of Polyethylene Glycol (Peg) 400 and CO<sub>2</sub> with Common Organic Solvents*. Fluid Phase Equilibria, 2009. **277**(2): p. 81-86.
169. Fan, Y.X. and J.Q. Qian, *Lipase Catalysis in Ionic Liquids/Supercritical Carbon Dioxide and Its Applications*. Journal of Molecular Catalysis B-Enzymatic, 2010. **66**(1-2): p. 1-7.
170. Hernaiz, M.J., A.R. Alcantara, J.I. Garcia, and J.V. Sinisterra, *Applied Biotransformations in Green Solvents*. Chemistry-a European Journal, 2010. **16**(31): p. 9422-9437.

171. Moniruzzaman, M., N. Kamiya, and M. Goto, *Activation and Stabilization of Enzymes in Ionic Liquids*. Organic & Biomolecular Chemistry, 2010. **8**(13): p. 2887-2899.
172. Zhao, H., *Methods for Stabilizing and Activating Enzymes in Ionic Liquids - a Review*. Journal of Chemical Technology and Biotechnology, 2010. **85**(7): p. 891-907.
173. Aki, S., A.M. Scurto, and J.F. Brennecke, *Ternary Phase Behavior of Ionic Liquid (II)-Organic-Co<sub>2</sub> Systems*. Industrial & Engineering Chemistry Research, 2006. **45**(16): p. 5574-5585.
174. Kroon, M.C., L.J. Florusse, and C.J. Peters, *Phase Behavior of the Ternary 1-Hexyl-3-Methylimidazolium Tetrafluoroborate Plus Carbon Dioxide Plus Methanol System*. Fluid Phase Equilibria, 2010. **294**(1-2): p. 84-88.
175. Zhang, Z.F., W.Z. Wu, B. Wang, J.W. Chen, D. Shen, and B.X. Han, *High-Pressure Phase Behavior of Co<sub>2</sub>/Acetone/Ionic Liquid System*. Journal of Supercritical Fluids, 2007. **40**(1): p. 1-6.
176. Doukyu, N. and H. Ogino, *Organic Solvent-Tolerant Enzymes*. Biochemical Engineering Journal, 2010. **48**(3): p. 270-282.
177. Tojo, G. and M.I. Fernandez, *Oxidation of Alcohols to Aldehydes and Ketones: A Guide to Current Common Practice*. 2006: Springer.
178. De Vos, D., I.F.J. Vankelecom, and P.A. Jacobs, *Chiral Catalyst Immobilization and Recycling 2000*, Weinheim: Wiley-VCH.
179. Baatz, C., N. Thielecke, and U. Prusse, *Influence of the Preparation Conditions on the Properties of Gold Catalysts for the Oxidation of Glucose*. Applied Catalysis B-Environmental, 2007. **70**(1-4): p. 653-660.